PHOTOPHYSICS AND PHOTOCHEMISTRY OF NATURAL WATERS WITH EMPHASIS ON RADICAL PROBE DEVELOPMENT AND APPLICATION

by

SARAH ELIZABETH HERBELIN

B. A., Chemistry
Reed College, 1991

submitted in partial fulfillment of the requirements of the degree of

MASTER OF SCIENCE

at the

MASSACHUSETTS INSTITUTE OF TECHNOLOGY

and the

WOODS HOLE OCEANOGRAPHIC INSTITUTION

August, 1994

Signature of Author _____
Joint Program in Oceanography
Massachusetts Institute of Technology/
Woods Hole Oceanographic Institution

Certified by _____
Neil V. Blough, Associate Scientist, Chemical Oceanography Department,
Woods Hole Oceanographic Institution

and _____
Philip M. Gschwend, Professor, Environmental Engineering Department,
Massachusetts Institute of Technology
Thesis Co-supervisors

Accepted by _____
Daniel J. Repeta, Chairperson, Joint Committee for Chemical Oceanography,
Massachusetts Institute of Technology/Woods Hole Oceanographic Institution

PHOTOPHYSICS AND PHOTOCHEMISTRY OF NATURAL WATERS WITH EMPHASIS ON RADICAL PROBE DEVELOPMENT AND APPLICATION

by

SARAH ELIZABETH HERBELIN

Submitted in partial fulfillment of the requirements for
the Degree of Master of Science in Oceanography

Abstract

The work presented here consists of a literature review and calculations to estimate the importance of photochemistry to carbon cycling in the oceans, followed by a photophysical study of a series of stable nitroxide radical probes that have been used for the quantitative detection of individual carbon-centered radicals and reducing species in natural waters. Two appendices follow. The first contains preliminary experiments utilizing one of the nitroxide probes in an investigation of hydroxyl radical production rates and steady-state concentrations in seawater. The second consists of an investigation of the singlet lifetimes of humic acids (HA), in order to aid in understanding their photochemical cycling and influence on other compounds.

The impact of photochemical reactions on global oceanic carbon cycling was calculated from literature values. The results indicate that between 1 and 13% of all dissolved organic carbon in the oceans is oxidized photochemically. This is a significant flux term, much larger than that of riverine input for example.

A photophysical study of nitroxide radical probes was undertaken. For all of the compounds studied, steady-state absorption and fluorescence spectra were identical to those of the parent fluorophores. A decrease in fluorescence lifetime and quantum yield of tens- to hundreds-fold was observed for the paramagnetic compounds relative to their diamagnetic counterparts. Very rapid fluorescence quenching rates (3 to 80 x 10^{10} s^{-1}) were calculated for the fluorescamine moiety of the paramagnetic nitroxide compounds in a variety of solvents. Calculated energy minimized geometries were very similar for all compounds which implies that geometric differences are not responsible for the variations found in fluorescence lifetimes and quantum yields between compounds. Calculated Förster and Dexter overlap integrals do not support deexcitation by these mechanisms. Time-resolved absorption measurements resulted in no evidence for transient species due to either intersystem crossing to the triplet state or charge transfer. Of the mechanisms considered, direct internal conversion to the ground state, is most likely given our results.

An investigation of the utility of 3-(aminomethyl)-2,2,5,5-tetramethyl-1-pyrrolidinyloxy free radical (3-amp) for detection and quantification of hydroxyl radicals in natural waters found that the addition of primary probe compounds resulted in the generation of secondary carbon-centered radicals that were successfully trapped by 3-amp. Competition kinetics experiments with dimethyl sulfoxide resulted in a natural scavenger rate constant that matched previous literature results for coastal seawater. As expected, the addition of formate resulted in decreases, and the addition of nitrite in increases, in the hydroxyl radical trapping rate by this method. The resulting quantum yield values were about an order of magnitude higher than previous literature results. However, probably

due to the use of different latitudes at which to estimate the incident solar radiation at the sea surface, hydroxyl radical production rate and steady-state concentrations calculated were about an order of magnitude lower than literature results.

One experiment showed no increase in the hydroxyl radical production rate from Milli-Q water to oligotrophic and coastal seawater although the sample absorption coefficients increase by a factor of more than 20. However a single experiment comparing three different coastal seawater samples did show a correlation between absorption and hydroxyl radical production rate. More detailed work is needed to recognize the full potential of this method.

Marine HA fluorescence lifetime measurements utilizing time-resolved single photon counting revealed a large portion of chromophores with very short (20-60 ps) lifetimes and low quantum yields. At least three distinct lifetimes could be distinguished by iterative deconvolution, although they probably result from the grouping of a multitude of individual chromophores. The theory of calculating the quantum yields of individual chromophores measured in a mixture is developed and calculations are made, although from an incomplete data set. Shorter fluorescent lifetimes for a given chromophore center within HA result in smaller quantum yields and are thought to be caused by very rapid competing intramolecular dark pathways such as energy or electron transfer

Preliminary work investigating changes in time-resolved fluorescent lifetimes due to different sources of HA (Orinoco vs. Suwanee Rivers) and solution types (seawater vs. standard buffer) showed little variability.

Thesis Supervisors:

Neil V. Blough, Associate Scientist, Chemical Oceanography Department,
Woods Hole Oceanographic Institution

Philip M. Gschwend, Professor, Environmental Engineering Department,
Massachusetts Institute of Technology

DEDICATION

To my family and friends who gave me the support to make this possible. Thank you.

Acknowledgments

I wish to give special thanks to my parents, Charlie and Maggy, my brother, Armando and my friend Paul for support, Nathalie, Sigi, Rebecca, and Amy for companionship and commiseration, and my classmates for numerous excuses for a party.

I thank Kelly Falkner and Sarah Green for instruction, advice, and for getting me interested in the first place, and John Edmond for advice and the opportunity of a trip to Russia to get me hooked. Thanks go to Meg Tivey for a superior job as a committee member. Also to Phil's lab group for helpful discussion of research questions. Jake, John, Abbie, and Ronnie all made the bureaucracy of the Joint Program work so easily.

My two advisors were very important to my education these last two years. Phil Gschwend provided much encouragement, great teaching and sound scientific advice. Neil Blough allowed me to make this thesis what it is by providing scientific advice, helping me to understand my results, always being available for consultation, and by reading and commenting on so many drafts! Many thanks to you both.

I wish to thank the captain and crew of the RV *Weatherbird II* and the RV *ARGO Maine* and Ken Buesseler and Bruce Keafer for taking me along to collect the samples for this work. Thanks go to Ted Loder for speedily supplying nutrient data from the GOM cruise. I am grateful for the assistance of Steve Atherton and Don Anderson at CFKR, Carl Johnson for high resolution mass spectrometer results and especially my brother, Armando Herbelin, at Western Washington University for molecular modeling work.

This material is based upon work supported under a National Science Foundation Graduate Research Fellowship. Any opinions, findings, conclusions or recommendations expressed in this publication are those of the author and do not necessarily reflect the views of the National Science Foundation.

Table of Contents

List of Figures

Appendix I

Appendix II

List of Tables

Chapter One: Background and Global Estimates

Introduction

Oceanic photochemical processes influence the cycling and bioavailability of carbon, oxygen, nitrogen and trace metals. Light mediated reactions have been shown to break down large macromolecules (Mopper and Stahovec, 1986; Amador et al., 1989; Ehrhardt et al., 1992) and may be responsible for some of the chemical differences including degree of saturation, nitrogen-to-carbon ratio and $^{12}C/^{13}C$ ratios between terrestrial and marine humic substances found by Hedges et al. (1992). Photolysis can partially transform biologically refractory compounds such as humic substance and crude oil (Kieber et al., 1989; Ehrhardt and Weber, 1991) into biologically available compounds such as pyruvate and low molecular weight carbonyl compounds, respectively. It is also possible to form a number of trace gases that are important to atmospheric chemistry, including COS, CO and CO_2 (Andreae and Ferek, 1992; Gammon and Kelly, 1990; Miller and Zepp, 1992). It has been argued that the photochemical degradation pathway is potentially the rate-limiting step in the removal of a large fraction of oceanic DOC (Mopper et al., 1991). In addition, the Fe(II)/Fe(III) redox couple in surface seawater can be driven photochemically as has been shown by Waite and Morel (1984) and O'Sullivan et al. (1991), with light increasing the bioavailability of Fe(II) and 'fresh' Fe(III) from aged Fe(III) compounds (Finden et al., 1984; Wells and Mayer, 1991; Wells et al., 1991).

In order to understand and quantify the importance of photochemistry in the oceans, the incident light field, available chromophores and the mechanisms of the resulting photochemical reactions must be thoroughly understood. Incident solar radiation at the sea surface is strongest and fairly constant between 400 and 850 nm. Below 400 nm the photon flux decreases sharply, undergoing a reduction of over two orders of magnitude between 300-400 nm (Baker et al., 1982). In addition to light energy, photochemistry requires the presence of chromophores that are capable of absorbing the available

wavelengths. In the ocean the principal photoreactive chromophores within the water column have been termed gelbstoff, yellow substance, or chromophoric dissolved organic matter (CDOM) (Fig. 1).

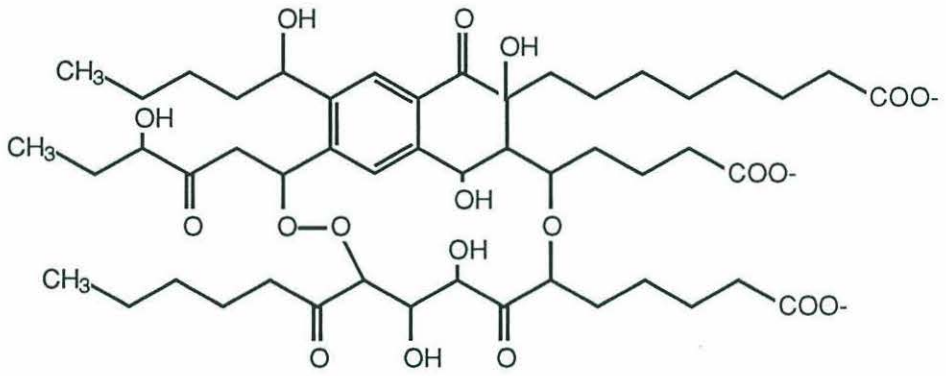

Figure 1. Proposed structure of seawater humic acid, (Harvey et al., 1983).

The specific absorptivity of CDOM decreases exponentially from the ultraviolet (UV) to the visible. In more highly colored coastal waters influenced by large riverine inputs, resuspension of sediments and high biological productivity, CDOM absorbs most of the incident photons in the photochemically important UV region of the spectrum. In oligotrophic (blue) waters where the concentrations of CDOM are much lower, water itself may absorb from one to three quarters of the solar radiation (Smith and Baker, 1979). The depth of effective light penetration (1/e) of the most photochemically productive photons (300-400 nm) in the oceans varies from between a few centimeters in some strongly absorbing coastal regions up to about 30 m in clear oligotrophic regions (Smith and Baker, 1979).

Once a photon has been absorbed by a chromophore (1), a number of outcomes are possible for the resulting excited state molecule. The extra energy can be reemitted as heat or light (quantum yield from Green, 1992) (2,3) or it can result in a transformation of the CDOM molecule that absorbed it either before or after undergoing intersystem crossing to the triplet state (4).

$$^1CDOM + h\nu \longrightarrow {}^1CDOM^* \quad (1)$$

$$^1CDOM^* \longrightarrow {}^1CDOM + \text{heat} \quad (2)$$

$$\xrightarrow{\Phi=\sim 0.01} {}^1CDOM + h\nu \quad (3)$$

$$\longrightarrow {}^3CDOM^* \quad (4)$$

$$^1CDOM^* \text{ or } {}^3CDOM^* \longrightarrow \text{direct photochemistry products} \quad (5)$$

$$^1CDOM^* \text{ or } {}^3CDOM^* \longrightarrow \text{indirect photochemistry products} \quad (6)$$

Transformations include direct photochemistry in which the individual excited CDOM molecule undergoes a chemical reaction (5) and indirect photochemistry in which some of the energy is transferred to another molecule sorbed or near the original molecule (6). Here we will focus on the indirect pathway (6). This last outcome is often accomplished by transient intermediates (TI) that can undergo further reactions. Dioxygen or molecular oxygen, due to their energy and high concentration in natural surface waters (~250 μM), are the predominant energy and electron acceptors available for the oxidation of CDOM. The resulting reactive oxygen species (ROS), which include $^1O_2(^1A_g)$, O_2^-, H_2O_2, OH, and RO_2, (Blough and Zepp, in press) sometimes exist long enough to react with additional molecules of CDOM or non-chromophoric DOM. Thus photochemical transformations may affect a larger portion of the carbon pool than that which absorbs solar photons directly. Although not discussed here, metals can also be instrumental in these processes, both as chromophores and as oxidizers when they undergo redox chemistry.

Global Photochemical Flux Estimates From Literature Values

The production of TI, including the ROS, has been recently summarized by Blough and Zepp (in press) and Blough (submitted). The known TI include: singlet oxygen ($^1O_2$), superoxide (O_2^-), hydrated electron ($e^-_{(aq)}$), hydrogen peroxide (H_2O_2), hydroxyl radical (OH), peroxy radicals ($RO_2^\bullet$, where R is some carbon compound), carbon-centered radicals ($R^\bullet$) and an experimentally defined group of one-electron reductants. The final

photochemical reaction products produced from TI and ROS include low molecular weight aldehydes, carbonyl sulfide, carbon monoxide and carbon dioxide.

A number of different researchers have measured the quantum yields of photochemical intermediates and products which can be transformed into global flux estimates with some simplifying assumptions (Table I,II,III).

Table I. Reactive Oxygen Species Production Rates

ROS	Annual Area Source (mol/y)[a]	Type of water, Location	Reference
O_2^-	4.1×10^{13}	Coastal, DE	Blough, submitted
H_2O_2	8.0×10^{12}	Coastal, DE	Blough, submitted
OH	2.6×10^{11}	Coastal, FL	Mopper and Zhou, 1990
All Available ROS	**3.6×10^{14}[b]**	**Global Ocean**	

[a]Assumes a global average photochemically effective sunlight flux equal to 3 hours of clear sky solar noon irradiation at 40° N (Mopper et al., 1991; Zepp and Cline, 1977), a coastal area of 4.9×10^{13} m^2 and an open ocean area of 3.1×10^{14} m^2. [b]Assumes identical quantum yields for coastal and oligotrophic waters.

Table II. Transient Intermediate Production Rates

TI	Annual Production Rate (mol/y)[a]	Type of water, Location	Reference
methyl radical	5.1×10^{10}	Coastal, DE	Blough, submitted
acetyl radical	1.9×10^{11}	Coastal, DE	Blough, submitted
1-e^- reductants	4.1×10^{13}	Coastal, FL	Blough and Kieber, 1992
1-e^- reductants	2.6×10^{14}	Oligotrophic	Blough and Kieber, 1992
All Available TI	**3×10^{14}**	**Global Ocean**	

[a]Assumes a global average photochemically effective sunlight flux equal to 3 hours of clear sky solar noon irradiation at 40° N (Mopper et al., 1991; Zepp and Cline, 1977), a coastal area of 4.9×10^{13} m^2 and an open ocean area of 3.1×10^{14} m^2.

Annual fluxes were calculated using the 'best estimate' of Mopper et al. (1991) for photon flux to the sea surface, wavelength dependencies from Zepp and Cline (1977) and the assumption that all photons arriving at the sea surface were absorbed by CDOM. It is of interest to compare the annual production rates of ROS, TI and photochemical products as they should all be related to each other. Excited chromophores create TI and ROS that then go on to create more TI which all eventually end up as products. Indeed, all three methods of estimation of global photochemical transformation rates do fall within the same range of values (Table I,II,III).

Table III. Product Production Rates

Product	Annual Production Rate (mol/y)[a]	Type of water, Location	Reference
formaldehyde, acetaldehyde, glyoxal, CO, glyoxylate, and pyruvate	1.7 to 7.2×10^{13} (text estimate)	Oligotrophic, SS	Mopper et al., 1991
CO	8.8×10^{11}	Coastal, DE	Blough, submitted
CO	3.2×10^{12}	Coastal, FL	Valentine and Zepp, 1993
CO	2.3×10^{13}[b]	Global	Valentine and Zepp, 1993
CO_2	2 to 5×10^{14}[c]	Global	Miller and Zepp, 1992
All Products except CO_2	**2.3×10^{13}**	**Global Ocean**	
All Products	**2 to 5×10^{14}**	**Global Ocean**	

[a]Assumes a global average photochemically effective sunlight flux equal to 3 hours of clear sky solar noon irradiation at 40^{o} N (Mopper et al., 1991; Zepp and Cline, 1977), a coastal area of 4.9×10^{13} m^2 and an open ocean area of 3.1×10^{14} m^2. [b]Assumes identical quantum yields for coastal and oligotrophic waters. [c]Assumes that production rate of CO = 5 to 10% of CO_2 production as found in terrestrial waters.

This may indicate that the ROS studied so far really lead to the TI identified that in turn form the reaction products measured, and thus, that most of the major players have been

identified and measured. However, it may also just be fortuitous that researchers have identified about the same fraction of important compounds from each of the three categories, or that reaction stoichiometries (see discussion below) happen to compensate. Clearly more work needs to be done in order to fully understand the mechanisms involved in photochemical transformations in natural waters.

Photochemical Impact On The Oceanic Carbon Cycle

There is much interest in understanding the mechanisms and magnitudes of the fluxes in the global biogeochemical carbon cycle, especially in how it relates to the issues of global warming. Carbon cycling in the ocean can be thought of in terms of the production and consumption of oxygen. Phytoplankton use solar energy to oxidize water and transform carbon dioxide into the reduced carbon (here generalized as 'CH_2O') needed for growth and storage of energy (7).

$$CO_2 + H_2O \longrightarrow \text{'}CH_2O\text{'} + O_2 \qquad (7)$$

The oxygen so produced can diffuse into the atmosphere, be advected away from the production site, accumulate in the water column, be consumed biologically to oxidize reduced carbon molecules for energy (respiration) (8) or be consumed photochemically in the oxidation of CDOM or DOC (9). Abiological dark consumption of oxygen is at most a small factor.

$$\text{'}CH_2O\text{'} + O_2 \xrightarrow{\text{biology}} CO_2 + H_2O \qquad (8)$$

$$\text{'}CH_2O\text{'} + O_2 \xrightarrow{\text{light}} CO_2 + H_2O \qquad (9)$$

The ratio of moles of oxygen produced per mole of carbon fixed in reaction (7) has been loosely constrained to between 1 and 1.8 : 1 (Williams et al., 1983). The stoichiometry of reaction (8) has been exhaustively studied. The most recent value is 1.45 moles of oxygen consumed per mole of carbon dioxide produced for depths below 400 m (Anderson and Sarmiento, 1994). The stoichiometry of reaction (9) is unknown, but for purposes of rough comparisons, a 1:1 ratio will be assumed here. It is expected that this should result in an error of no more than a factor of two to four.

Using current literature values of photosynthetic oxygen and reduced carbon production and riverine input (Table IV), we can evaluate the importance of photochemical oxidation of organic carbon compounds (shown in Tables I - III) to the oceanic carbon cycle. For example, marine oxygen production from primary productivity is estimated at from 4 to 8 x 10^{15} moles O_2/year by Williams et al. (1983) (Table IV).

Table IV. Global Annual Oxygen and Carbon Fluxes to the Oceans

	Flux (mol/m^2y)	Annual Global Source (mol/y)	Type of water	Reference
Oxygen				
Marine Primary Production	5		Sargasso Sea	Jenkins and Goldman, (85)
	7		Coastal	Laane et al., (85)
		$2x10^{15}$	[a]Combined	
		4 to $8x10^{15}$	[b]Combined	Williams et al. (83)
Carbon				
Marine Primary Production		$4x10^{15}$		Williams and Druffel (87)
Dissolved Riverine Input		$2x10^{13}$		Meybeck (82)

[a]Using a coastal area of 4.9 x 10^{13} m^2 and an open ocean area of $3.1x10^{14}$ m^2. [b]Obtained by multiplying the Williams and Druffel (87) carbon value by a photosynthetic ration of 1 to 1.8 moles of oxygen produced /mole carbon fixed .

Dividing the annual flux of ROS (3.6 x 10^{14} moles ROS/year) by the oxygen production indicates that between 5 and 9% of the annual ocean production of oxygen is used photochemically (Table V). Similar comparisons of the source magnitude of oxygen and carbon production from primary productivity with the three different photochemical sink measures (ROS, TI and reaction products) indicate that from 1 to 13% of the annual ocean production of reduced carbon is oxidized photochemically (Table V). This type of calculation also suggests that the annual photochemical oxidation of reduced organic carbon species is very large relative to other carbon-cycle contributions like yearly riverine input.

If the calculated flux of photons absorbed by CDOM is substantially lower than the assumed values, perhaps due to cloud albedo effects or the absorption of photons by water or non-reactive particulate matter, the calculated TI, ROS and product fluxes will be reduced. However, even with the assumption of a ten-fold lower photon flux, photochemistry must still play a significant part in the oxidative cycling of both terrestrial and marine derived DOC in the oceans.

Table V. Importance of Photochemical Reactions to Global Oceanic Carbon Cycling

Oceanic Source Measure (from Tables I - III)	Photochemical Consumption Measure (from Table IV)	Percent of Source Consumed Photochemically[a]
Oxygen Production from Primary Productivity[b]	ROS	5 to 9%
	TI	4 to 8%
	Products (without CO_2)	0.3 to 0.6%
	Products (including CO_2)	2.5 to 13%
Carbon Production from Primary Productivity	ROS	9%
	TI	8%
	Products (without CO_2)	0.6%
	Products (including CO_2)	5 to 13%
Riverine Carbon Input	ROS	1800%
	TI	1500%
	Products (without CO_2)	120%
	Products (including CO_2)	1000 to 2500%

[a]Method of calculation and sources contained in the text and Tables I-III. [b]Using the Williams et al. (83) values from Table III.

Motivation For and Overview of This Work

Given the difficulty of measuring reactive intermediates that are very short lived and only present at very low steady-state concentrations (micro to attomolar), the amount that is known is quite astonishing. However, as is clear from the rough nature of the above estimates, much more work needs to be done to better understand the sources, concentrations and mechanisms of the photochemical reactions occurring in natural waters. To accomplish this goal it is necessary to develop and evaluate extremely sensitive techniques for measuring TI, ROS and their products. Blough and Zepp (in press) have reviewed the current suite of TI trapping methods that have been employed. Of these the 3-aminomethyl-2,2,5,5-tetramethyl-1-pyrrolidinyloxy free radical (3-amp) (Fig. 1, Chapter

2) developed by Kieber and Blough (1990), is perhaps one of the most flexible. The reactivity of 3-amp with carbon-centered radicals (10^8-10^9 $M^{-1}s^{-1}$, Kieber and Blough, 1990a) is similar to that of dioxygen in that it reacts with the same types of TI as molecular oxygen does, but does not react facilely with the major reaction products of oxygen (superoxide and peroxyl radicals). The result of these reactions with 3-amp are stable diamagnetic alkoxyamines or the one-electron reduction product, the hydroxylamine. After coupling with fluorescamine, the diamagnetic products become highly fluorescent while the unreacted 3-amp is only very slightly fluorescent. This result is due to very efficient intramolecular fluorescence quenching of the fluorescamine moiety by the nitroxide radical as is further discussed in Chapter 2 and Green et al. (1990). The reaction products can be separated by high performance liquid chromatography (HPLC) (Kieber and Blough, 1990a,b) and positively identified by mass spectrometry (Kieber et al., 1992).

What follows is an investigation into the photophysics and photochemistry of natural waters. The main body consists of a photophysical study of the fluorescamine adducts of a series of stable nitroxide radicals that have been used for the quantitative detection of individual carbon-centered radicals and one-electron reductants in natural waters. With the use of secondary probes that produce carbon-centered radicals which can be trapped by 3-amp, quantification of additional radical intermediates is possible. One application of this approach is evaluated in this thesis and described in Appendix I.

In order to better understand the origins of these reactive intermediates in natural waters, the deexcitation processes of the chromophores themselves must be investigated. Humic substances have been shown to produce radicals that react with 3-amp (Kieber and Blough, 1992). Once a chromophore absorbs a photon, it can transfer its extra energy in one of the four ways discussed above. One method of studying the relative efficiency of these processes is to measure the singlet lifetimes of the chromophore via fluorescence lifetime measurements (Appendix II). The loss of energy by fluorescence competes with the other decay processes. Thus, in most situations, the shorter-lived the fluorescence, the

more rapid the competing processes must be, and vice versa. This work is one more step of the great many necessary to understand the photophysics and photochemistry of natural waters.

References

Amador, J. A., Alexander, M. and Zika, R. G., 1989. Sequential photochemical and microbial degradation of organic molecules bound to humic acid. Appl. Environ. Microbiol., 55: 2843-2849.

Anderson, L. A., Sarmiento, J. L., 1994. Redfield ratios of remineralization determined by nutrient data analysis. Glob. Biogeochem. Cycles, 8: 65-80.

Andreae, M. O., and Ferek, R. J., 1992. Photochemical production of carbonyl sulfide in seawater and its emission to the atmosphere. Global Biogeochem. Cycles, 6: 175-183.

Baker, K. S., Smith, R. C., and Green, A. E. S., 1982. Middle ultraviolet irradiance at the ocean surface: Measurements and models. In Calkins, J (Editor), The Role of Solar Ultraviolet Radiation in Marine Ecosystems, NATO conference series. IV, Marine sciences. Vol. 7, Plenum Press, NY., p 79-91.

Blough, N. V., and Simpson, D. J., 1988. Chemically-mediated fluorescence yield switching in nitroxide-fluorophore adducts: Optical sensors of radical/redox reactions. J. Am. Chem. Soc., 110: 1915-1917.

Blough, N. V., and Kieber, D. J., 1992. Photogenerated radical production in marine waters and its relationship to DOC photooxidation. Preprint extended abstracts, Division of Environmental Chemistry, ACS National Meeting, San Francisco, 32: 73-75.

Blough, N. V., and Zepp, R. G., in press. Reactive oxygen species (ROS) in natural waters. In: C. S. Foote, J. S. Valentine, A. Greenberg, and J.F. Liebman (Editors), Reactive Oxygen Species in Chemistry, Chapman and Hall.

Blough, N. V., Submitted. Photochemistry in the sea-surface microlayer.

Ehrhardt, M. G., Burns, K. A., Bicego, M. C., 1992. Sunlight-induced compositional alterations in the seawater-soluble fraction of a crude oil. Mar. Chem., 37: 53-64.

Ehrhardt, M. G., Weber, R. R., 1991. Formation of low molecular weight carbonyl compounds by sensitized photochemical decomposition of aliphatic hydrocarbons in seawater. Fresenius J. Anal. Chem., 339: 772-776.

Finden, D. A. S., Tiping, E., Jaworski, G. H. M., and Reynolds, C. S., 1984. Light-induced reduction of natural iron(III) oxide and its relevance to phytoplankton. Nature, 309: 783-784.

Gammon, R. H., and Kelly, K. C., 1990. Photochemical production of carbon monoxide in surface waters of the Pacific and Indian Oceans, in Effects of Solar Ultraviolet Radiation on Biogeochemical Dynamics in Aquatic Environments (eds. N. V. Blough and R. G. Zepp), Woods Hole Oceanographic Institution Technical Report, WHOI-90-09, pp. 58-60.

Green, S. A., 1992. Applications of Fluorescence Spectroscopy to Environmental Chemistry. Ph.D. Thesis. MIT/WHOI, WHOI-92-24.

Green, S. A., Simpson, D. J., Zhou, G., Ho, P. S., and Blough, N. V., 1990. Intramolecular quenching of excited singlet states by stable nitroxyl radical. J. Am. Chem. Soc., 112: 7337-7346.

Harvey, G. R., Boran, D. A., Chesal, L. A., and Tokar, J. M., 1983. The structure of marine fulvic and humic acids. Mar. Chem., 12: 119-132.

Hedges, J. I., 1992. Global biogeochemical cycles: progress and problems. Mar. Chem., 39: 67-93.

Hedges, J. I., Hatcher, P. G., Ertel, J. R., and Meyers-Schulte, K. J., 1992. A comparison of dissolved humic substances from seawater with Amazon River counterparts by ^{13}C-NMR spectrometry. Geochim. Cosmochim. Acta, 56: 1753-1757.

Jenkins, W. J., and Goldman, J. C., 1985. Seasonal oxygen cycling and primary production in the Sargasso Sea. J. Mar. Res., 43: 465-491.

Kieber, D. J., and Blough, N. V., 1990a. Fluorescence detection of carbon-centered radicals in aqueous solution. Free Rad. Res. Comm., 10: 109-117.

Kieber, D. J., and Blough, N. V., 1990b. Determination of carbon-centered radicals in aqueous solution by liquid chromatography with fluorescence detection. Anal. Chem., 62: 2275-2283.

Kieber, D. J., and Blough, N. V., 1992. Photoinitiated radical production in aquatic humic substances. Preprint extended abstracts, Division of Environmental Chemistry, ACS National meeting, San Francisco, 32: 84-87.

Kieber, D. J., Johnson, C. G., and Blough, N. V., 1992. Mass spectrometric identification of the radical adducts of a fluorescamine-derivatized nitroxide. Free Rad. Res. Comm., 16: 35-39.

Kieber, D. J., McDaniel, J., and Mopper, K., 1989. Photochemical source of biological substrates in sea water: implications for carbon cycling. Nature, 341: 637-639.

Laane, R. W. P. M., Gieskes, W. W. C., Kraay, G. W., and Eversdijk, A., 1985. Oxygen consumption from natural waters by photo-oxidizing processes. Neth. J. Sea Res., 19: 125-128.

Meybeck, M., 1982. Carbon, nitrogen and phosphorus transport by world rivers. Am. J. Sci., 282: 401-450.

Miller, W. L., and Zepp, R. G., 1992. Photochemical carbon cycling in aquatic environments: Formation of atmospheric carbon dioxide and carbon monoxide. Preprint extended abstracts, Division of Environmental Chemistry, ACS National Meeting, San Francisco, 32, 158-160.

Mopper, K. and Stahovec, W. L., 1986. Sources and sinks of low molecular weight organic carbonyl compounds in seawater. Mar. Chem., 19: 305-321.

Mopper, K. and Zhou, X., 1990. Hydroxyl radical photoproduction in the sea and its potential impact on marine processes. Science, 250: 661-664.

Mopper, K., Zhou, X., Kieber, R. J., Kieber, D. J., Sikorski, R. J. and Jones, R. D., 1991. Photochemical degradation of dissolved organic carbon and its impact on the oceanic carbon cycle. Nature, 353: 60-62.

O'Sullivan, D. W., Hanson, A. K., Miller, W. L., and Kester, D. R., 1991. Measurement of Fe(II) in surface water of the equatorial Pacific. Limnol. Oceanogr., 36: 1727-1741.

Smith, R. C., and Baker, K. S., 1979. Penetration of UV-B and biologically effective dose-rates in natural waters. Photochem. and Photobiol., 29: 311-323.

Valentine, R. L. and Zepp, R. G., 1993. Formation of carbon monoxide from the photodegradation of terrestrial dissolved organic carbon in natural waters. Environ. Sci. Technol., 27: 409-412.

Waite, T. D., and Morel, F. M. M., 1984. Photoreductive dissolution of colloidal iron oxides in natural waters. Environ. Sci. Technol., 18: 860-868.

Wells, M. L., and Mayer, L. M., 1991. The photoconversion of colloidal iron oxyhydroxides in seawater. Deep-Sea Res., 38: 1379-1395.

Wells, M. L., Mayer, L. M., Donard, O. F. X., de Souza Sierra, M. M., and Ackelson, S. G., 1991. The photolysis of colloidal iron in the oceans. Nature, 353: 248-250.

Williams, P. M., and Druffel, E. R. M., 1987. Radiocarbon in dissolved organic carbon in the central north Pacific Ocean. Nature, 330: 246-248.

Williams, P. J. LeB., Heinemann, K. R., Marra, J., and Purdie, D. A., 1983. Comparisons of ^{14}C and O_2 measurements of phytoplankton production in oligotrophic waters. Nature, 305: 49-50.

Zepp, R. G., and Cline, D. M., 1977. Rates of direct photolysis in aquatic environment. Environ. Sci. Technol., 11: 359-366.

Chapter 2: Intramolecular Quenching of Excited Singlet States in a Series of Fluorescamine-Nitroxide Compounds

Introduction

The mechanisms by which the excited singlet states of aromatic organic compounds are quenched by stable nitroxide radicals has been the subject of numerous studies over the last several decades (1-5). Much of this past work has been directed at disentangling the relative contributions of electron exchange, energy transfer and electron transfer to the quenching process (1). The more recent use of fluorescence quenching by nitroxides to examine dynamical processes in biochemical systems (6-9) and as the basis of a method for the fluorimetric detection of radicals in condensed phases (10-15) has significantly heightened the interest in these mechanisms and has pointed out the need to acquire additional information on the factors controlling the rates and distance-dependence of the quenching. This information is needed not only to identify the dominant quenching route(s) operating for a particular chromophore-nitroxide pair (1), but also to construct better optical radical sensors (10-12).

Depending on the particular chromophore-nitroxide pair under examination, as many as four mechanisms may contribute to the singlet state quenching (1). These mechanisms include electron exchange induced intersystem crossing (or internal conversion), energy transfer by electron exchange (Dexter mechanism), resonance energy transfer (Förster mechanism) and electron transfer. We previously reported the results of an extensive photophysical study on the intramolecular quenching of fluorescence in a series of covalently-linked nitroxide-naphthalene adducts (1). Based on the very weak solvent dependence of the intramolecular quenching rate constants, as well as on other factors, we concluded that the quenching arose primarily from an enhanced rate of intersystem crossing induced by electron exchange. However, more recent time-resolved

absorption measurements clearly indicate that the quenching in some of these compounds is more complicated than originally thought, and is composed of at least two solvent-dependent mechanisms which compensate to produce intramolecular quenching rate constants that vary only weakly with solvent polarity (16). These results clearly illustrate the need to examine a more diverse suite of compounds under a variety of solution conditions in order to gain a better understanding of the factors that control the intramolecular quenching of excited singlet states by nitroxides.

Here we extend our previous investigations to explore intramolecular singlet state quenching in a series of fluorescamine-nitroxide compounds (Fig. 1) by both time-resolved absorption and fluorescence measurements. Our choice of this particular series was motivated not only by our interest in expanding the available data on intramolecular quenching by nitroxides, but also by their recent use as highly sensitive optical probes for detecting radicals produced in aqueous systems (11,12) and by cells (15).

Experimental

Chemicals. Boric acid, sodium hydroxide, 4-(amino)-2,2,6,6-tetramethyl-1-piperidinyloxy free radical (4-at), 3-(aminomethyl)-2,2,5,5-tetramethyl-1-pyrrolidinyloxy free radical (3-amp), 4-hydroxy-2,2,6,6-tetramethyl-1-piperdinyloxy free radical (4-ht), and 3-carbamoyl-2,2,5,5-tetramethyl-1-pyrrolidinyloxy free radical (3-cp) were purchased from Aldrich. Distilled-in-glass grade diethyl ether was from Burdick & Jackson. 3-(amino)-2,2,5,5-tetramethyl-1-pyrrolidinyloxy free radical (3-ap) was obtained from Kodak and 4-phenylspiro [furan-2(3H), 1'-phthalan]-3,3'dione (fluorescamine) from Sigma. High performance liquid chromatography (HPLC) grade solvents were purchased from Aldrich and Sigma and used without further purification. Water used in all experiments was from a Millipore Milli-Q system. Standard buffer was 0.2 M, pH 8.1 borate.

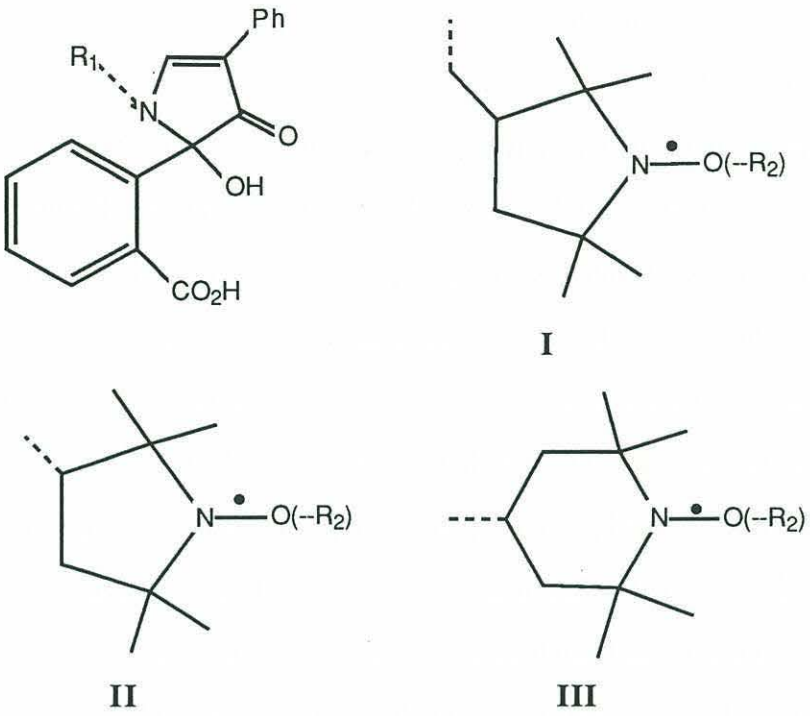

1a: R_1 = I; R_2 = —, parent nitroxide
1b: R_1 = I; R_2 = $COCH_3$
1c: R_1 = I; R_2 = $CH(CH_3)_2$
2a: R_1 = II; R_2 = —, parent nitroxide
2b: R_1 = II; R_2 = $COCH_3$
3a: R_1 = III; R_2 = —, parent nitroxide
3b: R_1 = III; R_2 = $COCH_3$
3c: R_1 = III; R_2 = $CH(CH_3)_2$

Figure 1. Fluorescamine derivatives examined in this study.

Preparation of compounds.

Syntheses of **1-3a**

The syntheses of **1-3a** employed procedures similar to that described by Bernardo et al. (17) for preparing the ethylamine adduct of fluorescamine. Equimolar amounts (~1 millimole) of fluorescamine and the appropriate amino-nitroxide dissolved in 15 and 6.5 mL of acetonitrile, respectively, were combined and let sit for 15 min in the dark. The reaction mix was placed on ice and its volume slowly reduced to ~5 mL by flushing with argon (Ar), and then placed overnight in a freezer at - 20 ^{o}C. The yellow, crystalline precipitate was collected by centrifugation using a table-top centrifuge, dried under Ar, and then washed three times with 5 mL of diethyl ether. In the preparation of **1a**, additional product was precipitated from the supernatent by the addition of 5 mL of water. The product was collected by centrifugation, dried and washed with ether as described above.

The purity of the products was checked by HPLC using equipment and procedures previously described (11,12) and employing both an absorption and fluorescence detector connected in series. The absorption detector was set to 390 nm (absorption maximum; Fig.2), while the excitation and emission wavelengths of the fluorescence detector were set to 390 and 490 nm, respectively (both with a 15 nm band-pass) (Fig. 2). Chromatograms acquired using absorption detection exhibited a major band corresponding to **1-3a** (≥90%) and a minor band (≤10 %) tentatively assigned to the lactone of **1-3a** based on the complete lack of fluorescence from this species (18). In contrast, chromatograms acquired with fluorescence detection revealed a number of other components that were comparable in magnitude to the very low fluorescence exhibited by **1-3a**; of these other components, only the one-electron reduction product of **1-3a**, the hydroxylamine, was clearly identified. These components, which represent minor contaminants with high fluorescence quantum yields (and long fluorescence lifetimes), did not seriously affect the time-resolved fluorescence measurements because of their small contribution to the total decay. Thus, as expected, time-resolved fluorescence measurements of **1-3a** showed a dominant

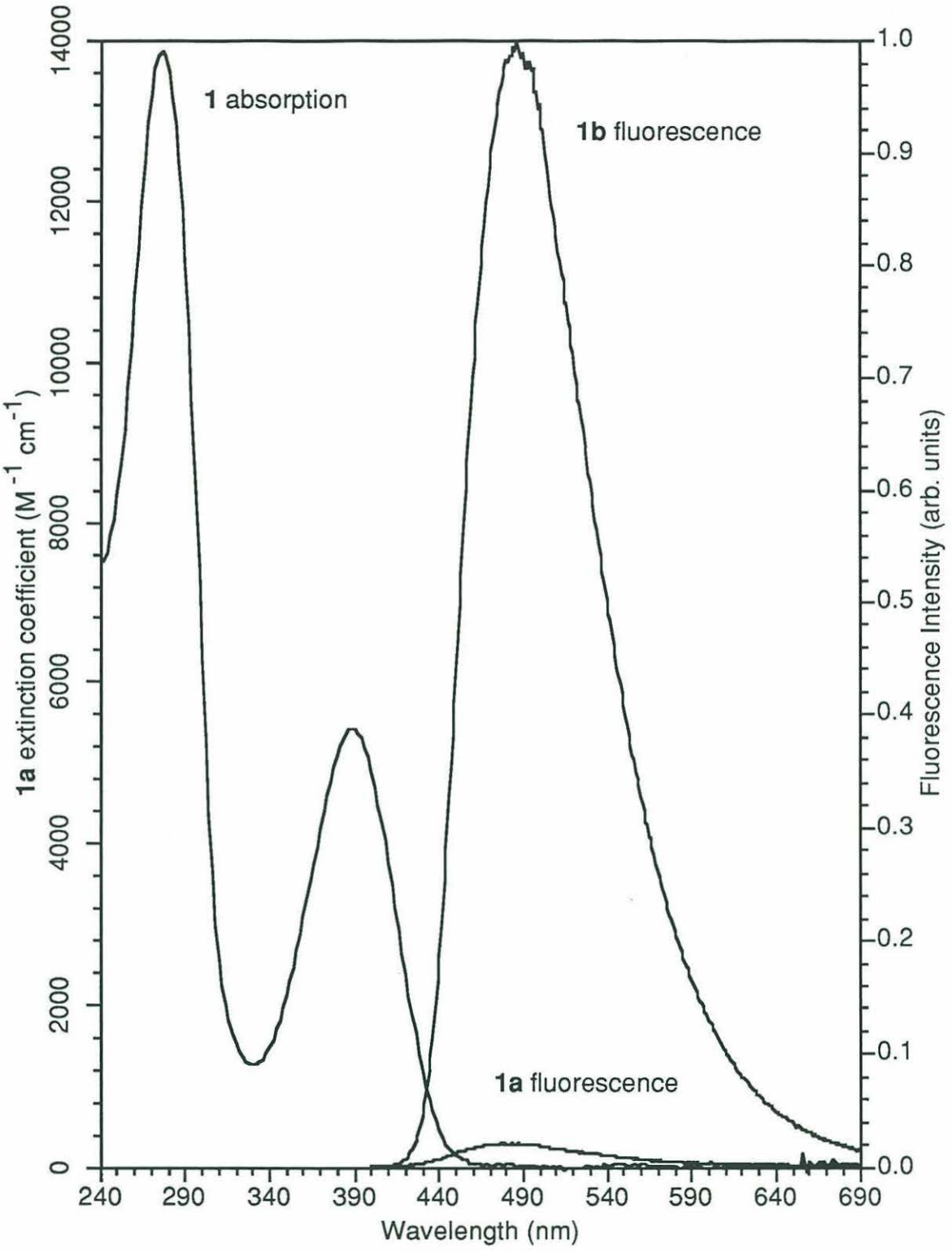

Figure 2. Absorbance and fluorescence spectra of **1a** and **1b** in standard buffer.

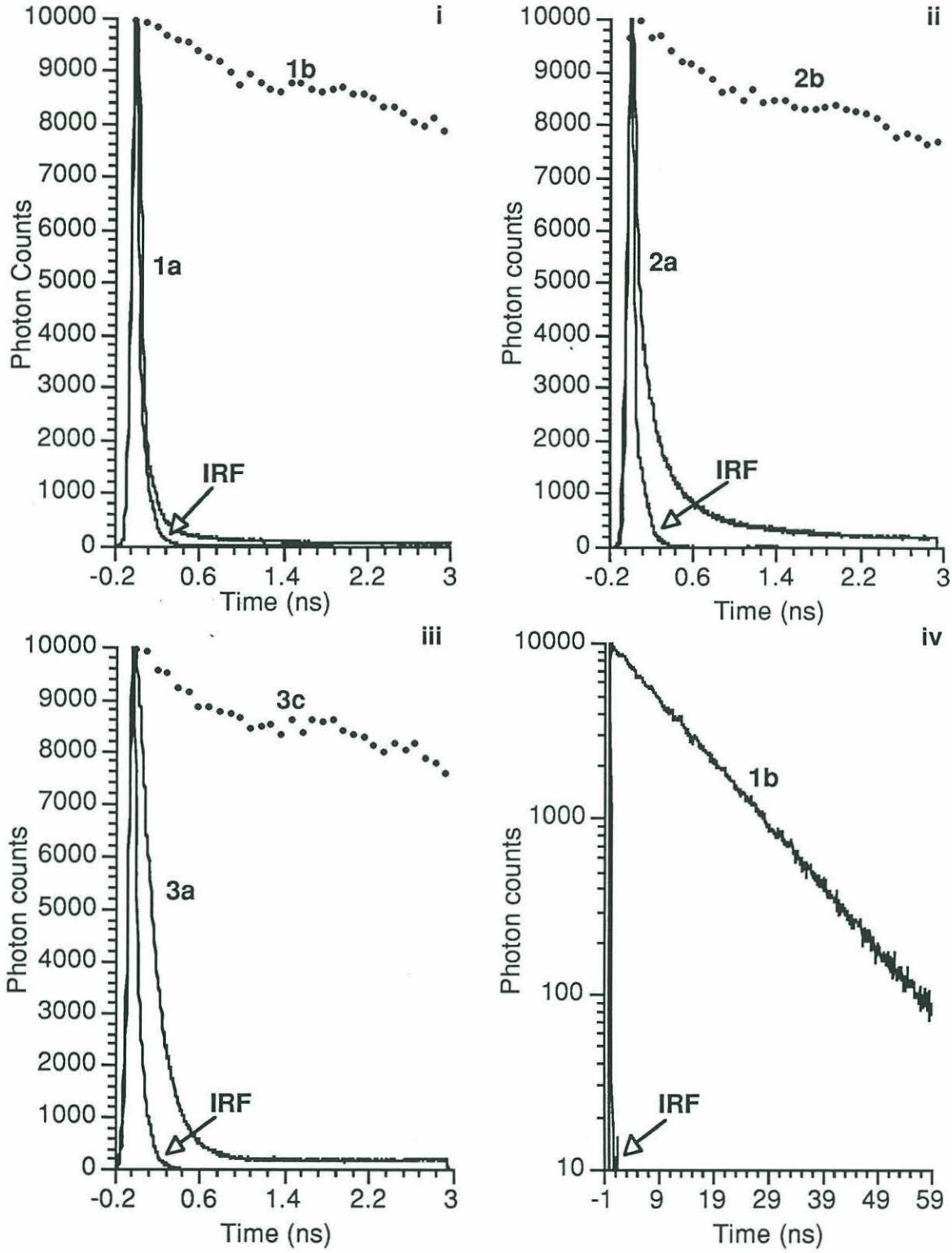

Figure 3. Fluorescence decays of nitroxide adducts (**1-3a**) and diamagnetic analogues (**1-2b, 3c**) in acetonitrile along with the instrument response function (IRF). (i) - (iii) are on a linear scale and a 3 ns timebase, (iv) is on a log scale and a 60 ns time base.

short-lived component (92-98 %; Fig. 3). Unfortunately, these minor contaminants did grossly interfere with determinations of fluorescence quantum yields and required us to purify **1-3a** further by HPLC immediately prior to the quantum yield measurements (vide infra).

For the determination of fluorescence quantum yields, **1-3a** were generated and purified by HPLC immediately prior to measurement. Approximately 4 to 9 mL of 1 mM amino-nitroxide in standard buffer was derivatized with a 2-fold molar excess of fluorescamine solution (1-4 mL of 5 mM in acetonitrile) in Teflon vials. The reaction time was less than 1 minute at room temperature and pH 8.1. Compounds were immediately purified by HPLC using procedures described previously (12,13), employing 1-4 enrichment columns (Upchurch Guard Column, 2 mm ID x 2 cm) within the injection loop. These columns were loaded with material from a Waters C_{18} Sep-Pak and allowed injections of up to 6 mL per run. Compounds **1-3a,** eluting after 12-13 minutes, were collected in Teflon vials and immediately diluted into other solvents for quantum yield determinations.

Syntheses of O-alkoxyamines

These compounds were produced photochemically by irradiating a 1 mM solution of 3-methyl-2-butanone in standard buffer containing 0.5 mM of an amino-nitroxide. Solutions were prepared in a 10 cm quartz cell and deoxygenated for 5 minutes with nitrogen (99.999% purity, Union Carbide) that had been passed through an oxygen trap (Alltech). Samples were irradiated with a broadband xenon lamp (300 W, Varian Model PS300-1), with the beam first passed through 22 cm of water and a pyrex filter (50% transmission at 290 nm). Samples were continuously purged with nitrogen during sample irradiations of between 60 and 90 min. The resulting alkoxyamines were derivatized with fluorescamine and purified by HPLC as described above. Compounds **1-3b** eluted at 15-

16 minutes and **1,3c** at 23-24 minutes. The compounds were collected and extracted with 1 mL of chloroform. The chloroform extracts were then washed three times with 5 mL aliquots of water, transferred to clean glass vials, and evaporated to yellow oils under nitrogen. The compounds were stored at -20 ^{o}C until needed. HPLC elution times matched those expected for these compounds (11,12). The mass spectra of these compounds (as the lactone form) were identical with those observed previously (13) and the structures were confirmed by high resolution mass spectrometry employing a VG Autospec Q and a desorption chemical ionization probe operated in the electron impact mode (50 keV): M^+ calcd for **1b** ($C_{28}H_{30}N_2O_5$) 474.2155, found 474.2143; M^+ calcd for **1c** ($C_{29}H_{34}N_2O_4$) 474.2518, found 474.2539; M^+ calcd for **2b** ($C_{27}H_{28}N_2O_5$) 460.1998, found 460.1998; M^+ calcd for **3b** ($C_{28}H_{30}N_2O_5$) 474.2155, found 474.2152; M^+calcd for **3c** ($C_{29}H_{34}N_2O_4$) 474.2518, found 474.2520.

Optical Measurements.

Absorption and Fluorescence Spectra and Fluorescence Quantum Yields

Absorption spectra were collected with a Hewlett-Packard 8451 A diode array spectrophotometer (2 nm resolution), while fluorescence spectra were recorded with a SLM-Aminco SPF-500C or an Aminco-Bowman 2 Luminescence spectrometer employing either 2/2 (**1-3b,c**) or 4 /4 (**1-3a**) nm excitation/emission bandpasses. Absorption and fluorescence spectra of **1-3a** were collected immediately following HPLC purification and dilution of 1-100 µl of the compound contained in HPLC mobile phase (64% methanol/36% pH 4 acetate buffer) into ~3 mL of the appropriate solvent. Solutions of **1-3b,c** were prepared by dissolving the oils in a small volume of dioxane (1-100 µl), which was then diluted into ~15 mL of the appropriate solvent. All spectra were recorded at room temperature. Quantum yields were determined relative to quinine sulphate as previously described (1).

Time Resolved Measurements

Solutions of **1-3a** were prepared by dissolving a small quantity of the solid in solvent or by diluting material synthesized immediately prior to the lifetime experiments as described above. Solutions of **1-3b,c** were prepared as in the steady-state measurements. The absorbance of solutions prepared for fluorescence lifetime measurements were between 0.1-0.2 O.D. at 290 nm and those for absorbance measurements ~1 O.D. at 266 nm (1 cm cell) as measured on a Hewlett-Packard 8450A diode array spectrophotometer.

Fluorescence lifetimes were measured by time-correlated single-photon counting, on an instrument at the Center for Fast Kinetic Research (Austin, TX). This system is described in detail elsewhere(19). Briefly, excitation was provided by a cavity-dumped tunable dye laser, synchronously pumped with the second harmonic of a mode-locked Nd-YAG (Coherent, Antares). The dye pulses (6 ps fwhm, 1.8 MHz) were frequency doubled with a KDP crystal to 290 nm. Fluorescence was collected at 90° and focused into a monochrometer tuned to 490 nm; entrance and exit slits were adjusted to obtain a counting rate of 4000-5000 photons per second impinging on the photomultiplier tube (PMT).

An Ortec 457 time-amplitude converter (TAC) received start pulses directly from the cavity dumper and stop pulses from the PMT. The TAC signal was passed to a multichannel analyzer and the data were saved in an IBM compatible computer for analysis, storage, and hardcopy. The decay curves were fit to 1-3 exponentials with iterative deconvolution software based on algorithms developed by O'Conner (20) and written in ASYST language by Paul Snowden at CFKR. The instrumental response limit for this system is ~20 ps.

Time resolved absorption measurements were performed with a conventional flash photolysis apparatus located at the Center for Fast Kinetic Research. This system employed the quadrupled output of a Quantel YG402 laser as the excitation source (266 nm). A 150 W xenon arc lamp, pulsed to high intensity during an experiment, served as the monitoring light source. The light from this source was passed through the 1 cm

sample cuvette and focused on the entrance slit of a SPEX monochromator. Transient absorption signals were detected with a Hamamatsu 928 phototube, captured with a Tektronix SCD 1000 transient digitizer, and passed to an IBM clone for analysis using software written by Paul Snowden (CFKR) in ASYST language. The instrumental response limit for this system is ~10 ns.

Energy Minimization. The molecular structures of **1-3a** were minimized using Nemesis 1.1, a 3-dimensional molecular modeling program running under the MicroSoft Windows GUI. The Nemesis program uses the COmputation and Structure Manipulation In Chemisty (COSMIC) algorithm (21) to supply the force field for energy calculations and the conjugate gradient optimiser used for structure optimization in energy calculations. Minimization was complete when either the difference in energy between successive iterations was less than 10^{-4} kcal/mol or the sum of the squares of the gradient vector comonents fell below 10^{-10} $kcal^2/mol^2/Å^2$. First the molecular fragment structures (fluorescamine, 3-amp, 4-at, and 3-ap) were entered into the program and the 3-dimensional structure was optimized for minimum electrostatic and van der Waals energy. Next, the three radicals, 3-amp, 4-at, and 3-ap were attached to the fluorescamine and the energy was again minimized. To search for local minima, the bonds between the radicals and the fluorescamine were rotated with 1 to 15° steps with new molecular energy calculated at each step, giving a plot of molecular energy vs. torsion angle. For compounds **2a** and **3a** rotation is only possible about the bond joining the nitroxide ring to the fluorescamine compound (N-R1 in Fig. 1). For compound **1a** two rotations are possible, both in the linkage between the nitroxide ring and the fluorescamine compound so a two-fold rotation was performed, resulting in a two-dimensional contour plot. Note that the molecular structure was not optimized at each step during the rotation. From the rotation results, each molecule was artificially rotated to the second deepest energy well and

minimized again. To keep the energy minimization from jumping back to the first minimum, other bonds were rotated to trap the process in the secondary well.

For **1-3a**, the fluorescamine to N-O radical nitrogen-nitrogen distance was calculated, as well as the angle between the planes of the five-membered fluorescamine ring and the radical ring (Fig. 1). Ring planes were defined by the nitrogen atoms and their adjacent ring carbons. The angle between the two ring planes was calculated from the atomic coordinants from the Nemesis minimized structures using a Matlab subroutine.

Results

Absorption and Fluorescence Spectra.

As observed previously for naphthalene-nitroxide adducts (1), the absorption spectra of **1-3a** were well described as a simple sum of the individual absorption contributions of the fluorescamine and nitroxide moieties. No obviously new transitions that could arise from strong electronic coupling between the chromophores were evident. The fluorescamine moiety exhibited absorption maxima at 272 and 392 nm, and an emission maximum at ~488 nm (Table I). While the emission maximum showed a weak

Table I: Fluorescamine and Nitroxide Spectral Characteristics[a]

	Singlet Energy (eV)	Fluorescence Peak Max (nm)	Absorbance Peak Max (nm) [Extinction Coefficient ($M^{-1}cm^{-1}$)]		
Solvent	fluorescamine	fluorescamine	fluorescamine	3-cp	4-ht
Buffer	2.82	492	386	398 [7.35]	430 [13.11]
Acetonitrile	2.84	486	386	426 [5.58]	466 [9.95]
Methanol	2.87	483	385	414 [6.83]	448 [10.73]
Dioxane	2.86	485	384	430 [4.62]	468 [11.13]

[a] Also see Fig. 4.

dependence on solvent polarity, the absorption maxima varied little. In contrast, the low energy absorption band ($n \rightarrow \pi^*$) of both the piperidinyl (4-ht) and pyrrolidinyl (3-cp)

nitroxides underwent significant blue shifts with increasing solvent polarity, with the pyrrolidinyl nitroxide always exhibiting the higher transition energy (Table I). The possible influence of these differences on the intramolecular quenching is discussed below.

Although the fluorescence yields were substantially smaller for **1-3a** (vide infra), the emission line shape and wavelength maximum were identical to those of the diamagnetic compounds, and exhibited the same dependence on solvent polarity. These results indicate that the remaining emission from **1-3a** originates from the locally excited singlet state of the fluorescamine moiety, consistent with results obtained previously with other adducts (1).

Fluorescence Quantum Yield Measurements. Very different fluorescence quantum yields were obtained for diamagnetic and paramagnetic compounds. Diamagnetic compounds (**1-3b,c**) exhibited a weak solvent effect of decreasing quantum yield with increasing polarity (Table II).

Table II: Quantum Yields of **1-3**

Compound	Buffer	Methanol	Dioxane
1a	0.0013	0.00081	0.00066
1b	0.095	0.13	0.13
1c	0.085	0.14	0.17
2a	0.00046	0.00023	0.00050
2b	0.097	0.17	0.17
3a	0.015	0.045	0.0055
3b	0.060	0.18	0.21
3c	0.060	0.21	0.21

Measurements showed 5-20% variation.

Results for **1-3b** and **1,3c** were nearly identical in magnitude, demonstrating that the quantum yield of these compounds is insensitive to the type of substituent group (acetyl or isopropyl). In contrast, quantum yields for the paramagnetic compounds (**1-3a**) were tens to hundreds of times smaller than the diamagnetic ones in agreement with previous results from our laboratory (12). Larger differences between paramagnetic and diamagnetic

quantum yields exist for **1, 2** than for **3**. The ratios for **1a** differ from those for **2a** somewhat as they are subject to some variations due to trace amounts of diamagnetic impurities which have much higher quantum yields. Even with this uncertainty, **3a** quantum yields are clearly higher than those for **1-2a**. A previous study has shown that quantum yields for amines coupled to fluorescamine fall between 0.09 and 0.34 with ethanol as the solvent (17), and our values for the diamagnetic species (**1-3b,c**) are within this range.

Lifetime Measurements and Quenching Rate Constants. As expected, the differences between the paramagnetic and diamagnetic fluorescence lifetimes reflect those evident in the quantum yields. Diamagnetic compounds show a substantial increase in lifetimes from water to less polar solvents (Table III).

Table III: Fluorescence Lifetimes of **1-3**

	lifetime (ns)[a]				
	buffer	acetonitrile	methanol	dioxane	cyclohexane
1a	0.029[b] (96%)[d]	≤0.019[b] (98%)[d]	≤0.020[b] (99%)[d]	0.031[b] (92%)[d]	[c]
1b	3.6 (100%)	12.1 (100%)	12.1 (62%), 2.2 (38%)	11.1 (55%), 1.1 (45%)	9.3 (72%), 1.8 (28%)
1c	3.7 (100%)	12.2 (100%)	9.6 (55%), 1.6 (45%)	11.3 (54%), 0.75 (46%)	9.9 (57%), 0.88 (43%)
2a	0.020[b] (96%)[d]	0.025[b] (91%)[d]	0.027[b] (76%), 0.39 (12%), 3.7 (12%)	0.029[b] (62%), 0.48 (22%), 23.4 (16%)	[c]
2b	4.6 (100%)	13.6 (100%)	11.9 (47%), 3.3 (53%)	12.1 (62%), 0.95 (38%)	11.1 (100%)
3a	0.12 (84%), 1.3 (16%)	0.059 (43%), 0.18 (57%)	0.054 (37%), 0.20 (59%)[d]	0.042 (43%), 0.22 (57%)	[c]
3b	1.99 (100%)	13.0 (100%)	11.5 (48%), 3.3 (52%)	11.7 (64%), 1.4 (36%)	9.3 (78%), 1.2 (22%)
3c	1.95 (100%)	13.5 (100%)	11.9 (71%), 1.7 (29%)	11.6 (55%), 0.80 (45%)	8.9 (51%), 2.0 (49%)

[a] Fitting program showed ~10% variation for **1-3a** and ~1% variation for **1-3b** and **1,3c**. All Chi^2 values were <6 for **1-3b** and **1,3c** and <3 for **1-3a**; most Chi^2 values were ~2 [b]Close to instrument time resolution. [c] Not soluble enough to measure. [d]Total is less than 100% due to diamagnetic impurities.

Values for **1-3b** and **1-3c** were again very similar. In acetonitrile and buffer all of the diamagnetic compounds were well-fit to a single exponential decay. However, in dioxane, methanol and cyclohexane two exponentials were needed for a similar fit. In all cases, the fluorescence decay was dominated by the longer lived component . Paramagnetic

compounds exhibited appreciably shorter fluorescence lifetimes than did the diamagnetic ones (Fig. 3) in ratios nearly identical to those for the quantum yields when corrections were made for diamagnetic impurities (percentages shown in Table III). As the lifetimes of **1,2a** were close to the time resolution of the instrument, differences between the two compounds and their solvent dependencies were not quantifiable. In contrast, lifetimes of **3a** were significantly longer (Fig. 3) and well above the time resolution of the instrument. However, decay kinetics for **3a** were more complicated, resulting in two measurable lifetimes.

When the fluorescence decays of **1-3a** were measured on longer timescales (50 - 90 ns), the lifetime of the longest lived component agreed closely with those of the corresponding diamagnetic compounds in a given solvent, indicating the presence of a small amount of diamagnetic contaminant. The diamagnetic fluorescence lifetimes of 9.6 to 12.1 ns in methanol and 2 to 4.6 ns in water are longer than those found by DeBernardo et al. (17) (3.3 ns in methanol and 1.7 ns in water). However, in methanol, the short-lived components [1.6 to 3.3 ns (12 to 52%)] agree well with their values.

Quenching rate constants, k_q, were calculated from the lifetime data (1)

$$k_q = \frac{1}{\tau_p} - \frac{1}{\tau_d} \quad (ns^{-1}) \qquad (1)$$

where τ is the lifetime of the paramagnetic (p) and diamagnetic (d) nitroxide compounds (Table IV). In the case of **3a** where more than one lifetime was measured, an average quenching rate constant, k_{qave}, was calculated (2)

$$k_{qave} = \frac{1}{(\tau_{p_1} c_{p_1} + \tau_{p_2} c_{p_2})} - \frac{1}{(\tau_{d_1} c_{d_1} + \tau_{d_2} c_{d_2})} \quad (ns^{-1}) \qquad (2)$$

where c is the percent contribution. The resulting quenching rates are very rapid and exhibit the same trends as the fluorescence lifetimes that they are calculated from. Again, values for compounds **1** and **2** (3-5 x 10^{10} s^{-1}) were significantly greater than those for **3** (3-8 x 10^9 s^{-1}).

Table IV: Quenching Rate Constants, k_q (x 10^{-9} s^{-1})

compound	buffer	acetonitrile	methanol	dioxane
1	≥ 34	≥ 53	≥ 50	≥ 32
2	≥ 50	≥ 40	≥ 37	≥ 34
3 ave	3.24	7.81	7.25	6.97
3 short	7.83	16.9	18.4	23.7
3 long	0.77	5.48	4.91	4.46

Time Resolved Absorbance. Time resolved absorbance measurements between 350 and 700 nm on diamagnetic compounds showed no evidence of absorption transients. Thus either i) intersystem crossing from the excited singlet state to the triplet is slow with respect to internal conversion, or ii) the extinction coefficient for the triplet state is extremely small. Unfortunately, no low temperature phosphorescence measurements or room-temperature triplet sensitization experiments have been performed to ascertain the triplet energy, extinction coefficient and decay rate to the ground state. However, triplet states are observable in the corresponding naphthalene-nitroxide compounds which supports i) above (16). Measurements of paramagnetic compounds also showed no evidence of any absorption transients, either triplet states or radical ions, despite the substantial quenching of the singlet state.

Energy Minimization. Energy minimized N(nitroxide)-N(fluorescamine) distances for **1-3a** varied in the manner expected with the largest being for **1a** where there are two carbon atoms in the connection between the nitroxide ring and the fluorescamine moiety, the next longest being for **3a** which contains a piperidinyl (six-member) instead of a pyrrolidinyl (five-member) nitroxide ring (Table V, Fig. 1).

Table V: Geometry Parameters from Nemesis 1.1

compound	N-N Distance (Å)	Angle[a]
1a	4.7	99.8°
2a	3.6	89.5°
3a	4.3	100.5°

[a]Angle between the planes of the five-membered fluorescamine ring and the radical ring (Fig. 1)

The angles between the plane of the nitroxide moiety in the ring and that of the fluorescamine chromophore were relatively constant for **1-3a**. All of the values were close to 90°, implying that the π orbital of the nitroxide nitrogen is almost perpendicular the π system on the five-membered ring of the fluorescamine. In addition to the global minimum, a secondary minimum was found corresponding to a ~180° rotation about the fluorophore-nitroxide bond(s) which is consistent with the steric factors in the geometry of these molecules. The absence of large variations in N-N distances and ring plane angles suggest that all of the compounds have similar ground state geometries.

Discussion

As discussed previously (1), a number of different singlet state quenching mechanisms are possible for nitroxide-fluorophore adducts. These include Förster (dipole-dipole) and Dexter (electron exchange) energy transfer, charge (or electron) transfer, electron exchange induced intersystem crossing and electron exchange induced internal conversion. Förster and Dexter energy transfer rates are proportional to their overlap integrals, J_F and J_D respectively (3,4)

$$J_F = \frac{\int_0^\infty F(\lambda)\varepsilon(\lambda)\lambda^4 d\lambda}{\int_0^\infty F(\lambda)d\lambda} \qquad (3)$$

$$J_D = \frac{\int_0^\infty F(\lambda)\varepsilon(\lambda)d\lambda}{\int_0^\infty F(\lambda)d\lambda \int_0^\infty \varepsilon(\lambda)d\lambda} \qquad (4)$$

where $F(\lambda)$ is the corrected fluorescence intensity of the fluorophore and $\varepsilon(\lambda)$ is the extinction coefficient of the acceptor (3-cp or 4-ht) at wavelength λ. Overlap integrals were calculated in the same manner as described previously (1) and it was found that J_F and J_D were larger for compounds **3b,c** than for compounds **1b,c** and **2b** (Table VI, Fig. 4).

Table VI: Dexter and Förster Overlap Integrals

comp	Dexter Integrals (cm)			Förster Integrals ($M^{-1}cm^3$)		
ound	buffer	methanol	dioxane	buffer	methanol	dioxane
1b,c	1.01×10^{-3}	2.18×10^{-3}	3.64×10^{-3}	3.58×10^{-18}	7.07×10^{-18}	8.96×10^{-18}
2b,c	1.08×10^{-3}	2.36×10^{-3}	3.74×10^{-3}	3.74×10^{-18}	7.50×10^{-18}	9.13×10^{-18}
3b,c	3.03×10^{-3}	4.71×10^{-3}	5.44×10^{-3}	2.37×10^{-17}	3.37×10^{-17}	4.23×10^{-17}

Better overlap should lead to more efficient quenching and shorter fluorescence lifetimes if either the Förster or Dexter mechanisms were operational. However, this prediction contradicts the lifetime data where **3a** is noticeably slower than **1a** and **2a** (Table III).

Förster transfer rates were calculated using (5)

$$k_{FT} = \frac{J_F \kappa^2 \phi_d}{R^6 \eta^4 t_d} 8.71 \times 10^{23} \qquad (5)$$

where κ^2 is the orientation factor (assumed to be 2/3), ϕ_d and τ_d are the quantum yield (Table II) and lifetime (Table III), respectively of the appropriate diamagnetic derivative, R is the donor-acceptor distance (Table V), and η is the solvent refractive index. The resulting lifetimes (Table VII) are much slower (108 to 670 ns) than those observed for compounds **1-2a** although for **3a** the values are close (42 to 53 ns) to the shorter lifetimes observed (42 to 54).

Table VII: Förster Transfer Rates, k_F ($\times 10^{-9}$ s^{-1})

compound	buffer	methanol	dioxane
1a	1.5	1.5	1.6
2a	6.7	9.3	8.5
3a	24	19	20

Sensitivity analysis shows that these values could be off by up to a factor of 5 if κ^2 is allowed vary from 0 to 4, although the actual value is close to 0 as κ^2 approaches 0 as the angle between the donor and acceptor plane approaches 90°, which is in the range of those calculated (Table V). Differences are not likely due to geometry as energy minimized N-N distances and the angles between the nitroxide radical plane and the fluorophore plane were

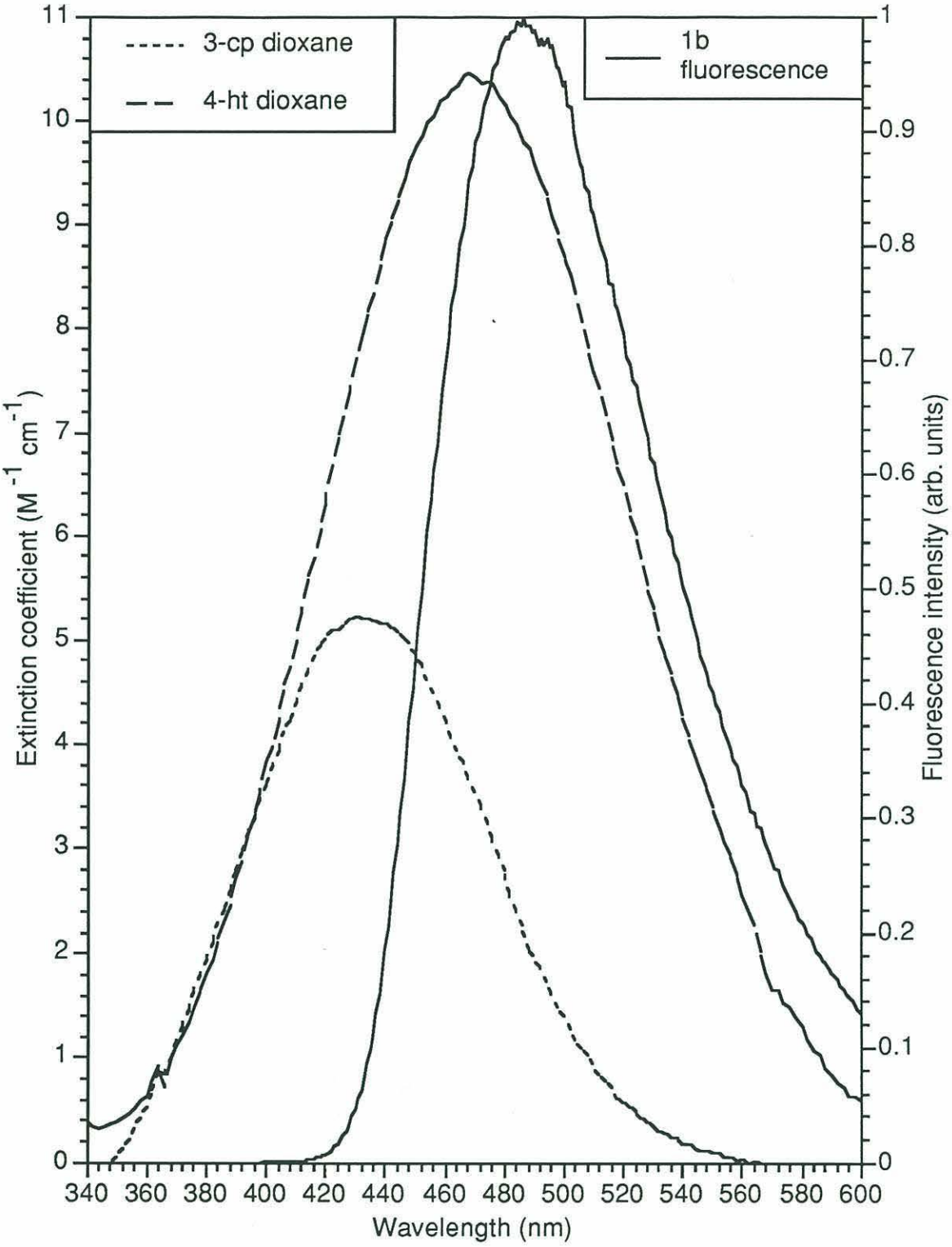

Figure 4. Absorption spectra of 3-cp and 4-ht in dioxane. Fluorescence emission spectrum of **1b** in standard buffer is included in order to illustrate the degree of spectral overlap between fluorescamine emission and nitroxide absorption.

similar for all three compounds (Table IV). The absorption dipole for the nitroxide group is perpendicular to the NO bond, lying in the CNC plane as discussed previously (1), and is perpendicular to the transition moment of the fluorophore which should lie in the plane of the 5-membered ring of the fluorescamine moiety. This geometry results in an unfavorable κ^2 value for Förster transfer. Further, while overlap integrals increase from buffer to the less polar solvents for both Dexter and Förster mechanisms, values of k_q do not change by the same magnitude as the overlap integrals do. Thus we attribute these solvent effects to the inherent photophysics of the molecule and not to the result of Förster or Dexter energy transfer as a singlet state quenching mechanism.

Although we do not have one electron reduction and oxidation potentials for fluorescamine and therefore can not calculate the thermodynamic driving forces for charge transfer, we saw no evidence for the formation of radical ions in time resolved absorbance measurements, making charge (electron) transfer less likely as a dominant quenching route.

No evidence for the formation of triplet states was obtained by time-resolved absorption measurements. Until triplet sensitization experiments are performed, we cannot exclude the possibilities that our inabiliby to observe these species is due to an extremely small triplet extinction coefficient or alternatively that the triplet decays more rapidly than the time resolution of the measurements (~10 ns). However for naphthalene-nitroxide compounds the triplet to ground intersystem crossing rate is about two orders of magnitude slower than the singlet intramolecular quenching rate and their extinction coefficients are not unusually small (16). Thus we believe that the possibility of excited singlet quenching via enhanced intersystem crossing is less likely.

The remaining quenching mechanism is enhanced internal conversion from the excited singlet to the ground state. While it is not clear how the unpaired electron in the nitroxide radical could directly enhance this process, this mechanism has been suggested by other experimenters (2,5).

Conclusions. For all of the compounds studied, steady-state absorbance and fluorescence spectra were identical with those of the parent fluorophore. There was no evidence for charge transfer processes. This resulted in a decrease in fluorescence lifetime and quantum yields of tens to hundreds-fold for the paramagnetic compounds over their diamagnetic counterparts. Very rapid quenching rates (3-5 x 10^{10} s^{-1} for **1-2a** and 3-8 x 10^{9} s^{-1} for **3a**) were calculated for the paramagnetic fluorescamine-nitroxide compounds in a variety of solvents. Calculated energy minimized geometries were very similar for all compounds which implies that geometric differences are not responsible for the variations found in fluorescence lifetimes and quantum yields between compounds. Calculated Förster and Dexter overlap integrals do not support deexcitation by these mechanisms. Time-resolved absorbance measurements resulted in no evidence for transient species due to either intersystem crossing to the triplet state or charge transfer. Of the mechanisms considered for singlet state quenching, we have ruled out Förster and Dexter energy transfer, and deem charge transfer and intersystem crossing to the triplet state less likely, but cannot rule them out without additional experiments. The remaining mechanism, direct internal conversion to the ground state, appears to be the most likely explaination of the data.

Acknowledgments. Special thanks to Armando Herbelin at Western Washington University for molecular modeling work, Carl Johnson for high resolution mass spectrometry results and Steve Atherton and Don O'Connor for assistance at CFKR. This work was supported by the Office of Naval Research under ONR Contract #N00014-91-J-1260 and the National Institute of Health under contract #1R01GM44966-01A1. Partial support for S. E. Herbelin was provided by a National Science Foundation graduate research fellowship. The time-resolved experiments and analyses of the data produced were performed at the Center for Fast Kinetics Research, which is supported jointly by the

Biomedical Research Technology Program of the Division of Research Resources of the National Institutes of Health (RR00886) and by the University of Texas at Austin.

References

(1) Green, S. A.; Simpson, D. J.; Zhou, G.; Ho, P. S.; Blough, N. V. *J. Am. Chem. Soc.* **1990**, *122*, 7337-7346.

(2) Karpiuk, J. and Grabowski, Z. R. *Chem. Phys. Let.* **1989**, *160*, 451-456.

(3) Chattopadhyay, S. K.; Das, P. K.; Hug, G. L. *J. Am. Chem.Soc.* **1983**, *105*, 6205-6210.

(4) Yee, W. A.; Kuzmin, V. A.; Kliger, D. S.; Hammond, G. S.; Twarowski, A. J. *J. Am. Chem. Soc.* **1979**, *101*, 5104-5106.

(5) Green, J. A.; Singer, L. A.; Parks, J. H. *J. Chem. Phys.* **1973**, *58*, 2690-2695.

(6) London, E. *Molec. Cell. Biochem.* **1982**, *45*, 181-188 and references cited therein.

(7) Yeager, M. D. and Feigenson, G. W. *Biochem.* **1990**, *29*, 4380-4392.

(8) Matko, J.; Ohki, K.; Edidin, M. *Biochem.* **1992**, *31*, 703-711.

(9) Abrams, F. S. and London, E. *Biochem.* **1992**, *31*, 5312-5322.

(10) Blough, N. V.; Simpson D. J. *J. Am. Chem. Soc.* **1988**, *110*, 1915-1917.

(11) Kieber, D. J.; Blough, N. V. *Free Rad. Res. Comm.* **1990**, *10*, 109-117.

(12) Kieber, D. J.; Blough, N. V. *Anal. Chem.* **1990**, *62*, 2275-2283.

(13) Kieber, D. J.; Johnson, C. G.; Blough, N. V. *Free Rad. Res. Comm.* **1992**, *16*, 35-39.

(14) Blough, N. V. and Zepp, R. G. in *Active Oxygen: Reactive Oxygen Species in Chemistry* (eds. C.S. Foote, J. S. Valentine, A. Greenberg and J. Liebman) Chapman and Hall, New York, Chapter 8, in press.

(15) Pou, S.; Huang, Y.; Bhan, A.; Bhadti, V. S.; Hosmane, R. S.; Wu, S. Y.; Cao, G.; Rosen, G. M. *Anal. Biochem.* **1993**, *212*, 85-90.

(16) Blough, N. V., unpublished observations.

(17) De Bernardo, S.; Weigele, M.; Toome, V; Manhart, K; Leimgruber, W.; Bohlen, P.; Stein, S.; Udenfriend, S. *Arch. Biochem. Biophys.* **1974**, *163*, 390.

(18) Weigele, M.; Blount, J. F.; Tengi, J. P.; Czajkowski, R. C.; Leimgruber, W. *J. Am. Chem. Soc.* **1972**, *94*, 4052-4.

(19) Chandler, R. R.; Coffer, J. L.; Atherton, S. J.; Snowden, P. T. *J. Phys. Chem.* **1992**, *96*, 2713.

(20) O'Conner, D. V.*Time Correlated Single Photon Counting*, Academic Press: Orlando, **1984**.

(21) Vinter, J. G.; Davies, A.; Saunders, M. R. *J. Comput.-Aided Mol. Design*, **1987**, *1*, 31-51.

(22) Turro, N. J. *Modern Molecular Photochemistry*; University Science Books: Mill Valley, **1991**.

Appendix I: Investigation Into the Use of a Stable Nitroxide Radical as a Secondary Trap for Hydroxyl Radicals Generated in Sea Water

Introduction

The hydroxyl radical has been termed the "most reactive, photochemically produced free radical in the environment" (Mopper and Zhou, 1990) and is believed to be an important photooxidant in natural waters. The production and consumption mechanisms for hydroxyl radical in natural waters have recently been reviewed by Blough and Zepp (in press) and Blough (submitted). Among those most studied are the direct photolysis of nitrate and nitrite (1-3),

$$NO_3^- + h\nu \xrightarrow{\Phi = 0.017} NO_2 + O^- \quad (1)$$

$$NO_2^- + h\nu \xrightarrow{\Phi = 0.07} NO + O^- \quad (2)$$

$$O^- + H^+ \longrightarrow OH \quad (3)$$

where Φ is the photochemical quantum yield.

The NO produced by (2) can further react with superoxide to form additional hydroxyl radical (or a species with similar reactivity), although the production of nitrate competes with this process (4-7).

$$NO + O_2^- \xrightarrow{k=6.7(+/-0.9)x10^9\ M^{-1}s^{-1}} {}^-OONO \quad (4)$$

$${}^-OONO + H^+ \xrightarrow{pK_a = 6.5} HOONO \quad (5)$$

$$HOONO \longrightarrow NO_3^- + H^+ \quad (6)$$

$$\longrightarrow OH + NO_2 \quad (7)$$

Hydrogen peroxide can also react with reduced metal species to produce hydroxyl radical (8), or undergo direct photochemistry and dissociate into two hydroxyl radicals (9). The latter process is not an important contributor in natural waters due to the poor overlap of hydrogen peroxide absorption and the solar radiation spectra at the sea surface.

$$H_2O_2 + M^{n+} \longrightarrow M^{(n+1)+} + OH + OH^- \quad (8)$$

$$H_2O_2 + h\nu \xrightarrow{\Phi=0.98} 2\ OH \quad (9)$$

It has been proposed (Zhou and Mopper, 1990; Mopper and Zhou, 1990; Mill, 1980; Mill et al., 1980) that an additional source of hydroxyl radical is through the photolysis of colored or chromophoric dissolved organic matter (CDOM) (10). Although the precise mechanism by which hydroxyl radical is formed is currently unknown, one possible mechanism may involve the follwing steps (Ononye et al., 1986; Ononye and Bolton, 1986).

$$^1\text{CDOM} + h\nu \longrightarrow {}^1\text{CDOM}^* \qquad (10)$$

$$^1\text{CDOM}^* \xrightarrow{\Phi=0.01-0.04} {}^3\text{CDOM}^*$$

$$^3\text{CDOM}^* + H_2O \longrightarrow \text{CDOMH}^\cdot + OH$$

Although this last production mechanism has not been verified, it may be important for understanding the oceanic cycling of dissolved organic carbon as photochemical degradation has been proposed as the rate-limiting step for the removal of a large fraction of oceanic DOC (Mopper et al., 1991).

Sinks for the hydroxyl radical in seawater are dominated by reaction with bromide ion (11) (rate constant from Zehavi and Rabani, 1972).

$$OH + Br^- \xrightarrow{k=1.1\times10^{10}\,M^{-1}s^{-1}} Br^\cdot + OH^- \quad [Br^-] = \sim 1\ mM \qquad (11)$$

In fresh waters, reactions with the carbonate ion (12) and dissolved organic matter (DOM) (13)(rate constants from Anbar and Neta, 1967) are the major sink for the hydroxyl radical.

$$OH + CO_3^= \xrightarrow[\text{(typical seawater concentrations)}]{k'=<8\times10^4\,s^{-1}} CO_3^{\cdot -} + OH^- \qquad (12)$$

$$OH + DOM \xrightarrow{k=\sim2\times10^8\,M^{-1}s^{-1}} DOM^\cdot + H_2O \quad \text{or} \quad HO\text{-}DOM^\cdot \qquad (13)$$

Because of the high reactivity of the hydroxyl radical in natural waters, special methods are needed for its study. Previous methods have included the use of cumene (Mill et al., 1980), n-butyl chloride (Haag and Hoigné, 1985; Zepp et al., 1987b), methyl mercury, nitrobenzene and anisole (Zepp et al., 1987b; 1992), octanol (Haag and Hoigné, 1985; Zepp et al., 1987a; 1992), benzoic acid and methanol (Zhou and Mopper, 1990; Mopper and Zhou, 1990), benzene, 2-propanol and formate (Warneck and Wurzinger, 1988).

In order to further investigate the possible influence on CDOM on the production of hydroxyl radical and to improve sensitivity, we have worked to develop an additional method of trapping hydroxyl radicals. This new method involves a two-step trapping scheme. First the hydroxyl radical generated by the laboratory irradiation of natural seawater reacts with one of three primary traps, DMSO, t-butanol, or octanol, to produce a carbon-centered radical intermediate (14-16) (rate constants from Veltwisch et al., 1980; Scholes and Willson, 1967; Buxton et al., 1988, respectively) Then, a second compound, the probe, 3-(aminomethyl)-2,2,5,5-tetramethyl-1-pyrrolidinyloxy free radical (3-amp) traps these carbon-centered radicals. In the absence of oxygen, 3-amp reacts with carbon centered radicals to form stable alkoxyamine adducts (17).

$$\underset{\text{DMSO}}{OH + CH_3SOCH_3} \xrightarrow{k=7\times10^9\ M^{-1}s^{-1}} \cdot CH_3 \qquad (14)$$

$$\underset{\text{octanol}}{OH + CH_3(CH_2)_7OH} \xrightarrow[\text{(pH 2, RT, in water)}]{k=7.7\times10^9\ M^{-1}s^{-1}} \text{carbon-centered radicals} \qquad (15)$$

$$\underset{\text{t-butanol}}{OH + C(CH_3)_3OH} \xrightarrow[\text{(RT, in water)}]{k=6\times10^8\ M^{-1}s^{-1}} H_2O + \cdot CH_2C(CH_3)_2OH \qquad (16)$$

$$\text{carbon-centered radical} + \text{3-amp} \xrightarrow{k=10^8 \text{ to } 10^9\ M^{-1}s^{-1}} \text{alkoxyamines} \qquad (17)$$

The alkoxyamines are then derivatized by fluorescamine, separated by high performance liquid chromatography (HPLC), and detected by monitoring the fluorescamine fluorescence at 480 nm, utilizing techniques developed by Kieber and Blough (1990a,b).

As a test of whether hydroxyl radical produces the carbon-centered reaction intermediates, reaction kinetics were studied in the presence of formate. Formate reacts with hydroxyl radical in direct competition with natural scavengers (Br^-) to form $CO_2^{\cdot -}$ which reduces 3-amp to the hydroxylamine (18) (rate constant from Buxton et al., 1988).

$$OH + HCOO^- \xrightarrow{k=3.2\times10^9\ M^{-1}s^{-1}} CO_2^{\cdot -} \qquad (18)$$

$$CO_2^{\cdot -} + \text{3-amp} \xrightarrow{k=10^8 \text{ to } 10^9\ M^{-1}s^{-1}} \text{hydroxylamine}$$

Further, nitrite was employed as a well-defined photochemical source of hydroxyl radical. The addition of NO_2^-, a compound which photolyzes to hydroxyl radical (vide supra), was used as an additional check that hydroxyl radical was indeed the compound trapped. The expected result of nitrite addition is an increased product signal (2).

We found that the addition of the primary probe compounds resulted in the generation of secondary carbon-centered radicals that were efficiently trapped by the 3-amp. Competition kinetics experiments with DMSO resulted in a natural scavenger hydroxyl radical consumption rate constant, k_{ns} ($M^{-1}s^{-1}$), that matched previous literature results for coastal waters. The addition of formate resulted in decreases, and the addition of nitrite in increases in the hydroxyl radical trapping rate by the two step probe method that we employed.

Experimental

Sample Collection

Surface coastal sea water was obtained during a cruise aboard the RV *ARGO Maine* in the Gulf of Maine (Table I).

Table I. Station Locations and Ancillary Data

Stn #	Date	Time EDST	Latitude	Longitude	Temp. °C	Water Depth (m)	Salin. ‰
GOM 10	5/24/93	23:07	43° 31.47'	69° 35.77'	9.4	150	31.7
GOM 12	5/25/93	00:02	43° 34.54'	69° 38.16'	8.6	124	31.4
GOM 14	5/25/93	00:48	43° 37.66'	69° 40.49'	8.6	84	30.6
GOM 16	5/25/93	01:42	43° 40.79'	69° 42.76'	8.3	74	29.1
GOM 18	5/25/93	02:33	43° 44.20'	69° 45.31'	8.0	14	29.8
GOM 22	5/25/93	04:33	43° 42.79'	69° 55.68'	9.5	30	28.1
GOM 32	5/25/93	09:10	43° 18.07'	69° 50.91'	9.8	189	31.5
GOM 54	5/26/93	01:11	42° 48.95'	70° 20.80'	11.6	102	29.7
GOM 56	5/26/93	02:23	42° 48.95'	70° 29.11'	11.9	112	29.6
GOM 58	5/26/93	03:27	42° 48.90'	70° 37.83'	11.5	82	29.7
GOM 60	5/26/93	04:29	42° 48.79'	70° 46.66'	11.2	23	29.5
BATS	7/8/93	17:21	31° 40.47'	64° 05.63'			36.6

Shelf water near the outflow of the Kennebec and Merrimack Rivers and in Lumbo's Hole was sampled using a pole sampler and trace-metal clean techniques for photochemical measurements and a 5 L Niskin for nutrient measurements. An additional sample was collected in 5 L Niskins from 10 m depth at the BATS site southwest of Bermuda on the RV *Weatherbird II*. All water was stored at room temperature in polyethylene containers in the dark. Absorption and fluorescence measurements were made within four days of collection.

Chemicals

HPLC grade dimethyl sulfoxide (DMSO), *tert*-butanol, *n*-octanol, reagent grade sodium formate and 3-amp were obtained from Sigma-Aldrich. Reagent grade sodium nitrite was purchased from Fisher. All chemicals were used as received, except for the 3-amp which was purified as described elsewhere (Caron and Blough, in preparation). HPLC solvents were made up as previously described (Kieber and Blough, 1990a,b). Water used in all experiments was from a Millipore Milli-Q system. Standard buffer was 0.2 M, pH 8.1 borate.

Nutrient Analysis

Samples were collected in polyethylene scintillation vials and immediately frozen to -10 °C. Analyses were performed following the Technicon AutoAnalyzer method (1970) in T. C. Loder's lab at the University of New Hampshire.

Absorption and Fluorescence Measurements

Filtered (0.2 μm) water samples were analyzed with a Hewlett-Packard 8451A spectrophotometer using 5 cm cells and Milli-Q water as the blank (Blough et al., 1993). Absorption coefficients were calculated using:

$$a_{CDOM}(\lambda) = 2.303\ A(\lambda)/L \qquad (19)$$

where $A(\lambda)$ is the absorbance and L is the cell path length in meters. Fluorescence emission spectra were collected on a SLM-Aminco SPF-500C spectrofluorometer in 1 cm cells with 4 nm excitation and emission bandpasses. Samples were excited at 337 and 355 nm and the resulting in Raman bands centered at 381 and 404 nm, respectively and an emission peak at ~450 nm. After the Milli-Q water blank was subtracted, the spectra were normalized to the fluorescence of 0.01 mg/liter quinine sulfate in 0.1 N H_2SO_4 (qs). Fluorescence is reported in normalized fluorescence units (N.Fl.U.) using the technique of Hoge et al. (1993)

$$F_n(\lambda)\ (\text{N.Fl.U.}) = [(F_{sample}: R_{sample})/(F_{qs}:R_{qs})] \times 10 \qquad (20)$$

where λ is the excitation wavelength, F the fluorescence peak height and R the water Raman signal height.

Sample Irradiation

Irradiation solutions consisted of filtered sea water (0.45 μm nylon syringe filter) buffered with 10% standard buffer, and containing 5-100 mM of primary trap (DMSO, t-butanol or octanol) and 200-250 μM 3-amp. In a 1 cm quartz cell, the sample was completely deaerated (~5 minutes) with argon (99.995% purity, Union Carbide) passed through an oxygen trap (Alltech). Irradiations lasted for 10 to 30 minutes at 310 nm (unless otherwise noted) with continuous head space flushing. The output of a 1000 W Hg-Xe arc lamp was passed through a Spectral Energy GM 252 monochromator set to a 10 nm bandpass. Lamp intensities were measured with an International Light 1700 research radiometer with a SUD 400 photodetector, calibrated for the specific experimental set-up using potassium ferrioxalate actinometry as is described elsewhere (Caron and Blough, in progress). After irradiation, 2 ml of sample were derivatized with 200 μl of fluorescamine (5 mM in acetonitrile) in an all-Teflon vial.

Compound Detection and Quantification

The HPLC method of Kieber and Blough (1990a,b) was used to analyze the trapped compounds. Compounds were detected with a Spectroflow 783 absorbance detector set to 390 nm and a Hitachi Model F1000 fluorescence spectrometer. Excitation and emission monochromators of the fluorometer were set to 390 and 480 nm, respectively. Fluorescence peak areas were converted to concentrations by first multiplying by the absorbance to fluorescence peak area ratio, and then using an absorbance standard addition curve created with known concentrations of 3-amp:

$$C_{std} * \frac{A_{std}}{F_{std}} * \frac{F_s}{A_s} = C_s \qquad (21)$$

where F is the fluorescence area, A the absorbance area for the peak of interest, and C the concentration of the sample (s) and standard (std).

Results and Discussion

Nutrient Data

The nutrient values fell within a fairly narrow range (Table II). Absorption by nitrate and nitrite is less than 0.5% of the total absorption of the samples (calculated using extinction coefficients from Zafiriou and True, 1979 and Zafiriou and Bonneau, 1987).

Table II. Nutrient Data[a]

Stn #	Depth (m)	$NO_3^- + NO_2^-$ (μM)	NO_2^- (μM)	NO_3^-[b] (μM)
10	1.3	0.26	0.08	0.18
12	1.8	0.07	0.04	0.03
14	1.2	0.10	0.04	0.06
16	1.6	0.04	0.05	0.0
18	1.8	0.15	0.04	0.11
22	1.3	0.45	0.09	0.36
32	1.8	0.10	0.09	0.01
54	1.6	0.06	0.04	0.02
56	1.1	0.45	0.07	0.38
58	1.5	0.15	0.06	0.09
60	1.6	0.12	0.13	0.0

[a]Data provided by T. Loder. [b]By difference of $NO_3^- + NO_2^-$ and NO_2^-.

Absorption and Fluorescence Measurements

Absorption and fluorescence spectra and ratios closely matched those for other North Atlantic samples (Table III). For the Gulf of Maine water samples, only slight deviations from linearity were found in the relationships between salinity and a_{CDOM} at 310, 337 and 355 nm (R^2 = 0.934, 0.917 and 0.898, respectively) (Fig. 1), and salinity and F_n at 355 nm and 337 nm (R^2 = 0.902, 0.792, respectively) (Fig. 2).

Table III. Absorption and Fluorescence Data

Sample ID	a_{CDOM}(310) m-1	a_{CDOM}(337) m-1	a_{CDOM}(355) m-1	F_n(337) N.Fl.U.	F_n(355) N.Fl.U.
GOM 10	0.623	0.357	0.268	1.32	0.872
GOM 12	0.918	0.595	0.523	1.98	1.25
GOM 14	1.573	0.985	0.795	2.97	1.98
GOM 16	2.154	1.357	1.031	4.29	2.69
GOM 18	2.438	1.564	1.194	4.79	3.31
GOM 22	3.470	2.253	1.700	7.23	4.63
GOM 32	0.725	0.437	0.380	1.73	0.975
GOM 54	1.895	1.170	0.896	3.50	2.19
GOM 56	1.977	1.193	0.888	3.58	2.46
GOM 58	2.109	1.329	1.025	3.61	2.34
GOM 60	2.222	1.371	1.036	4.06	2.79
BATS	0.099	0.066	0.040		

These results indicate that the fluorescence and absorbance are mainly due to riverine organic matter that is being diluted into the sea water. Deviations from linearity in absorbance or fluorescence to salinity relationships may be due to photobleaching of the riverine material with time spent at the surface, biological production of distinct or additional CDOM in situ, or upwelling of high salinity water masses which have picked up CDOM from the bottom sediments (Blough et al., 1993; Carlson and Mayer, 1983). Very good linear relationships were found between a_{CDOM} and F_n at 337 and 355 nm (R^2 = 0.979 and 0.977, respectively) (Fig. 3) These relations are close to those found by Hoge et al. (1993) for other Western North Atlantic sites and furthers their finding of only slight variations in the fluorescence per unit absorption (or quantum yield) of marine waters.

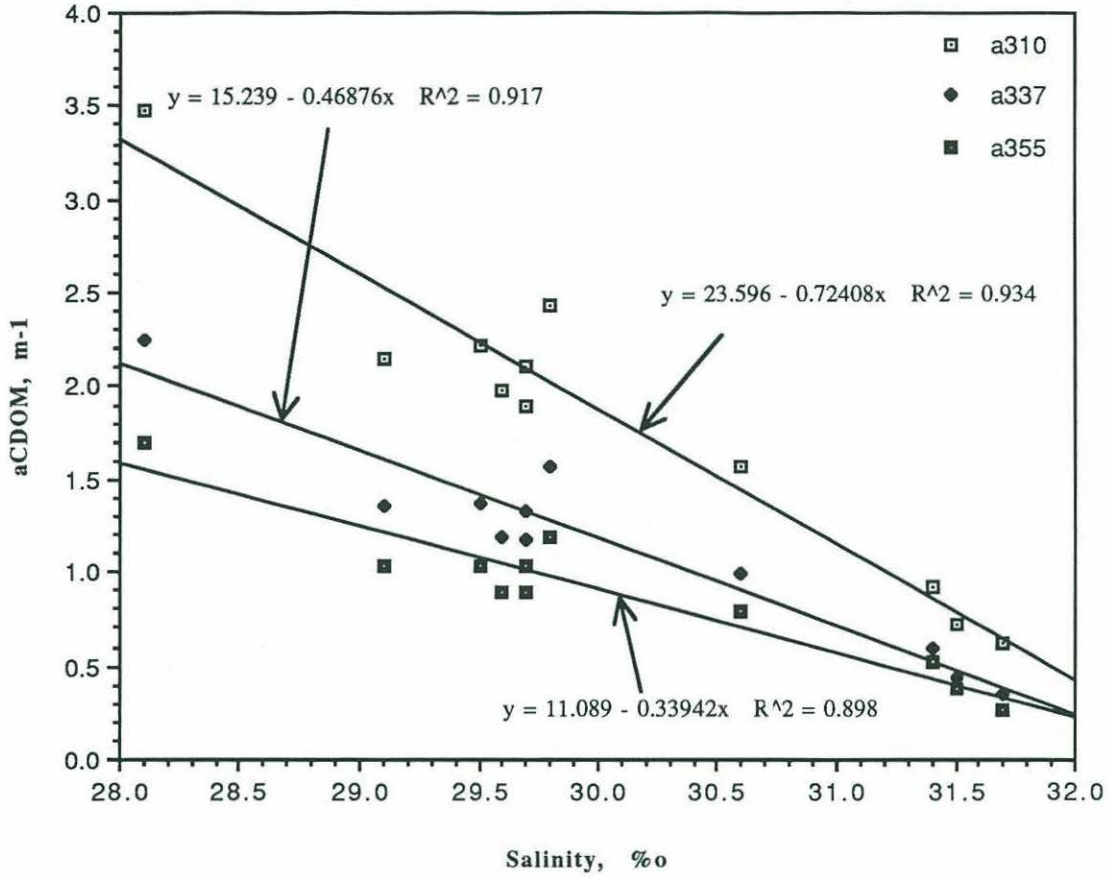

Figure 1. Correlation of absorption coefficient at 310, 337 and 355 nm (m^{-1}) with salinity (‰) for the GOM samples.

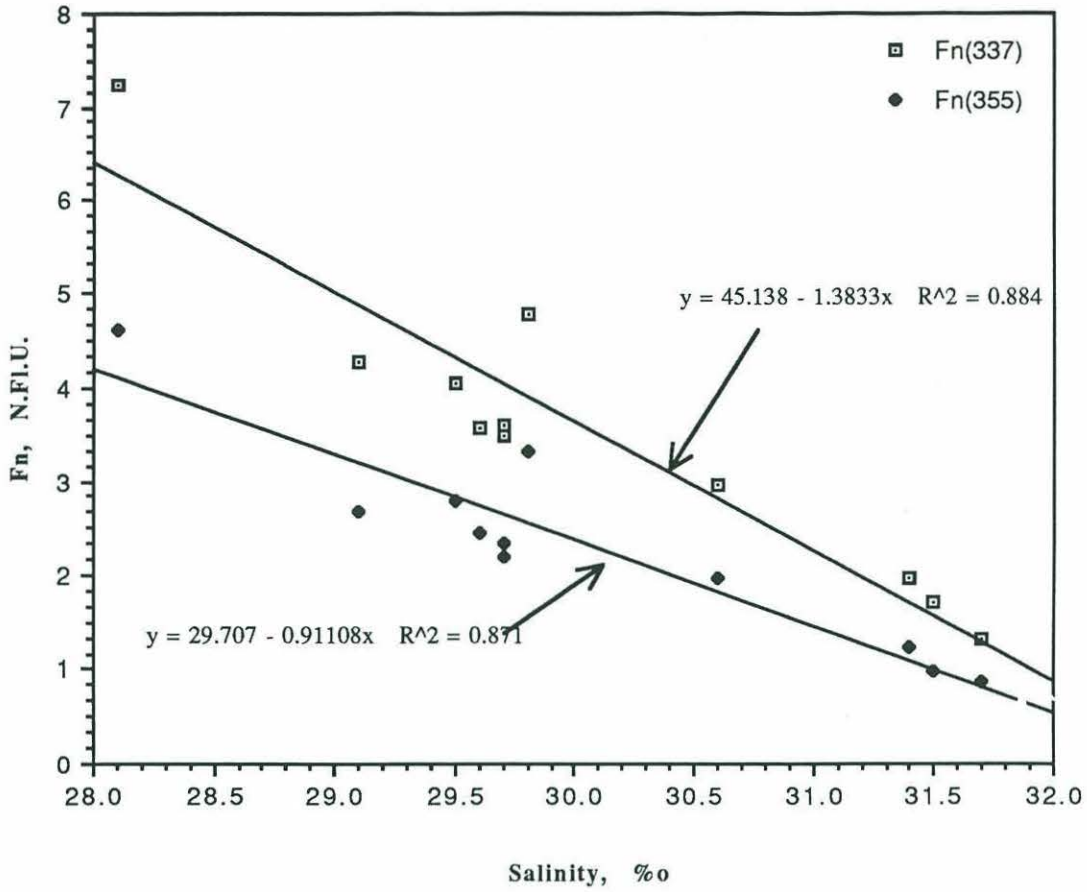

Figure 2. Correlation of fluorescence at 337 and 355 nm (N.Fl.U.) with salinity (‰) for the GOM samples.

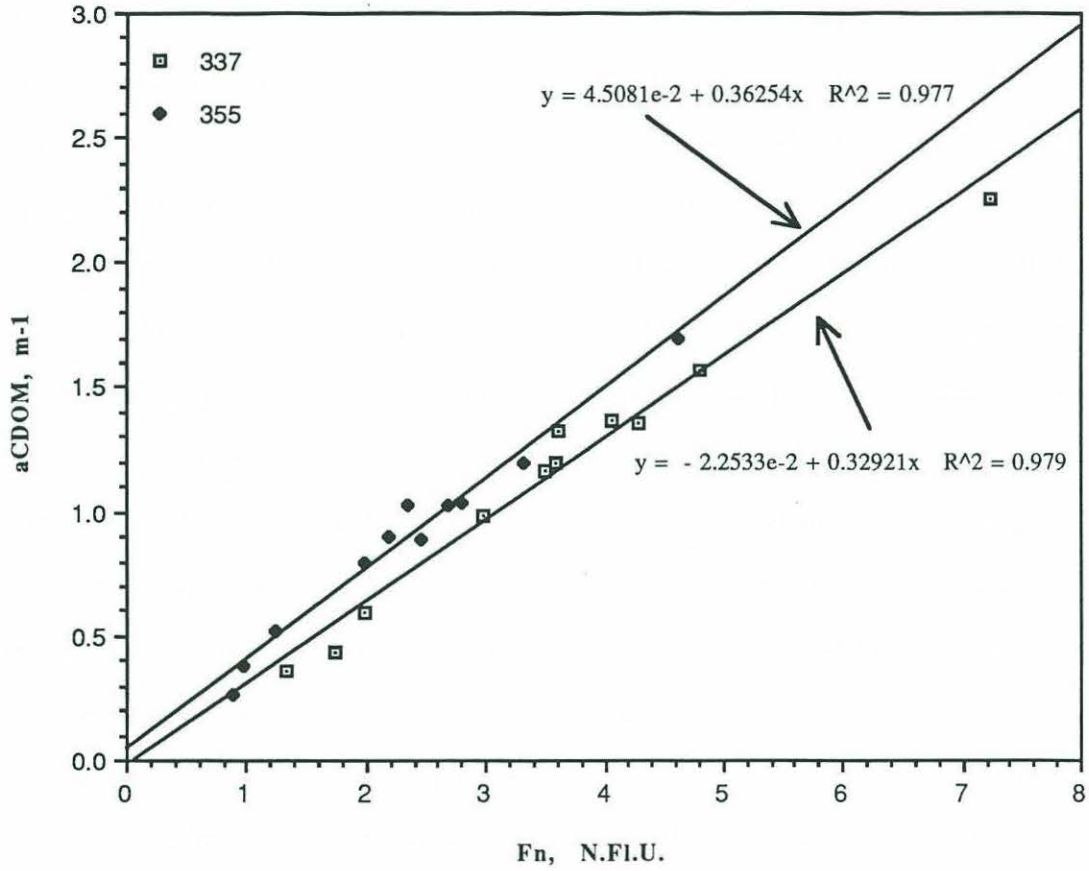

Figure 3. Correlation of absorption coefficient at 310, 337 and 355 nm (m^{-1}) with fluorescence at 337 and 355 nm (N.Fl.U.) for the GOM samples.

Method Evaluation

No background problems were encountered, but day to day variability has not yet been eliminated. Dark reactions contributed less than 1% of the methyl radical fluorescence peak area (as measured by dark blanks). The background production rate of methyl radical from photolysis of CDOM (0.66 nM/min in GOM water and 0.65 nM/min in BATS water at 310 nm and a light intensity of 1.1×10^{-8} E/cm^{2}sec) is also negligible compared to the signal generated in the presence of DMSO as a primary radical trap (Fig. 4). The background methyl radical production rate was about three fold lower in Milli-Q water (0.46 nM/min). The methyl radical signal increased with increasing concentration of 3-amp up to 200 μM 3-amp at which point the methyl radical signal flattened out. This indicates that above this concentration, 3-amp is present in enough excess to quantitatively trap the methyl radical. Concentrations of 200-250 μM were used in the experiments reported here. Generally runs on a single day showed good agreement (± 25%) and the data discussed below comes from such runs. Experiments on different days showed up to a factor of five variability. The cause of this variability has not yet been determined, but might be due to small amounts of product-destroying cleaning acid remaining in incompletely rinsed reaction vessels.

DMSO as Primary Trap

When various amounts (0.5 to 11 mM) of DMSO were added to the sample before irradiation, the methyl radical fluorescence peak area increased, corresponding to the production of secondary methyl radicals by reaction (14). The production rate reached a plateau after the addition of 5 mM DMSO (Fig. 5) at a value of 54 nM/min. Irradiation of buffered Milli-Q water for 10, 20 and 30 minutes with DMSO as the primary trap, resulted in hydroxyl radical production rates that were constant within experimental error indicating that the amount of hydroxyl radical trapped increases linearly with time. Unlike the results for the primary production of methyl radicals, irradiations of three different types of

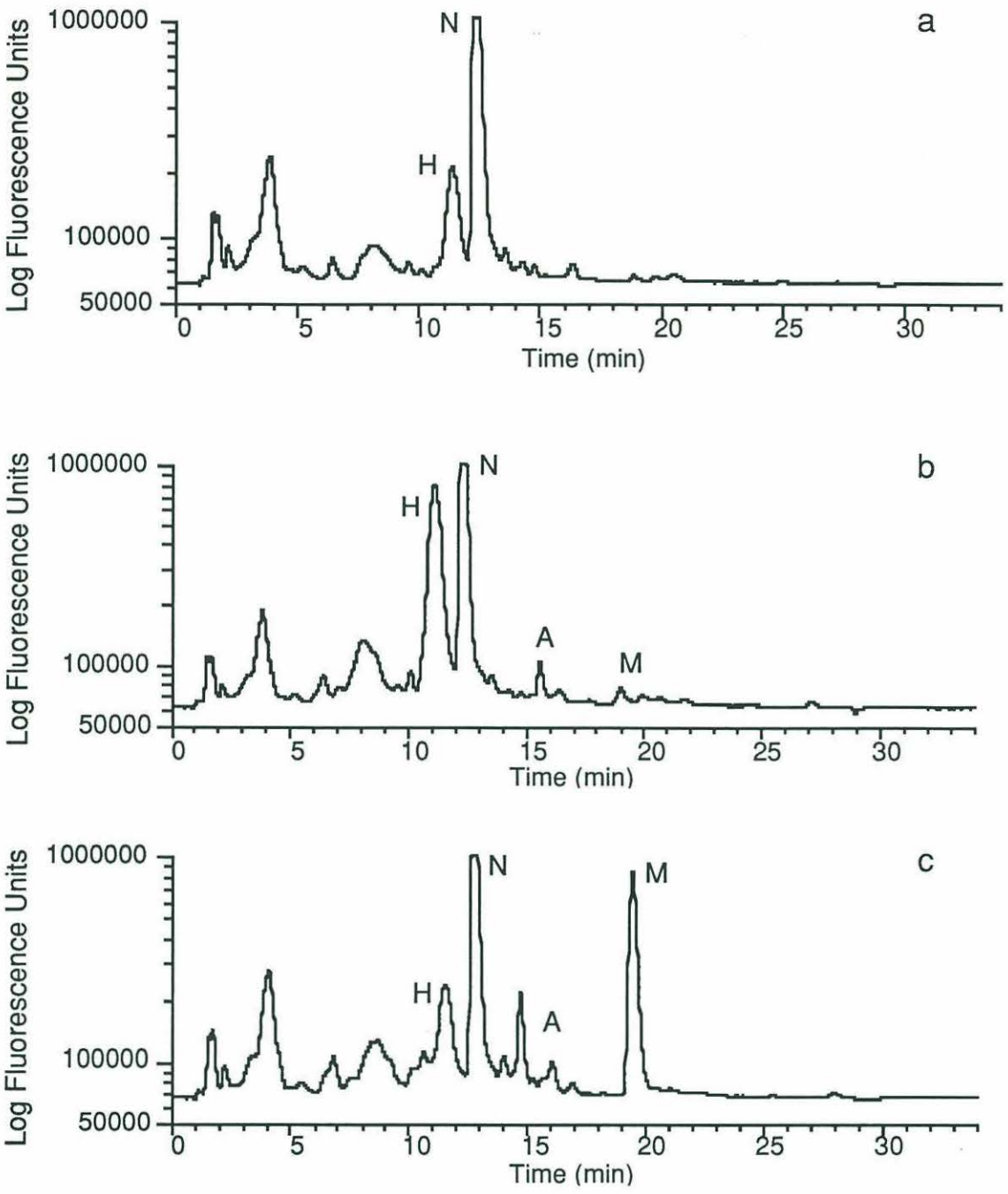

Figure 4. Log-linear plot of HPLC fluorescence chromatograms illustrating the pattern of adduct formation produced by an irradiation of GOM #18 water at 310 (± 5) nm. Initial 3-amp concentration was 250 μM; light intensity was 1.1×10^{-8} E/cm^{2}sec except for **a**. Adduct designations ar as follows: N=3-amp, H=hydroxylamine, A=acetyl radical, M=methyl radical. **a** is a dark blank, **b** is a light blank, and **c** is with 5 mM DMSO added. Unlabeled peaks were caused by fluorescent contaminants in the 3-amp. Hydroxylamine concentrations are not quantitative.

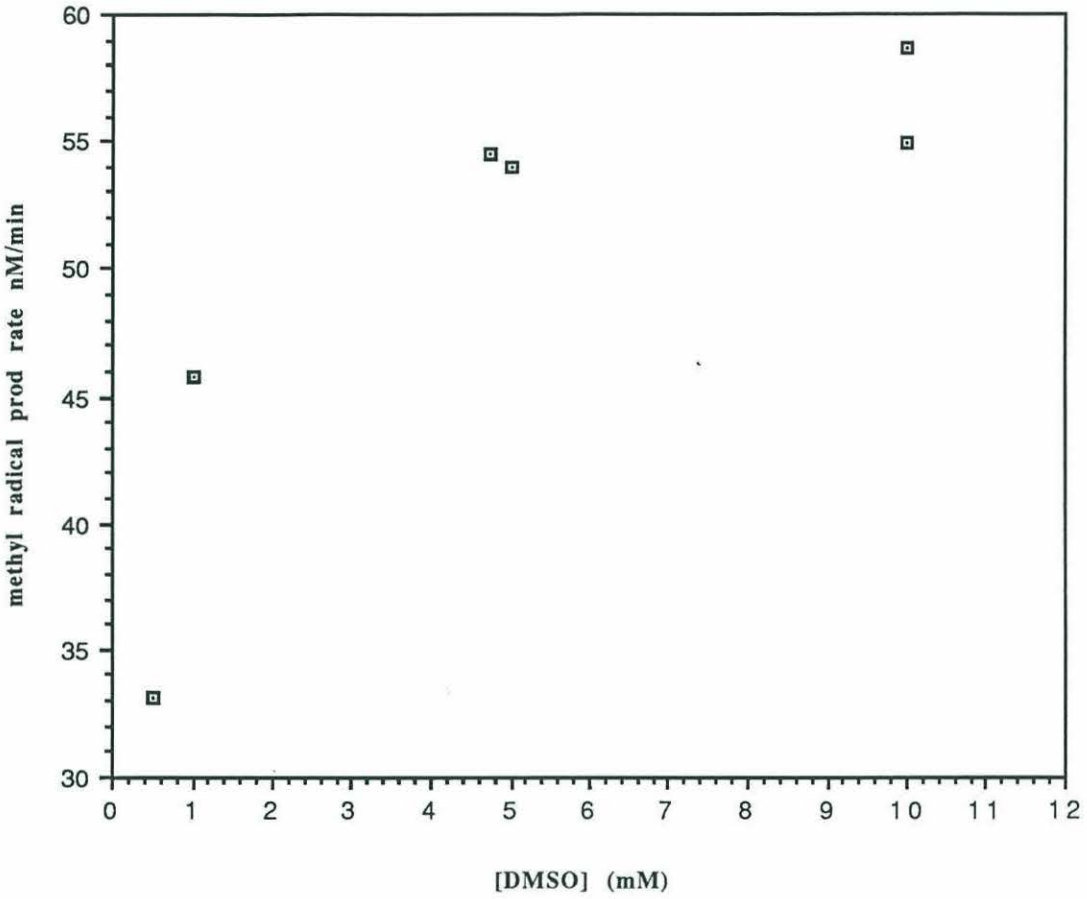

Figure 5. The effect of increasing concentrations of DMSO on the trapping rate of methyl radicals (generated from reaction of hydroxyl radical with DMSO). All points are from irradiations of GOM #18 water at 310 (± 5) nm and a light flux of 1.1 x 10^{-8} E/cm^2sec with an initial 3-amp concentration of 200 μM.

waters, GOM, BATS and Milli-Q with DMSO as the primary trap gave the rather uniform results of 17.1, 16.7 and 23.5 nM/min, respectively. This suggests a problem (possibly left over acid) with the technique, the presence of equal amounts of hydroxyl radical producing CDOM in the two waters or another source of hydroxyl radical in the samples which overwhelms the contribution of the CDOM-originated hydroxyl radical. Up to a factor of five variability was found in runs on different days. An average of six irradiations at 310 nm in GOM water that did not appear to be affected by acid or any other problems results in a hydroxyl radical production rate of ~45 (± 10) nM/min.

Preliminary evidence from the irradiation of three different GOM samples (10, 18 and 22) shows that it may be possible to correlate absorbance and fluorescence with hydroxyl radical production rate. There is a general trend of increasing hydroxyl radical production rate with increasing absorption (Fig. 6), although clearly more data is needed before it can be quantified. The non-zero x-intercept for the data set suggests blank problems and not necessarily that hydroxyl radical is being generated.

Octanol as Primary Trap

Hydroxyl radical reacts with octanol (15) to form a suite of product carbon-centered radicals that are trapped by 3-amp. Abstraction of a hydrogen atom from the carbon next to the alcohol group in octanol leads to the formation of the 3-amp one electron reduction product, the hydroxylamine. Abstraction of any of the other hydrogens should result in stable alkoxyamine adducts. Consistent ratios of 0:5:6:1:1:1:1 were found for the six stable alkoxyamine product peaks observed (Fig. 7) This differs from the ratios of the number of protons on each carbon (2:2:2:2:2:2:3) because all of the protons are not extracted with equal efficiency as has been seen previously (Asmus et al., 1973). As this is a region of changing HPLC gradient, the varying quantum yields of the alkoxyamines in different solvents effect the peak ratios (although by no more than a factor of two) (see Chapter 1, Table I. for quantum yields of 3-amp in methanol and buffer.)

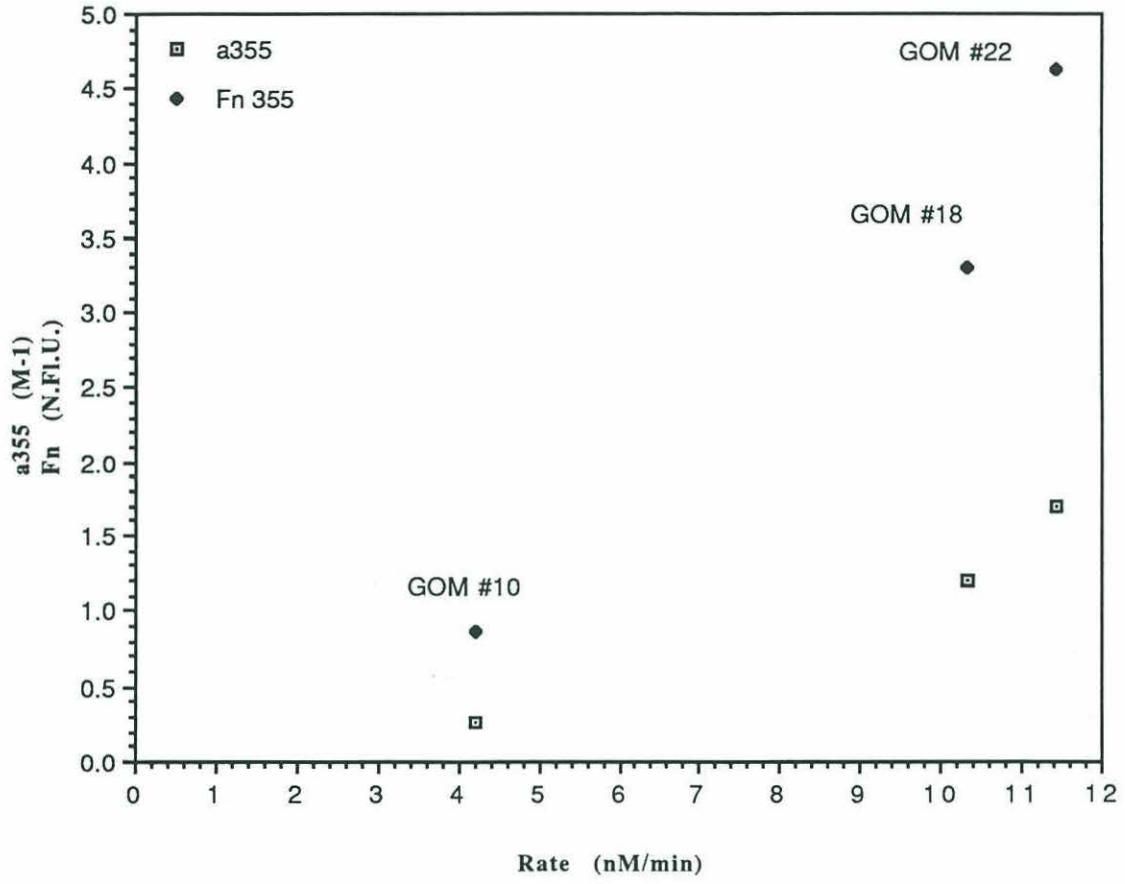

Figure 6. Correlation of absorption coefficient (m^{-1}) and fluorescence from excitation at 355 nm (N.Fl.U.) with the trapping rate of methyl radicals (generated from reaction of hydroxyl radical with DMSO) for three GOM samples (#10, 18 and 22). All points are from irradiations at 310 nm, a light flux of 1.1×10^{-8} E/cm^2sec, an initial 3-amp concentration of 200 μM and an initial DMSO concentration of 5 mM.

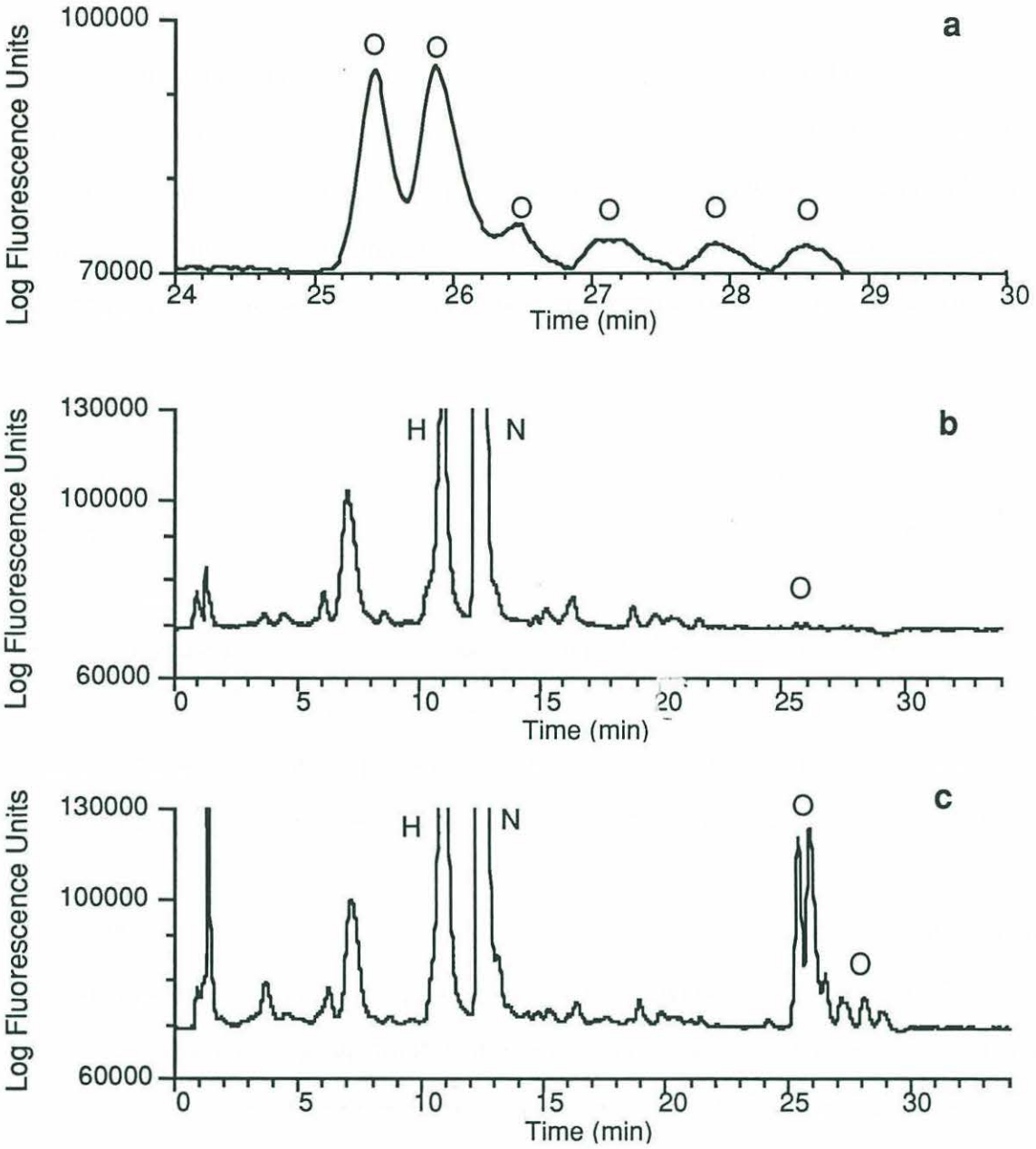

Figure 7. Log-linear plot of HPLC fluorescence chromatograms illustrating the pattern of adduct formation produced by an irradiation of Milli-Q water at 310 (± 5) nm. Initial 3-amp concentration was 250 μM initial octanol concentration was 5 mM; light intensity was 1.1 x 10^{-8} E/cm^{2}sec for **a** and 1.2 x 10^{-8} E/cm^{2}sec for **b** and **c**. Adduct designations are as follows: N=3-amp, H=hydroxylamine, O=radical formed from reaction of hydroxyl radical and octanol. **a** is at 310 nm **b** is at 360 nm and **c** is at 360 nm with 100 μM nitrite added. Hydroxylamine concentrations are not quantitative.

Irradiation in the presence of ~5 mM octanol (due to the limited aqueous solubility of octanol {4.47 mM, Tewari et al., 1982}, the exact concentration present is not known) resulted in an estimated hydroxyl radical production rate of 6.6 nM/min (achieved by summing the area of the six peaks.) Irradiation at 360 nm instead of 310 nm resulted in lower production rates, in accordance with the absorption coefficient at this wavelength.

t-Butanol as Primary Trap

Hydroxyl radical reacts with t-butanol (16) both by extracting a proton from one of the methyl groups (95.7%) and by extracting the proton from the alcohol which rearranges to generate a methyl radical (4.3%) (Asmus et al., 1973). These radicals are trapped by 3-amp and elute at around 18.5 and 19 minutes, respectively, and in the expected ratio. Four additional small peaks were observed as well which are probably due to contaminants in the t-butanol as they do not increase with the addition of nitrite (Fig. 8) Preliminary studies indicate that at least 50 to 100 mM of t-butanol are needed for complete trapping.

Product Check

The addition of 100 μM NO_2^- to the cuvette before irradiation with either octanol or t-butanol as the secondary probe, resulted in a 50 to 100 fold increase in production rate (Figs. 7,8) as expected due to the generation of hydroxyl radicals by NO_2^- (2). In both cases, the addition of nitrite resulted in increased production of the same compound peaks that resulted from the primary traps alone, thus showing that these products are indeed the result of reactions with hydroxyl radical. Dark blanks for octanol and t-butanol with NO_2^- showed no peaks in the region of interest.

Kinetics

The rate of hydroxyl radical consumption by natural scavengers can be arrived at considering the following reactions:

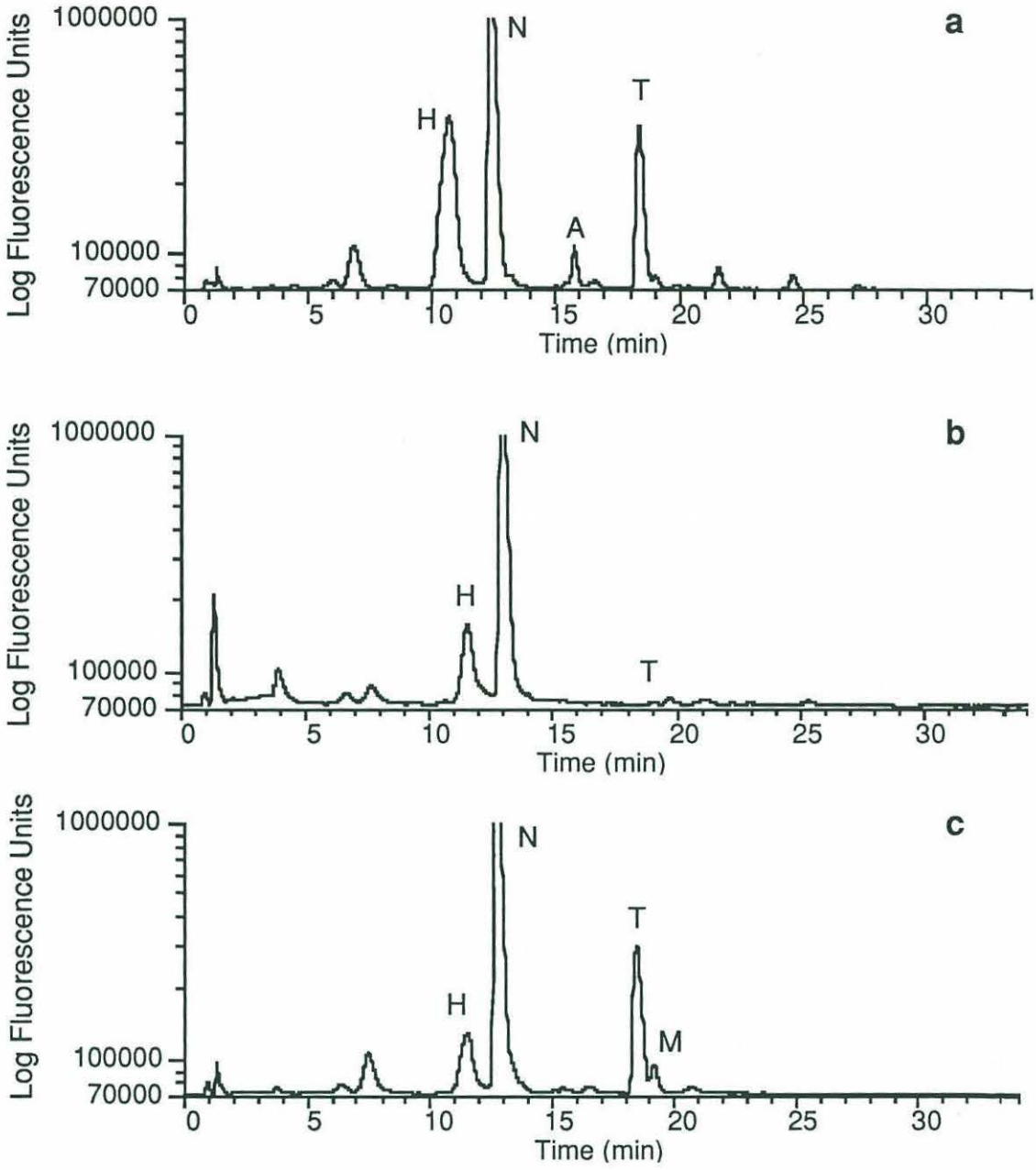

Figure 8. Log-linear plot of HPLC fluorescence chromatograms illustrating the pattern of adduct formation produced by an irradiation of Milli-Q. Initial 3-amp concentration was 250 μM initial t-butanol concentration was 100 mM; light intensity was 1.1 x 10^{-8} E/cm^2sec for **a** and 1.2 x 10^{-8} E/cm^2sec for **b** and **c**. Adduct designations are as follows: N=3-amp, H=hydroxylamine, T=radical formed from reaction of hydroxyl radical and t-butanol, A=acetyl radical, M=methyl radical. **a** is at 310 nm **b** is at 360 nm and **c** is at 360 nm with 100 μM nitrite added. Hydroxylamine concentrations are not quantitative.

$$\text{OH sources} + h\nu \xrightarrow{P_{OH}} OH \quad (22)$$

$$OH + ns \xrightarrow{R_{ns}} \text{mostly } Br_2^- \text{ in seawater} \quad (23)$$

$$OH + p \xrightarrow{R_p} \text{alkoxyamines} \quad (24)$$

where P_{OH} is the production rate (s^{-1}) of hydroxide radical and R_{ns} and R_p are the rates of consumption ($M^{-1}s^{-1}$) by natural scavengers (ns) and probe compounds (p), respectively. In the presence of probe compounds,

$$\frac{d[OH]}{dt} = P_{OH} - k'_{ns}[OH]'_{ss} - k_p[P][OH]'_{ss}. \quad (25)$$

where k'_{ns} and $[OH]'_{ss}$ are the pseudo first order rate constants (s^{-1}) and hydroxyl radical concentration (M), respectively, in the presence of the probe (which can cause a decrease in the steady-state concentration of hydroxyl radical due to an increased sink), k_p is the rate constant ($M^{-1}s^{-1}$) and [P] the concentration of the probe (M). At steady-state (which is rapidly achieved as all of the

species involved are very reactive), the rate of change of hydroxyl radical with time is equal to zero. Taking this into account and solving for $[OH]'_{ss}$ in (25) leads to

$$[OH]'_{ss} = \frac{P_{OH}}{k'_{ns} + k_p[P]} \quad (26)$$

Taking the rate of probe consumption (and trapped methyl radical production),

$$R_p = k_p[P][OH]'_{ss} \quad (27)$$

rearranging and substituting into (26) gives

$$R_p = \frac{k_p[P]P_{OH}}{k'_{ns} + k_p[P]} \quad (28)$$

A linear transformation arrives at

$$\frac{1}{R_p} = \frac{1}{[P]}\frac{k'_{ns}}{P_{OH}k_p} + \frac{1}{P_{OH}} \quad (29)$$

A plot of inverse production rate of methyl radical versus inverse DMSO concentration (1/[P]) in GOM # 18 water (Fig. 9) results in a k'_{ns} of 2.6×10^6 s^{-1} (recall $k_p = 7 \times 10^9$ $M^{-1}s^{-1}$ for DMSO). This matches the k'_{ns} value obtained by Zhou and Mopper of 2.4 ($\pm$ 0.2) x 10^6 s^{-1} in coastal seawater. Also obtained is the laboratory hydroxyl radical production rate

(9.9×10^{-10} M s^{-1}), from which it is possible to calculate the natural water hydroxyl radical production rate in the GOM samples by dividing by laboratory photon fluxes (obtained using potassium ferrioxalate actinometry) and multiplying by the clear-sky, summer noon photon fluxes at 40°N (Zepp and Cline, 1977)

$$P_{OH(40°N\{\lambda\})} = \frac{P_{OH(exp\{\lambda\})} * E_{(40°N\{\lambda\})}}{E_{(exp\{\lambda\})}} \quad (30)$$

where E is the photon flux of either 40°N or the experiment (exp) for a given wavelength, λ. From this calculated production rate (Table IV), the steady-state surface hydroxyl radical concentration can be calculated as follows. In the absence of probe compounds, the rate of change of hydroxyl radical concentration (25) becomes

$$\frac{d[OH]}{dt} = P_{OH} - k'_{ns}[OH]_{ss} \quad (31)$$

which at steady-state gies

$$[OH]_{ss} = \frac{P_{OH}}{k'_{ns}} \quad (32)$$

The values obtained in this manner agree well with those obtained from single experiment values at a number of wavelengths (Table IV). Rearranging (26) leads to

$$P_{OH} = \frac{(k'_{ns} + k_p[P])R_p}{k_p[P]}$$

which, when substituted into (32) gives

$$[OH]_{ss} = \frac{(k'_{ns} + k_p[P])R_p}{k'_{ns} * k_p[P]} \quad (33)$$

Again we normalize to clear-sky, summer noon photon fluxes at 40°N (Zepp and Cline, 1977)

$$[OH]_{ss(40°N\{\lambda\})} = \frac{[OH]_{ss(exp\{\lambda\})} * E_{(40°N\{\lambda\})}}{E_{(exp\{\lambda\})}} \quad (35)$$

the resulting average value between 310 and 400 nm is 2.4 (±1.1) x 10^{-18} M which is about a factor of four to five smaller than values obtained by Zhou and Mopper (1990) of 9.5 to 13.5 x 10^{-18} M for coastal sea water.

The hydroxyl radical production rate, P_{OH}, can be calculated from the steady-state concentration, $[OH]_{SS}$, and the natural scavenger rate constant, k'_{ns} (s^{-1}) using (33). The resulting average value (Table IV) is also about a factor of 10 lower than that obtained by Zhou and Mopper (1990). This is due, in part, to the fact that these values are calculated using solar photon data from 40° N whereas Zhou and Mopper (1990) use values for 26° N.

Table IV. Hydroxyl Radical Production Rate and Steady-State Concentration

wavelength (nm)	$[OH]_{SS}$[a] (M)	P_{OH}[a] (Ms^{-1})
275 (one value)	5.74×10^{-18}	1.51×10^{-23}
310 (linear fit)	2.48×10^{-18}	6.52×10^{-12}
310(one value)	3.02×10^{-18}	7.95×10^{-12}
350 (one value)	1.52×10^{-18}	4.00×10^{-12}
390 (one value)	1.26×10^{-18}	3.32×10^{-12}
400 (one value)	3.67×10^{-18}	9.64×10^{-12}
average (single measurements) (310-400)	$2.4(\pm1.1)\times10^{-18}$	$6.2(\pm3.1)\times10^{-12}$

[a] Using clear-sky summer photon fluxes at 40°N (Zepp and Cline, 1977).

A quick check for the influence of 10 mM HCO_2^- (5) showed about a five-fold decrease in hydroxyl radical trapping rate due to HCO_2^- comparing two 20 minute irradiations at 310 nm, one with and one without HCO_2^-. The presence of an additional sink, in this case formate, results in the following modification to equation (29)

$$\frac{1}{R'_p} = \frac{1}{[P]}\frac{(k'_{ns}+k'_f)}{P_{OH}k_p} + \frac{1}{P_{OH}} = \frac{1}{[P]}\frac{(k'_{ns}+k_f[F])}{P_{OH}k_p} + \frac{1}{P_{OH}} \qquad (30)$$

where k'_f (s^{-1}) is the pseudo first order reaction rate constant for hydroxyl radical with formate, k_f ($M^{-1}s^{-1}$) the rate constant, [F] the concentration of formate and R'_p the rate of consumption ($M^{-1}s^{-1}$) of probe in the presence of formate. Rearranging (30) we can solve for k'_f

$$k'_f = -\left(k'_{ns} + \frac{(R'_p - P_{OH})k_p[P]}{R'_p}\right) \qquad (31)$$

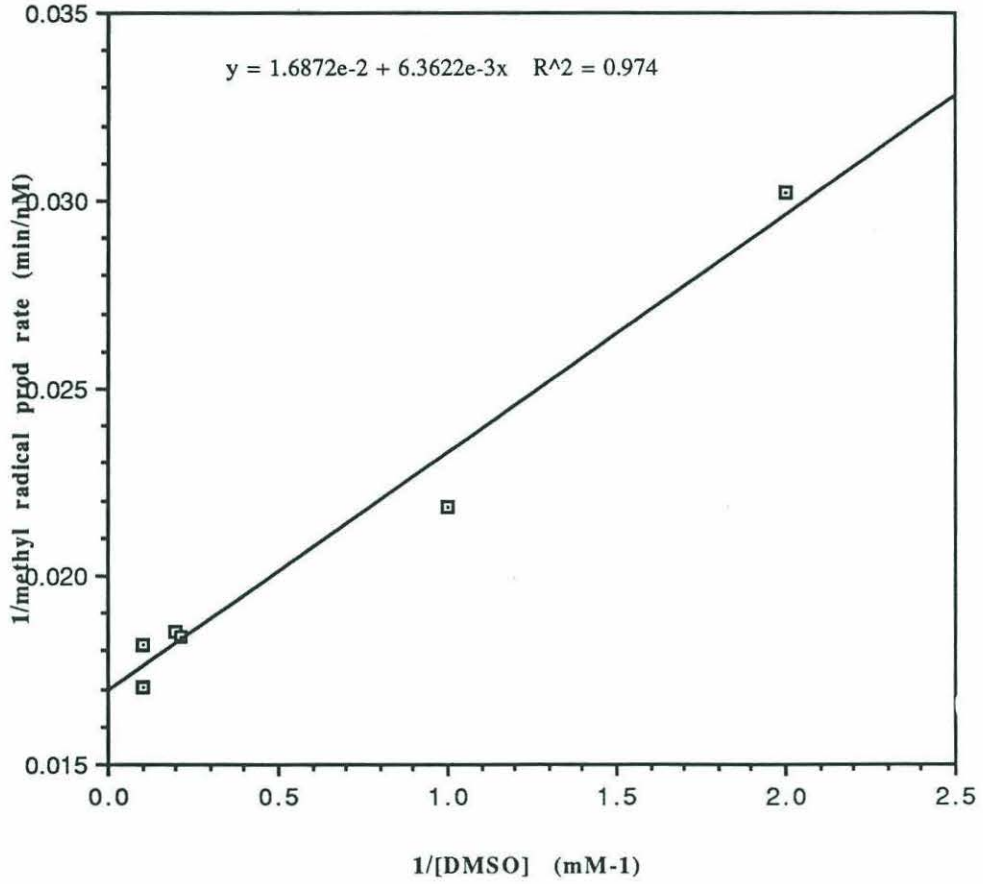

Figure 9. Double reciprocal plot of the effect of increasing concentrations of DMSO on the trapping rate of methyl radicals (generated from reaction of hydroxyl radical with DMSO). All points are from irradiations of GOM #18 water at 310 (± 5) nm and a light flux of 1.1 x 10^{-8} E/cm^2sec with an initial 3-amp concentration of 200 μM.

The value obtained in the one experiment was $k_f = 16 \times 10^9\ M^{-1}s^{-1}$ which is about five-fold faster than the literature value of $3.2 \times 10^9\ s^{-1}M^{-1}$ (Buxton et al., 1988). This indicates that there was a problem with this competitive kinetics experiment which is not surprising given the observed variability in results.

Wavelength Dependence of the Hydroxyl Radical Production Quantum Yield

Previous researchers have shown that there is a strong wavelength dependence of the hydroxyl radical production quantum yield (Mopper and Zhou, 1990). The measurements from our experiments follow the same pattern, but result in values higher by about a factor of 10 (Fig. 10). Until the uncertainty in our technique is worked out, it is not possible to tell if there is really a conflict between these values.

Relative Contribution of NO_3^-, NO_2^- and other sources to P_{OH}

The relative contribution of NO_3^-, NO_2^- and other sources (including CDOM photolysis) to P_{OH} can be calculated from their concentrations and rate constants. When concentrations of nitrate and nitrite (Table II) are multiplied by the production rate constants that Mopper and Zhou (1990) calculated for nitrate ($3.0 \times 10^{-13}\ Ms^{-1}/\mu M\ NO_3^-$) and nitrite ($2.3 \times 10^{-11}\ Ms^{-1}/\mu M\ NO_2^-$), they only account for 0.53 and 15% of the production of hydroxyl radical in GOM sample #18, respectively. The remaining ~85% of the source term in as yet unaccounted for, but could be due to CDOM photolysis is argued by Mopper and Zhou (1990). The possible correlation between sample absorption and/or fluorescence and hydroxyl radical production rate (vide supra) suggests a significant contribution by CDOM photolysis.

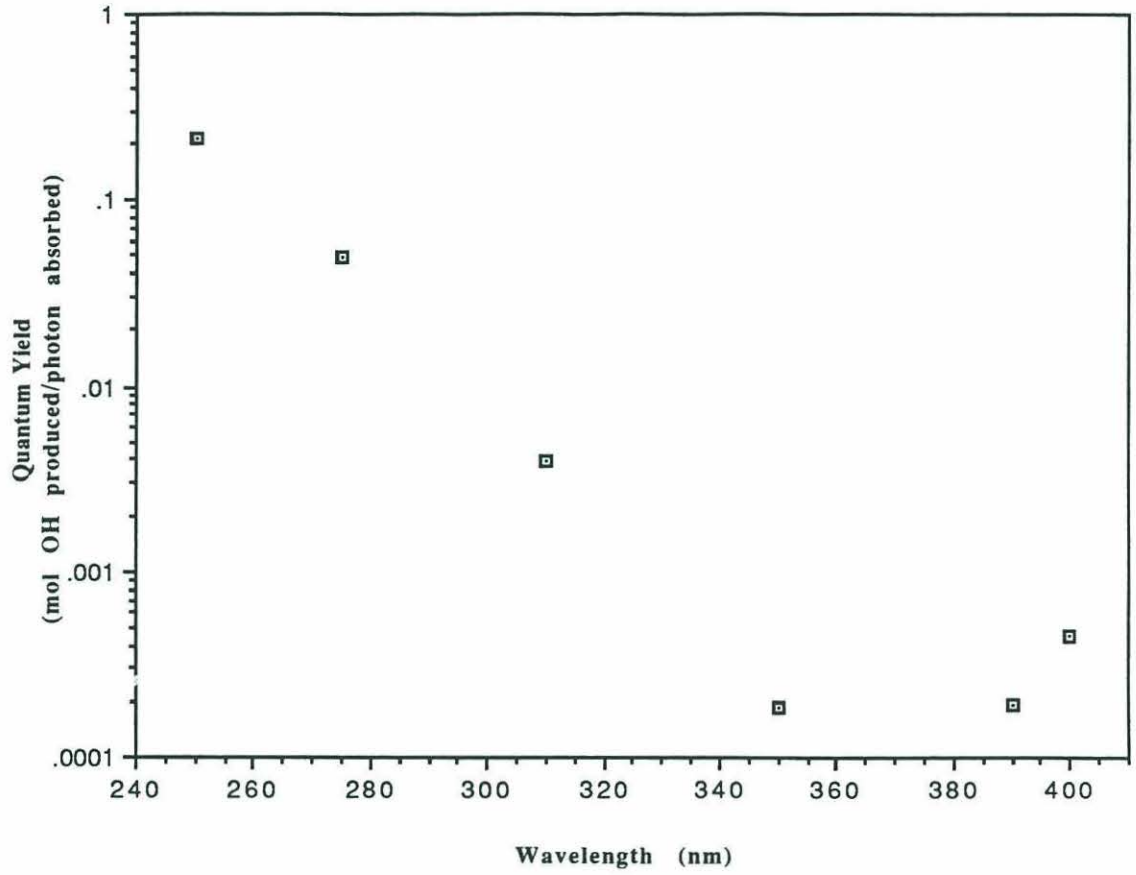

Figure 10. Log-linear plot of the wavelength dependence of the hydroxyl radical production quantum yield.

Conclusions

The relatively low background natural production rate of methyl radical (0.5 to 1 nM/min) without a primary trap makes this double trapping method feasible. Tests of the method had favorable results. The addition of nitrite to the reaction mixture results in an expected increase in the area of the fluorescence peaks, indicating that it is indeed hydroxyl radical that causes the HPLC fluorescence peaks. Competitive kinetics calculations result in a calculated k'_{ns} that is identical, within experimental error, to that obtained by Zhou and Mopper (1990) using two different trapping methods in coastal seawater. Addition of formate causes a decrease (of a factor of two more than expected from literature results) in the trapping efficiency of DMSO as is expected as it is a competitor for hydroxyl radical. The large amount of variability between runs has interfered with the results, but can probably be eliminated with more method development work.

Within the uncertainty of the technique, there does not appear to be an increase in the hydroxyl radical production rate of Milli-Q, BATS, and GOM #18 water with increasing sample absorption coefficient. However a single experiment comparing three different GOM samples (#10, 18, 22) did show a correlation between absorbance and hydroxyl radical production rate.

The values obtained here do not closely match other literature values. Hydroxyl radical production rate and steady-state concentrations were about an order of magnitude lower than those calculated by Zhou and Mopper (1990), although this may be due to latitudinal differences (vide supra). Quantum yield values were about an order of magnitude higher than those of Mopper and Zhou (1990). More detailed work is needed to recognize the full potential of this method.

Future Work

A central question in interpreting these results is the reason for the similarity of hydroxyl radical production rates obtained for GOM #18, Milli-Q and BATS waters. This

needs to be investigated further. Also, a thorough study of reproducibility needs to be done to improve consistency between days and irradiations. To do this a number of irradiations using constant primary trap and 3-amp concentrations should be done on a single sample. Experiments employing different primary trap and nitroxide concentrations should be performed to test these results further. A detection limit study should be undertaken using a well defined hydroxyl radical source such as nitrite to see if some of the measurements here are in the noise level. A systematic model study of hydroxyl radical production quantum yields should be undertaken so that experimental results can be compared with natural waters irradiated with sunlight. Also, some terrestrial water samples should be analyzed to expand the area of relevance of the study. In addition, the effects of metals, such as iron, on hydroxyl radical production rates (8) could be studied using this method.

References

Anbar, M., and Neta, P. A., 1967. Compilation of specific bimolecular rate constants of hydrated electrons, hydrogen atoms and hydroxyl radicals with inorganic and organic compounds in aqueous solution. Int. J. Appl. Radiat. Isotopes, 18: 493-523.

Asmus, K. -D., Möckel, H., and Henglein, A., 1973. Pulse radiolytic study of the site of •OH radical attack on aliphatic alcohols in aqueous solution. J. Phys. Chem., 77: 1218-1221.

Blough, N. V., Zafiriou, O. C., and Bonilla, J., 1993. Optical absorption spectra of waters from the Orinoco River outflow: Terrestrial input of colored organic matter to the Caribbean. J. Geophys. Res., 98: 2271-2278.

Blough, N. V., and Zepp, R. G., in press. Reactive oxygen species (ROS) in natural waters. In: C. S. Foote and J. S. Valentine (Editors), Reactive Oxygen Species in Chemistry, Chapman and Hall.

Blough, N. V., Submitted. Photochemistry in the sea-surface microlayer.

Buxton, G. V., Greenstock, C. L., Helman, W. P., and Ross, A. B., 1988. Critical review of rate constants for reactions of hydrated electrons, hydrogen atoms and hydroxyl radicals (•OH/•O$^-$) in aqueous solution. J. Phys. Chem. Ref. Data, 17: 513-886.

Carlson, D. J., and Mayer, L. M., 1983. Relative influences of riverine and macroalgal phenolic materials on UV absorbance in temperate coastal waters. J. Fish. Aq. Sci., 40: 1258-1263.

Caron, S., and Blough, N. V., in progress. Photochemical formation of free radicals and hydrogen peroxide in natural waters and their relationship to DOM photooxidation.

Haag, W. R., and Hoigné, J., 1985. Photo-sensitized oxidation in natural water via OH radicals. Chemosphere, 14:1659-1671.

Hoge, F. E., Vodacek, A., and Blough, N. V., 1993. Inherent optical properties of the ocean: Retrieval of the absorption coefficient of chromophoric dissolved organic matter from fluorescence measurements. Limnol. Oceanogr., 38: 1394-1402.

Kieber, D. J., and Blough, N. V., 1990a. Determination of carbon-centered radicals in aqueous solution by liquid chromatography with fluorescence detection. Anal. Chem., 62: 2275-2283.

Kieber, D. J., and Blough, N. V., 1990b. Fluorescence detection of carbon-centered radicals in aqueous solution. Free Rad. Res. Comms., 10: 109-117.

Mill, T., 1980. Chemical and photo oxidation. In: O. Hutzinger (Editor), The Handbook of Environmental Chemistry, Vol. 2, Part A. Springer, Berlin, pp. 77-105.

Mill, T., Hendry, D. G. and Richardson, H., 1980. Free-radical oxidants in natural waters. Science, 207: 886-887.

Mopper, K. and Zhou, X., 1990. Hydroxyl radical photoproduction in the sea and its potential impact on marine processes. Science, 250: 661-664.

Mopper, K., Zhou, X., Kieber, R. J., Kieber, D. J., Sikorski, R. J. and Jones, R. D., 1991. Photochemical degradation of dissolved organic carbon and its impact on the oceanic carbon cycle. Nature, 353: 60-62.

Ononye, A. I., McIntosh, A. R., Bolton, J. R., 1986. Mechansim of the photochemistry of *p*-benzoquinone in aqueous solutions. 2. Optical flash photolysis. J. Phys. Chem., 90, 6270-6274.

Ononye, A. I., and Bolton, J. R., 1986. Mechansim of the photochemistry of *p*-benzoquinone in aqueous solutions. 1. Spin trapping and flash photolyxix electron paramagnetic resonance studies. J. Phys. Chem., 90,·6266-6270.

Scholes, G. and Willson, R. L., 1967. γ-Radiolysis of aqueous thymine solutions. Determination of relative reaction rates of OH radicals. Trans. Faraday Soc., 63: 2983-2993.

Technicon AutoAnalyzer Method for Nitrate and Nitrite Determination, 1970. Technicon Industrial Method #, 158-71W in Manual #TN0-0210-00, Technicon Industrial Systems.

Tewari, Y. B., Miller, M. M., Wasik, S. P., and Martine, D. E., 1982. Aqueous solubility and octanol-water partition coefficients of organic compounds at 25°C. J. Chem. Eng. Data, 27: 451-454.

Veltwisch, D., Janata, E., and Asmus, K.-D., 1980. Primary processes in the reaction of hydroxyl-radicals with sulphoxides. J. Chem. Soc., Perkin Trans. 2: 146-153.

Warneck, P. and Wurzinger, C., 1988. Product quantum yields for the 305-nm photodecomposition of NO_3 in aqueous solution. J. Phys. Chem., 92: 6278-6283.

Zafiriou, O. C. and Bonneau, R., 1987. Wavelength-dependent quantum yield of OH radical formation from photolysis of nitrite ion in water. Photochem. Photobiol., 45: 723-727.

Zafiriou, O. C. and True, M. B., 1979. Nitrate photolysis in seawater by sunlight. Mar. Chem., 8: 33-42.

Zehavi, D. and Rabani, J., 1972. The oxidation of aqueous bromide ion by hydroxyl radicals. A pulse radiolytic investigation. J. Phys. Chem., 76: 312-319.

Zepp, R. G., Braun, A., Hoigné, J., 1987a. Photoproduction of hydrated electrons from natural organic solutes in aquatic environments. Environ. Sci. Technol., 21: 485-90.

Zepp, R. G., and Cline, D. M., 1977. Rates of direct photolysis in aquatic environment. Environ. Sci. Technol., 11: 359-366.

Zepp, R. G., Hoigné, J. and Bader, H., 1987b. Nitrate-induced photo-oxidation of organic chemicals in water. Environ. Sci. Technol., 21: 443-450.

Zepp, R. G., Faust, B. C. and Hoigné, J., 1992. Hydroxyl radical formation in aqueous reactions (pH 3-8) of iron(II) with hydrogen peroxide: The photo-Fenton reaction. Environ. Sci. Technol., 26: 313-319.

Zhou, X. and Mopper, K., 1990. Determination of photochemically produced hydroxyl radicals in seawater and freshwater. Mar. Chem., 30: 71-88.

Appendix II: Humic Acid Fluorescence Lifetime Study Utilizing Time-Resolved Single Photon Counting

Introduction

The photochemistry and photophysics of chromophoric dissolved organic matter (CDOM) (and humic acids (HA) as a subset) found in natural waters are of interest for a number of reasons. In addition to playing a part in the geochemical cycling of carbon species (Introduction), and its potential importance in the production of hydroxyl radicals (Appendix I), it has been shown that CDOM can act as a direct sensitizer in reactions with a number of organic pollutants. Sensitizers are compounds which absorb light directly, and then either transfer the energy to oxygen or other compounds to initiate reactions or produce reactive transient intermediates (free radicals) that react with other compounds. CDOM can act as a sensitizer for both dissolved (Zepp et al., 1985) and sorbed compounds (Fisher et al., 1987, and references therein,; Zepp et al., 1981a,b; Amador et al., 1989; Gauthier et al., 1986). This is of interest as a number of studies have shown that organic pollutants, including polycyclic aromatic hydrocarbons and some pesticides, extensively sorb to CDOM (McCarthy and Jimenez, 1985; Hatcher et al., 1993; Carter and Suffet, 1982; Chiou et al., 1986). To better understand the photophysics and photochemistry of these materials, and quantify CDOM sensitization of organic pollutant reactions, it is necessary to know the kinetics of both quenching and sensitization. In addition, studies of the photophysical lifetimes and emission energies can give insight into the properties and nature of the underlying chromophores of the CDOM and how they are influenced by changes in solvent matrix such as salinity and pH.

Some of the transient intermediates produced in CDOM photochemistry have been identified (solvated electron, radical cations, triplet states; Power et al., 1987). However, all of the previous measurements of fluorescence lifetimes were performed with equipment that was laser pulse-width limited and therefore was not able to examine lifetimes shorter

than hundreds of picoseconds (Milne et al., 1987). The apparatus used here allows examination of lifetimes down to ~20 picoseconds and a significant population of the CDOM chromophore lifetimes were found in this range. The following work examines the fluorescence lifetimes of two different humic acids both in seawater and buffered Milli-Q water at two excitation wavelengths and a suite of emission wavelengths.

Theoretical Development

Mechanisms

There are two deexcitation pathways that produce photons from excited state CDOM (1) (denoted as CDOM*). In addition to direct fluorescence from the singlet state (2) which we measured, CDOM can undergo intersystem crossing (ISC) to the triplet state and phosphoresce (3-4). Since ISC involves a non-allowed electron spin flip, the triplet state (and thus phosphorescence) exhibits longer lifetimes than direct fluorescence.

$$^1\text{CDOM} + h\nu \longrightarrow {}^1\text{CDOM}^* \quad (1)$$

$$^1\text{CDOM}^* \xrightarrow{k_F(\phi = \sim 0.01)} h\nu + {}^1\text{CDOM} \quad (2)$$

$$\xrightarrow{k_{ISC}} {}^3\text{CDOM}^* \quad (3)$$

$$^3\text{CDOM}^* \xrightarrow{k_{PH}} h\nu + {}^1\text{CDOM} \quad (4)$$

In competition with the photon-producing deexcitation pathways are the various dark pathways. These unimolecular reactions include internal conversion (IC) within the molecule either from the singlet state (5) or inter-system crossing (ISC) from the triplet state after ISC from the singlet state (6) and direct photochemical reactions to make a product (P) (7,8). Bimolecular reactions include short-range collisional transfer (SRX) (9,10) and long-range, Förster transfer (LRX) (11,12) to an acceptor molecule (A).

Unimolecular Reaction

$$^1\text{CDOM}^* \xrightarrow{k_{IC}} {}^1\text{CDOM} \quad (5)$$

$$^3\text{CDOM}^* \xrightarrow{k_{ISC}} {}^1\text{CDOM} \quad (6)$$

$$^1\text{CDOM}^* \xrightarrow{k_p} p \quad (7)$$

$$^3CDOM^* \xrightarrow{k_p} p \quad (8)$$

Bimolecular Sensitization

$$^1CDOM^* + {}^1A \xrightarrow{k_{SRX}} {}^1CDOM + {}^1A^* \quad (9)$$

$$^3CDOM^* + {}^3A \xrightarrow{k_{SRX}} {}^1CDOM + {}^3A^* \quad (10)$$

$$^1CDOM^* + {}^1A \xrightarrow{k_{LRX}} {}^1CDOM + {}^1A^* \quad (11)$$

However, normally these reactions (9-11) do not occur because the lifetimes are too short and the concentrations too low. The most common mechanisms are fluorescence, internal conversion, intersystem crossing to the triplet, intramolecular quenching and product formation.

Quantum Yields and Lifetimes

Both steady-state and time-resolved experiments give information on the photophysical parameters of chromophores. The combination of the two can yield even more information. Here we will explore the measurements and calculations necessary to obtain as many parameters as possible from a combination of steady-state and time-resolved measurements for two chromophores. Later we will demonstrate it for HA lifetimes divided into three groups.

Different chromophores generally absorb differently at a given wavelength (Fig. 1) and can emit light at distinct or identical wavelengths (Fig. 2,3). The theory for both cases will be developed after some basic definitions.

Basic Definitions

The fluorescence quantum yield, ϕ, of a species is related to the ratio of photons emitted to those absorbed (12) which is also the ratio of the fluorescence, or radiative, rate constant to the sum of all rate constants, radiative and non-radiative (13).

$$\phi = \frac{\text{number of photons emitted}}{\text{number of photons absorbed}} \quad (12)$$

$$\phi = \frac{k_F}{k_F + k_{ISC} + k_{IC} + k_P + k_{SRX}[A] + k_{LRX}[A]} = \frac{k_r}{k_r + k_{nr}} \quad (13)$$

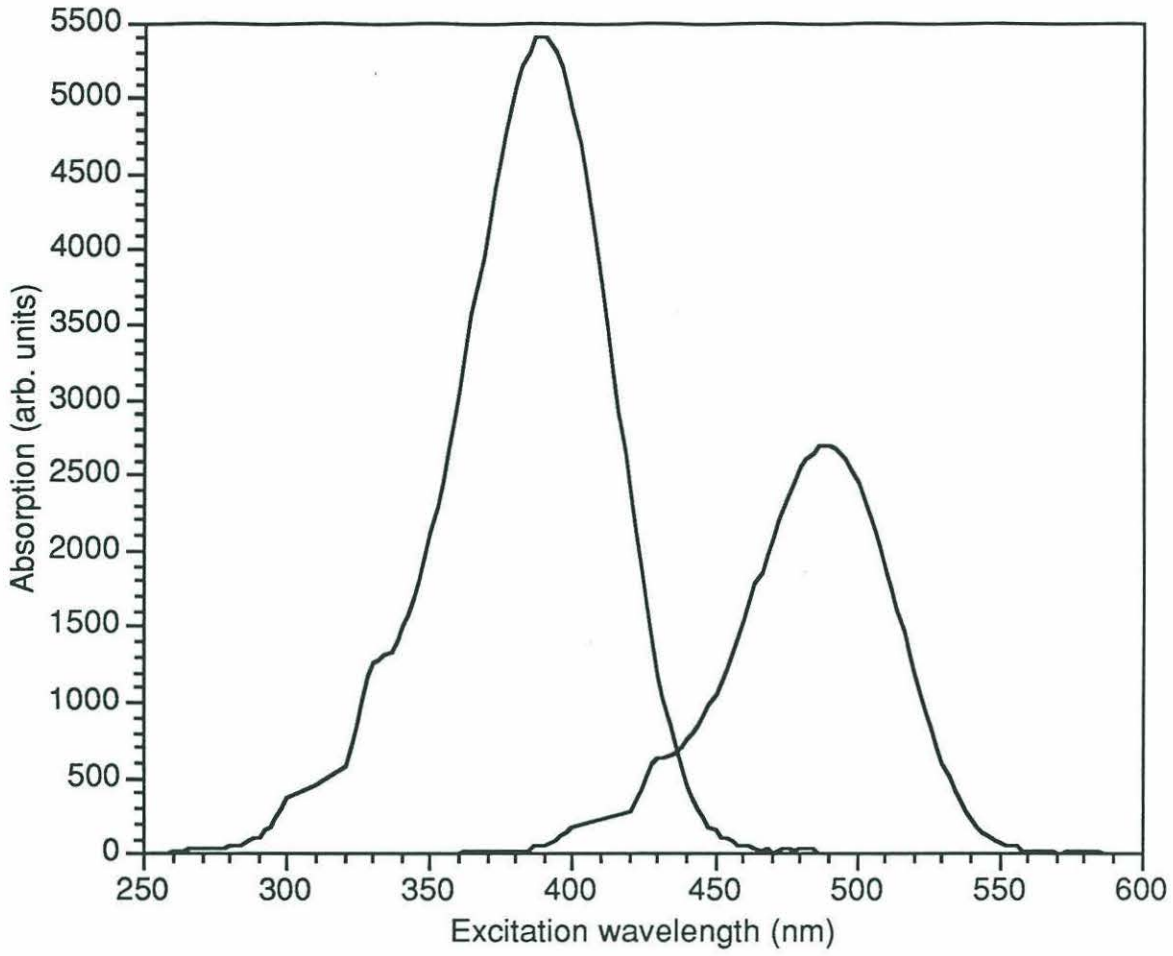

Figure 1. Plot of two stylized chromophores with distinct absorption spectra.

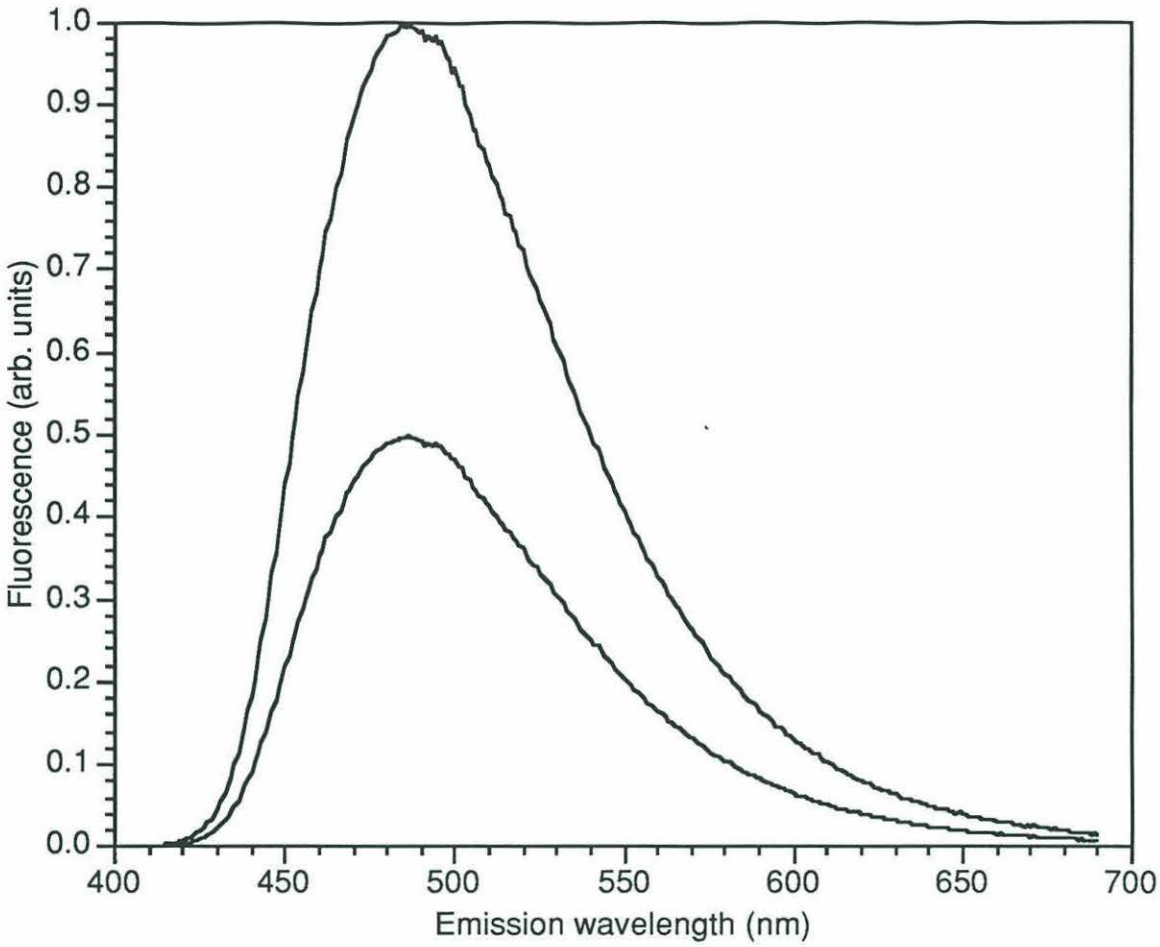

Figure 2. Plot of two stylized chromophores with identical fluorescence emission spectra.

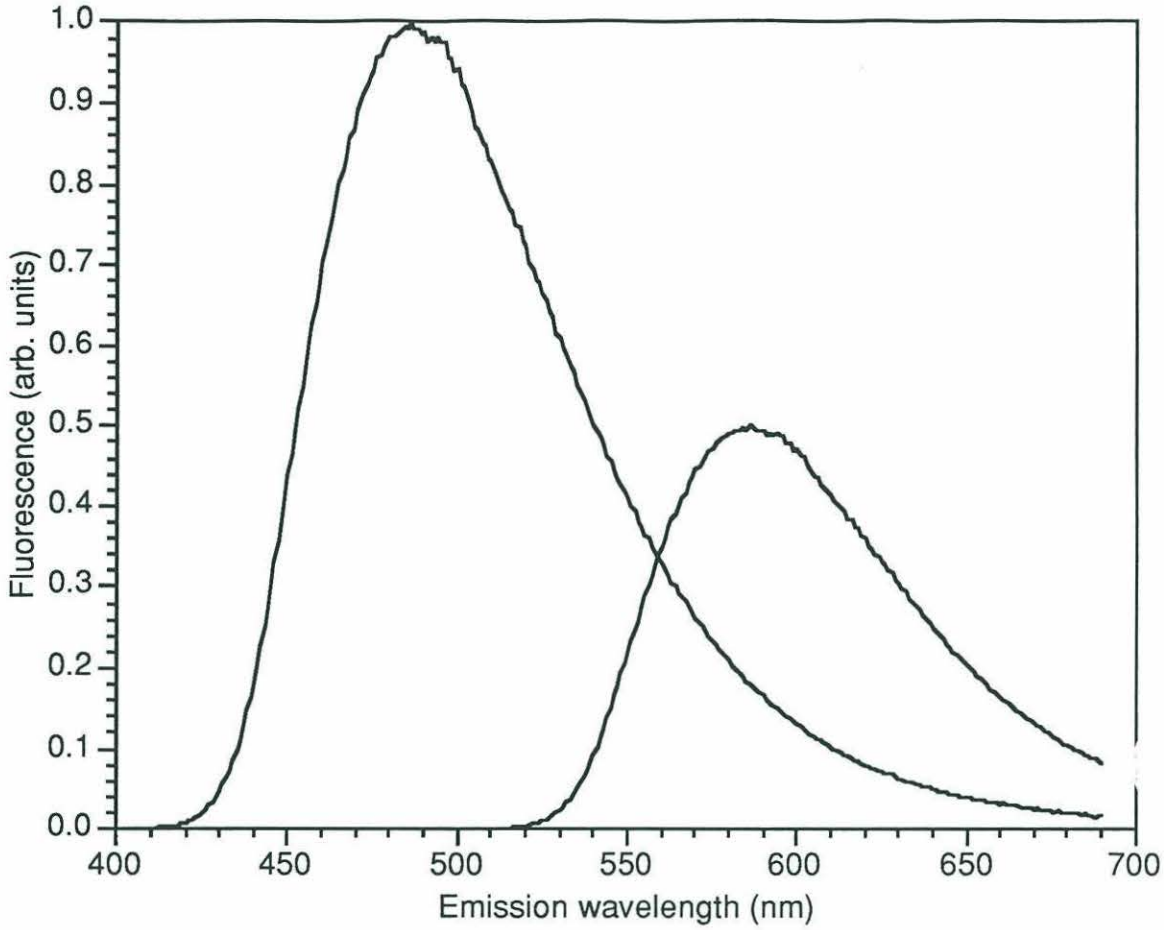

Figure 3. Plot of two stylized chromophores with distinct fluorescence emission spectra.

The total quantum yield of a multi-component system such as humic acids can be determined experimentally with respect to a compound of known fluorescence quantum yield such as quinine sulfate,

$$\phi_T = \frac{F_s A_{qs} \phi_{qs}}{A_s F_{qs}} \tag{14}$$

where ϕ_T and ϕ_{qs} are the quantum yields of the mixture and quinine sulfate (qs), respectively, A the absorbance at the excitation wavelength and F the integrated fluorescence of the sample (s) or quinine sulfate (qs).

When analyzing a mixture of chromophores, it is necessary to know the fractional absorption contribution, c_i, of each component at the excitation wavelength used before the individual component quantum yields, ϕ_i, can be calculated, as

$$\phi_T = \Sigma c_i \phi_i \tag{15}$$

where, by definition,

$$\Sigma c_i(\lambda) = 1 \tag{16}$$

Steady-state fluorescence spectra are used to calculate the total quantum yield, ϕ_T, and also give the photon per wavelength information necessary to gain more information from time-resolved fluorescence measurements. Time-resolved fluorescence spectra consist of an initial rise due to the laser pulse and then an exponential decrease in photon counts with increasing time after the pulse (Fig. 4). Individual lifetimes are deconvoluted using an exponential fitting program. The output of the program consists of the lifetimes and the contribution of each lifetime to the whole as is consistent with an exponential fit of the form

$$<\tau> = \int_0^\infty a_1 e^{-\frac{1}{\tau_1}t} = a_1\tau_1 \tag{17}$$

for one fluorescent component and

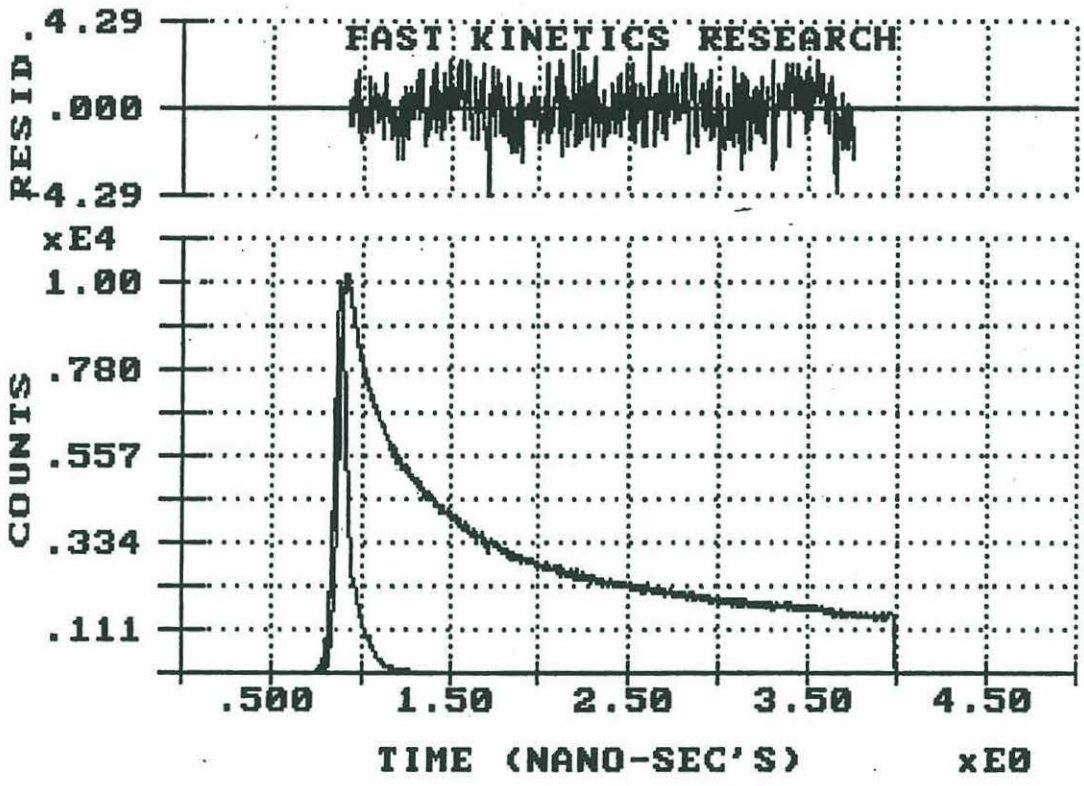

Figure 4. Time-resolved fluorescence spectrum of SRHA in standard buffer along with the instrument response function (IRF) on a 3 ns scale. Excitation was at 290 nm and emission at 440 nm.

$$<\tau>=\int_0^{\infty}\Sigma a_i(\lambda)e^{-\frac{1}{\tau_i}t}=\Sigma a_i(\lambda)\tau_i \qquad (18)$$

for three fluorescent components where $<\tau>$ is the average lifetime, t is time, τ_i is the lifetime and $a_i(\lambda)$ the fractional amplitude of the ith fluorescing component at wavelength, λ. By definition

$$\Sigma a_i(\lambda) = 1 \qquad (19)$$

The fluorescence lifetime of a component, τ_i, is determined by the reciprocal of the sum of the rate constants

$$\tau_i = \frac{1}{k_r + k_{nr}} \qquad (20)$$

It should be noted that the value of τ_i is dependent on the mechanism of deexcitation and is generally constant over all emission wavelengths for a given component. We can now relate ϕ_i and τ_i by taking the ratio of (13) to (20) and rearranging to get

$$\phi_i = \tau_i k_r \qquad (21)$$

The fractional fluorescence contribution of an individual component at wavelength λ, $f_i(\lambda)$, to the total time-resolved fluorescence can be calculated from the time-resolved data as follows

$$f_i(\lambda) = \frac{\tau_i a_i(\lambda)}{\Sigma \tau_i a_i(\lambda)} \qquad (22)$$

This can be converted into the fraction of total steady-state fluorescence, $F_i(\lambda)$ by multiplying $f_i(\lambda)$ by the total fluorescence at each wavelength, $F_T(\lambda)$

$$F_i(\lambda) = f_i(\lambda) * F_T(\lambda) \qquad (23)$$

These are all of the basic quantities that will be used in the following discussion.

Calculation of c_i and ϕ_i when all components have identical emission spectra

In the case of a multi-component system in which all of the components have identical emission spectra (Fig. 2),

$$\phi_T = \Sigma c_i \phi_i(\lambda) \qquad (24)$$

as the relative time-resolved fluorescence contribution of each of the components is constant with emission wavelength (Fig. 5). Thus, the ratio of the quantum yield of (fluorescence by) an individual component to the total quantum yield (fluorescence) is

$$\frac{c_i\phi_i(\lambda)}{\phi_T} = \frac{F_i(\lambda)}{F_T(\lambda)} = f_i(\lambda) = \frac{a_i(\lambda)\tau_i}{\Sigma a_i(\lambda)\tau_i} \tag{25}$$

In a two component system, the ratio of the first and second components leads to

$$\frac{c_1\phi_1(\lambda)}{\phi_T} * \frac{\phi_T}{c_2\phi_2(\lambda)} = \frac{a_1(\lambda)\tau_1}{\Sigma a_i(\lambda)\tau_i} * \frac{\Sigma a_i(\lambda)\tau_i}{a_2(\lambda)\tau_2} \tag{26}$$

which simplifies to

$$\frac{c_1\phi_1(\lambda)}{c_2\phi_2(\lambda)} = \frac{a_1(\lambda)\tau_1}{a_2(\lambda)\tau_2} \tag{27}$$

Substituting in (20) leads to

$$\frac{c_1\tau_1(\lambda)k_{r1}}{c_2\tau_2(\lambda)k_{r2}} = \frac{a_1(\lambda)\tau_1}{a_2(\lambda)\tau_2} \tag{28}$$

If the radiative rate constants, k_{r1} and k_{r2} are the same, then

$$\frac{c_1}{c_2} = \frac{a_1(\lambda)}{a_2(\lambda)} \tag{29}$$

and, recalling (16,20)

$$c_1=a_1(\lambda) \qquad \text{and} \qquad c_2=a_2(\lambda) \tag{30}$$

Substituting into (25) we obtain,

$$\phi_1(\lambda) = \frac{F_1(\lambda)\phi_T}{a_1(\lambda)F_T(\lambda)} \quad \text{and} \quad \phi_2(\lambda) = \frac{F_2(\lambda)\phi_T}{a_2(\lambda)F_T(\lambda)} \tag{31}$$

which can be calculated as we can measure $a_1(\lambda)$,$a_2(\lambda)$,ϕ_T,$F_T(\lambda)$ and calculate $F_1(\lambda)$,$F_2(\lambda)$ from $F_T(\lambda)$, $a_1(\lambda)$,$a_2(\lambda)$,τ_1 and τ_2. More generally for systems of greater than two component chromophores with identical emission spectra

$$\phi_i = \frac{\tau_i\phi_T\Sigma_i F_i'}{F_T} \tag{32}$$

If k_{r1} and k_{r2} are not the same, then it is necessary to collect data at two excitation wavelengths to calculate the individual quantum yields, ϕ_i.

In the more common case of a multi-component system in which the individual chromophores have distinct emission spectra, the process of calculating the individual

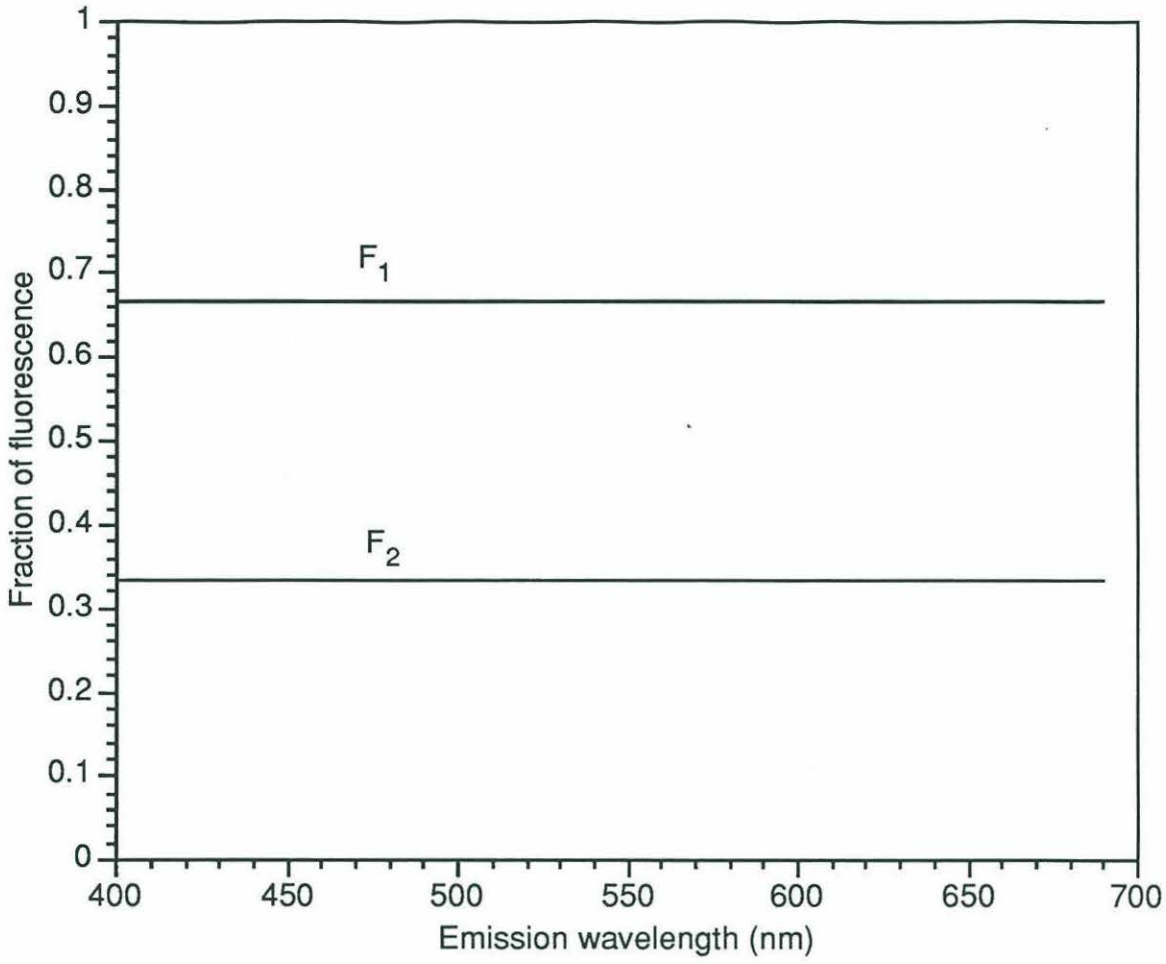

Figure 5. Change in fractional fluorescence contribution, $f_i(\lambda)$, of two chromophores with identical excitation wavelength and emission spectra wavelength.

quantum yields is a bit more complex, but can still be done as long as all of the lifetimes can be satisfactorily resolved and data is collected over all relevant emission wavelengths.

Calculation of c_i and ϕ_i when all components have distinct emission spectra

In the more common case of a multi-component system in which the individual chromophores have distinct emission spectra (Fig. 3), the process of calculating the individual quantum yields is more complex, but can still be done if fluorescence lifetimes can be resolved and are determined for all relevant emission wavelengths.

For this case, (15) holds true, but (24) no longer does,

$$\phi_T \neq \Sigma c_i \phi_i(\lambda) \tag{33}$$

as the relative time-resolved fluorescence contribution of each of the components changes with emission wavelength (Fig. 6). We find it convenient to define

$$f_i'(\lambda) = \frac{f_i(\lambda)}{\tau_i} = \frac{a_i(\lambda)}{\Sigma a_i(\lambda)\tau_i} \tag{34}$$

In order to compensate for the distinct emission spectra of the individual components, we must calculate the sum of $F_i(\lambda)$ over all emission wavelengths

$$F_i = \int_\lambda F_i(\lambda)d\lambda = \tau_i \int_\lambda f_i'(\lambda)F(\lambda)d\lambda \tag{35}$$

so that now

$$F_T = \Sigma_i F_i \tag{36}$$

In this case, the ratio of the quantum yield of an individual component to the total quantum yield is equal to the ratio of the fluorescence due to an individual component to the total fluorescence of all of the components

$$\frac{c_i\phi_i}{\phi_T} = \frac{F_i}{F_T} = \frac{F_i'\tau_i}{F} \tag{37}$$

Substituting in (15) leads to

$$\frac{c_i\tau_i k_{ri}}{\phi_T} = \frac{\tau_i F_i'}{F} \tag{38}$$

Which rearranges to

$$c_i = \frac{F_i'\phi_T}{k_{ri}F} \tag{39}$$

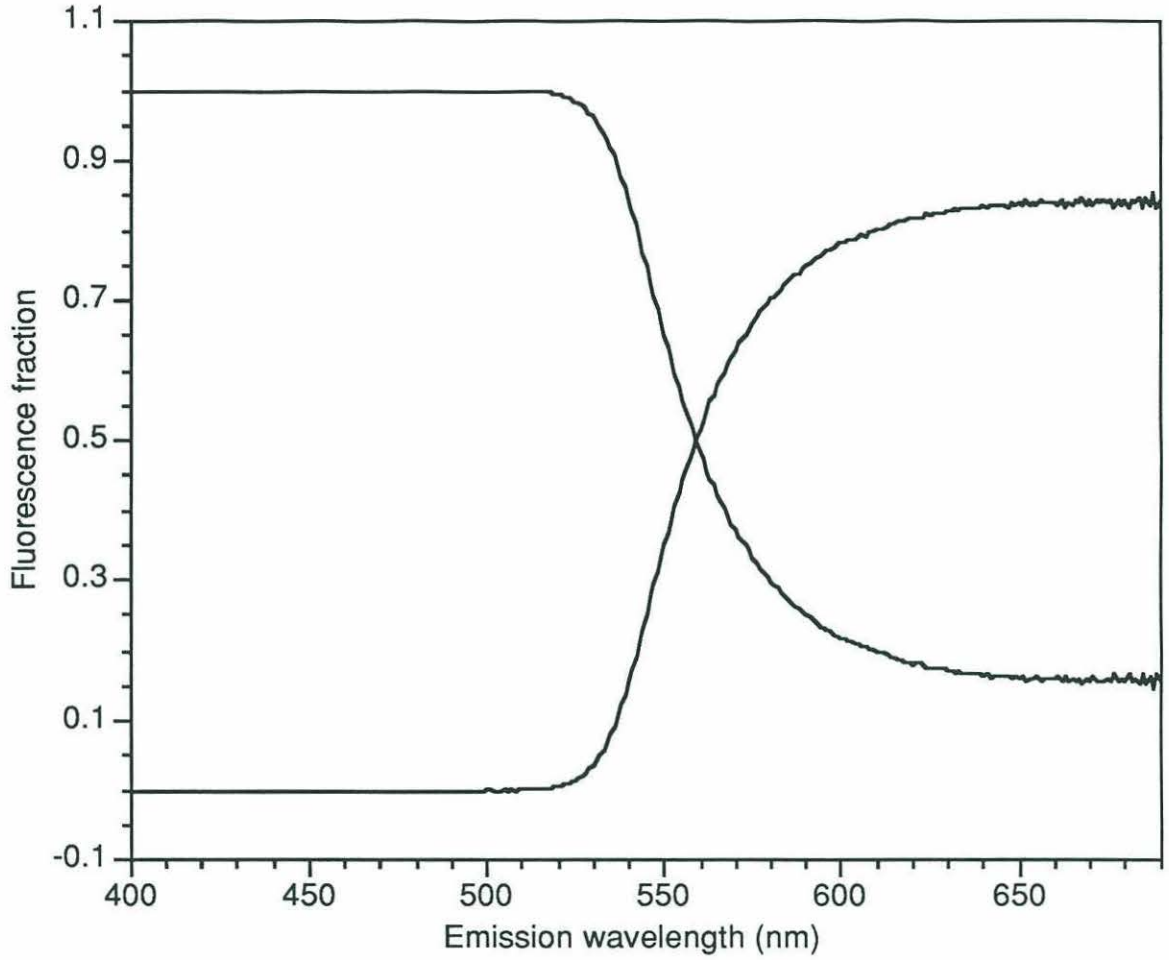

Figure 6. Change in fractional fluorescence contribution, $f_i(\lambda)$, of two chromophores with distinct emission spectra wavelength.

In a two component system, the ratio of the first and second components leads to

$$\frac{c_1}{c_2} = \frac{F_1'\phi_T}{k_{r1}F_T} * \frac{k_{r2}F_T}{F_2'\phi_T} \tag{40}$$

If the radiative rate constants, k_{r1} and k_{r2} are the same, then

$$\frac{c_1}{c_2} = \frac{F_1'}{F_2'} \tag{41}$$

and, recalling (15)

$$c_1 = \frac{F_1'}{F_1'+F_2'} \qquad \text{and} \qquad c_2 = \frac{F_2'}{F_1'+F_2'} \tag{42}$$

Rearranging (37) and substituting in (42) gives

$$\phi_1 = \frac{\tau_1(F_1'+F_2')\phi_T}{F_T} \qquad \text{and} \qquad \phi_2 = \frac{\tau_2(F_1'+F_2')\phi_T}{F_T} \tag{43}$$

which can be calculated as we can measure τ_1,τ_2,ϕ_T,F_T and calculate F_1' and F_2' from F_T, $a_1(\lambda),a_2(\lambda),\tau_1$ and τ_2.

For a two component system, if k_{r1} and k_{r2} are not the same, then it is necessary to collect data at two excitation wavelengths as well as all of the important emission wavelengths in order to calculate the individual quantum yields, ϕ_i.

Thus, with a combination of steady-state absorbance and fluorescence data and time-resolved fluorescence life-times, the quantum yields of individual components can be calculated. It should be noted however, that in the case of SRHA and ORHA there may be a continuum of components that are artificially grouped (into three categories for our data) by the nature of the analysis.

Experimental

Reagents

Water used in all experiments was from a Millipore Milli-Q system. Standard buffer was 0.2 M, pH 8.1 borate. Sea water was collected from 10 m depth at the BATS site southwest of Bermuda on the RV *Weatherbird II* and stored at room temperature in the dark. Suwanee River humic acid (SRHA) was purchased from the U.S. Geological

Survey, Denver and used as received. Orinoco River humic acid (ORHA) was collected and concentrated as described by Blough et al. (1993).

Apparatus

Time-Resolved

A mode-locked, cavity-dumped, synchronously-pumped Nd-YAG laser exciting at 290 nm (Rhodamine 6G dye, doubled) or 590 nm (Rhodamine 6G dye) was used to perform single photon counting fluorescence measurements on humic acids (Chapter 2). At the 290 nm excitation wavelength, <290 nm and >310 nm cutoff filters were placed in front of the monochromator to reduce scatter. The monochromator was tuned between 350 and 650 nm; entrance and exit slits were adjusted to obtain a counting rate of 4000-5000 photons per second impinging on the photomultiplier tube. Before collecting lifetime data, a rough emission spectrum of photon intensity versus wavelength was collected by averaging a series of 10 to 15 readings from the photomultiplier bin readout at the wavelengths of interest. Between 5000 and 10000 photon counts were collected for most samples. For the experiment with excitation at 290 nm and emission at 650 nm only 1200-1500 counts were collected due to the very slow photon emission rate at this wavelength. Varying time bases were used (between 5 and 100 ns) to collect information on different decay processes. Decay curves were deconvoluted and fit to three exponentials with software described above (Chapter 2). The temporal resolution of this system is ~20 picoseconds.

Steady-State

Absorption spectra were collected with a Hewlett-Packard 8451 A diode array spectrophotometer (2 nm resolution), while steady-state fluorescence spectra were recorded with an Aminco-Bowman 2 Luminescence spectrometer employing 4 nm excitation and emission bandpasses, an excitation wavelength of 290 nm. Samples were thermostated to

23°C. Quantum yield measurements were made relative to quinine sulfate in 0.1N H_2SO_4 where $\phi_{qs} = 0.55$ (14).

Sample Preparation

Sufficient Suwanee River or Orinoco River humic acid was added to Milli-Q water or filtered (0.45 μm nylon syringe filter) sea water in a 1 cm quartz cuvette to achieve an optical density of ~0.1 at 290 nm. Some samples were deaerated with nitrogen before analysis but, not surprisingly, this was found to be unnecessary for the short lifetimes encountered (0.02 to 6 ns). In air-saturated aqueous solutions where oxygen is the primary quencher, it only becomes efficient when the lifetimes of the compounds or interest are close to the quenching rate of oxygen in solutions which is 20 to 50 ns.

Results and Discussion

Steady-State Measurements

As has been seen previously (Zepp and Schlotzhauer, 1981; Bricaud et al., 1981; Blough et al., 1993), the absorption spectrum of humic acids consists of a featureless exponential decrease in absorbance from the ultraviolet into the visible wavelengths (Fig. 7).

The rough emission spectrum of photon intensity versus wavelength from the laser measurements is shifted about 50 nm to the blue (450 nm) from that obtained with the AB2 steady-state fluorescence instrument (500 nm) (Fig. 8). This offset may be due to the gating of the photons measured on the time-resolved laser system which causes it to be biased towards the shorter lifetimes. An effect has also been seen in the values of the deconvolved fluorescence lifetimes on different time bases (vide infra).

The fluorescence quantum yield of SRHA in standard buffer (Table 1) was similar to those measured by Zepp and Schlotzhauer (1981) and Green and Blough (submitted) for a number of different soil and riverine humic materials. In addition to the total quantum

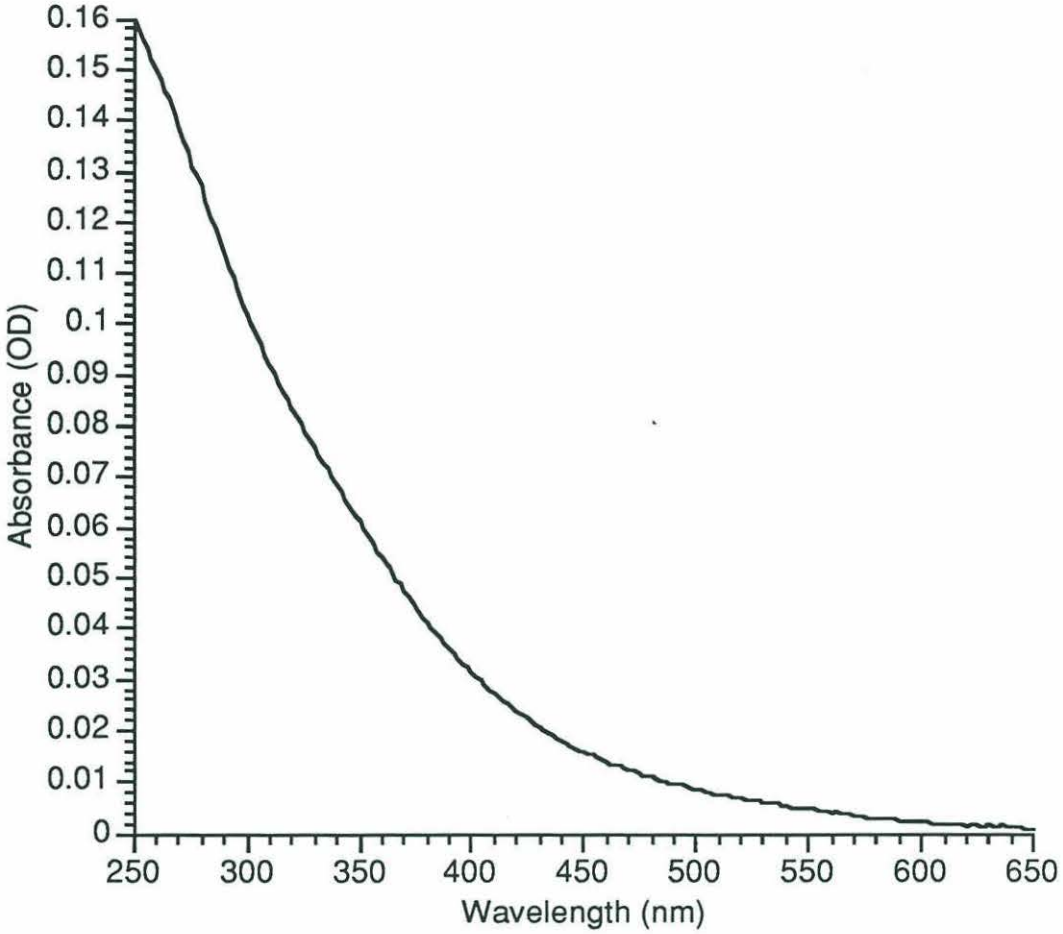

Figure 7. Absorption spectrum of SRHA in standard buffer.

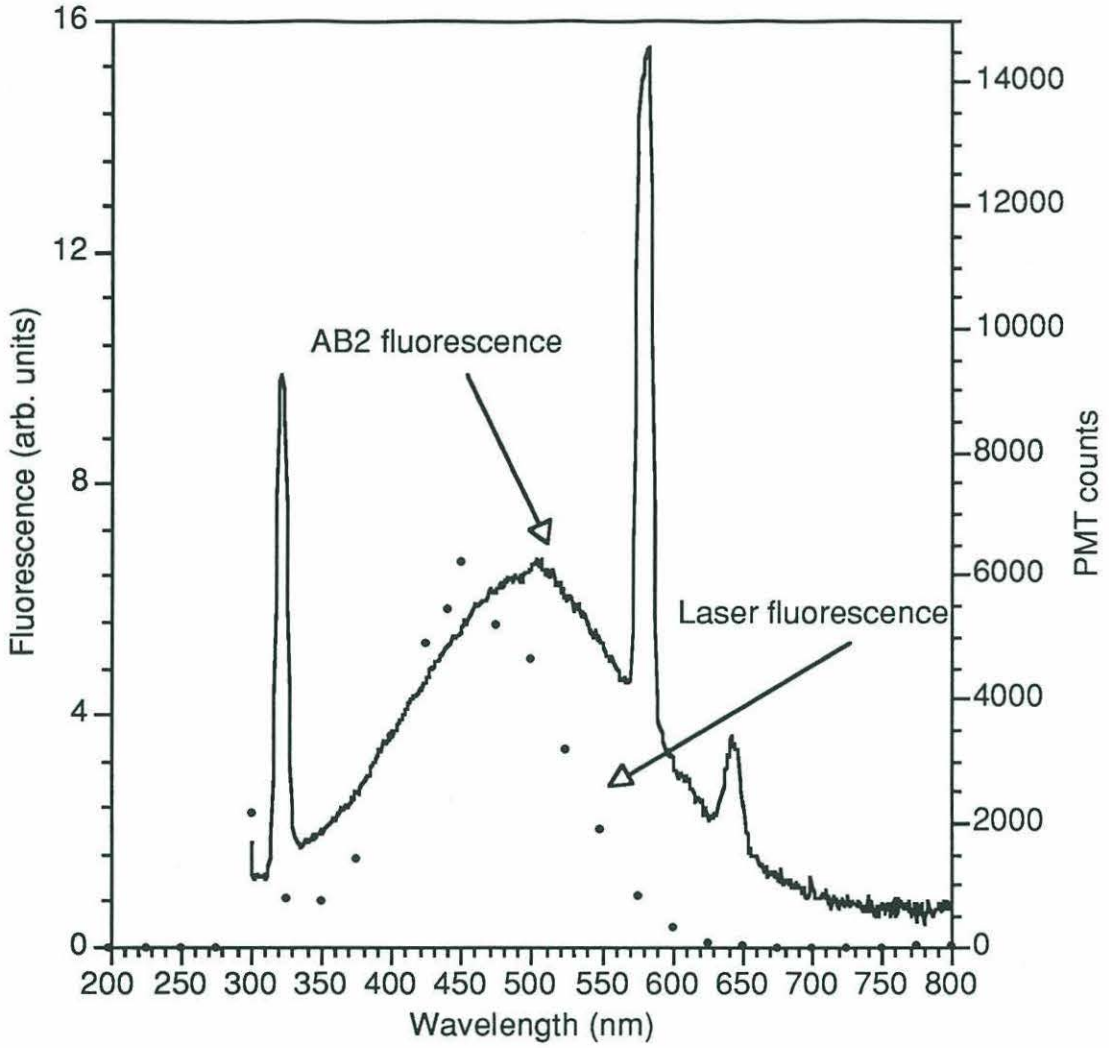

Figure 8. Comparison of laser and steady-state fluorescence spectra of SRHA in standard buffer. The peak at 300 nm in the laser fluorescence spectrum is due to scatter from the 290 nm excitation line. In the steady-state spectrum, the peak at 580 nm is the second-order excitation line and peaks at 322 and 644 nm are water Raman lines. Excitation was at 290 nm.

yield (300 to 800 nm), two partial quantum yields were measured over the wavelengths at which time-resolved fluorescence lifetimes were measured.

Table I. Fluorescence Quantum Yields

Material	Quantum Yield over		
	300 to 800 nm	350 to 650 nm	350 to 550 nm
SRHA	0.0030	0.0025	0.0019

Time-Resolved Measurements

Deconvolution

For both SRHA and ORHA, three lifetimes were clearly distinguishable using a three exponential fitting program (Fig. 4). The output of the program consists of the three lifetimes and the contribution of each lifetime to the total photon output, as is consistent with an exponential fit (18) (Table II). Fitting with fewer exponentials was not tried, but the program did not cause two of the lifetimes to converge to a single value (as it has done with other compounds when they had fewer distinguishable lifetimes than the number of exponentials selected for fitting.)

The use of different time bases for data collection caused some variation in the lifetime values obtained. For the shortest lived component, τ_1, the use of a 5 ns timebase resulted in values that ranged from 0.019 to 0.064 ns while use of 20 to 100 ns timebases resulted in values between 0.046 to 0.28 ns. This is probably an effect of a preferential weighting of the data available to the deconvolution and fitting program and the fact that there is probably a large number of components that we are artificially grouping into three categories. The short lived components are better resolved on a shorter timebase as they constitute a greater portion of the fit; similarily, the long lived components are better resolved on a longer timebase (Chapter 2).

Table II. Time-Resolved Fluorescence Lifetime Data

Emission λ (nm)	time base	τ_1 (ns)	c_1 (%)	f_1 (%)	τ_2 (ns)	c_2 (%)	f_2 (%)	τ_3 (ns)	c_3 (%)	f_3 (%)
SRHA excited at 290 nm										
350	5	0.019	85	9	0.50	12	35	2.9	3.3	55
350	20	0.060	71	11	0.78	26	52	5.2	2.9	37
360	20	0.16	59	14	0.96	36	50	5.1	4.8	36
360	5	0.039	67	6	0.51	27	33	4.2	5.9	60
370	5	0.039	68	6	0.51	26	30	4.2	6.6	64
380	5	0.036	69	6	0.49	24	26	4.0	7.4	68
390	5	0.043	66	5	0.49	26	24	4.2	8.7	70
400	5	0.045	65	5	0.50	26	23	4.4	9.1	72
410	5	0.046	66	5	0.49	25	21	4.4	9.8	74
420	5	0.042	67	5	0.48	24	20	4.6	9.6	76
430	5	0.048	64	4	0.51	26	19	5.3	10	77
440	5	0.035	71	4	0.44	19	15	4.2	11	81
440	20	0.22	61	12	1.5	29	41	5.7	9.1	47
440	40	0.20	64	13	1.5	28	41	5.8	8.0	46
440	100	0.28	69	18	1.8	25	42	6.2	6.7	40
450	5	0.052	64	5	0.50	24	18	4.2	12	77
450	20	0.090	70	9	1.2	22	36	5.2	7.7	56
460	5	0.044	64	4	0.48	26	17	5.9	10	80
470	5	0.047	64	4	0.49	26	16	6.1	10	80
480	5	0.053	63	5	0.47	24	16	4.0	13	79
490	5	0.064	61	5	0.51	26	17	4.5	13	78
500	5	0.048	67	5	0.47	22	17	4.5	11	78
510	5	0.058	64	5	0.51	25	17	5.1	12	78
520	5	0.052	64	5	0.44	25	17	4.2	12	78
520	20	0.16	67	12	1.2	24	34	5.4	8.9	54
530	5	0.043	67	5	0.39	22	17	3.7	11	78
540	5	0.041	69	6	0.38	21	17	3.6	10	77
550	5	0.043	69	5	0.43	21	15	5.1	9.5	80
550	20	0.16	67	12	1.2	23	31	5.2	9.8	57
650	5	0.034	87	18	0.37	10	22	3.2	3.1	60
650	20	0.046	88	21	0.64	10	32	3.8	2.4	47
SRHA excited at 590 nm										
640	20	0.022	90	14	0.50	8	28	3.5	2.4	58
650	20	0.030	86	14	0.48	11	29	3.3	3.1	57
660	20	0.033	86	16	0.52	11	31	3.5	2.8	53
ORHA excited at 590 nm										
650	20	0.018	90	10	0.57	7	27	3.7	2.7	63
ORHA excited at 290 nm										
440	20	0.15	60	8	1.4	29	36	5.4	11	56
550	20	0.19	63	11	1.5	27	35	6.1	10	54
650	20	0.080	72	11	0.72	20	29	3.9	7.8	60
SRHA in seawater excited at 290 nm										
440	20	0.11	61	7	1.1	26	28	4.8	13	65

τ_i is the lifetime, c_i the contribution, and f_i the fractional contribution of the ith component. Chi^2 values were between 0.93 and 2.7 for this data set.

Wavelength Dependence of Fluorescence Lifetimes

As expected, (vide supra) fluorescence lifetimes were nearly constant across all emission wavelengths examined (Fig. 9) The anomalously short lifetime at 650 nm may be real, but could also result from the collection of a lesser number of counts at this wavelength. The intermediate lifetimes, τ_2, ranged from 0.37 to 0.51 ns on the 5 ns timebase (0.63 to 1.8 ns on 20 to 100 ns timebases), and the shortest lifetimes, τ_1, ranged from 34 ps to 64 ps (with one 19 ps value) on the 5 ns timebase (46 to 280 ps on the 20 to 100 ns timebases) (Table I). All except for the single 19 ps value are above the detection limit of about 20 ps.

Individual Chromophore Contribution to Time-Resolved Fluorescence and Quantum Yields

The fractional contribution to time-resolved fluorescence, $F_i(\lambda)$, varies with emission wavelength as is expected for chromophores with distinct emission spectra (Fig. 6,10). $F_1(\lambda)$ remains relatively constant across the wavelengths examined, while $F_2(\lambda)$ decreases from 350 to 550 and $F_3(\lambda)$ increases to a plateau (and maybe decreases to 650 although this data point is questionable as discussed above.) Thus the second set of equations, (33) to (44), is used to calculate the component quantum yields.

Table III. Calculated Relative Absorption and Quantum Yields for each Component[a]

	350 to 650		350 to 550	
Component	c_i	ϕ_i	c_i	ϕ_i
1	0.68	2.0×10^{-4}	0.67	1.4×10^{-4}
2	0.227	2.1×10^{-3}	0.234	1.6×10^{-3}
3	0.095	2.0×10^{-2}	0.100	1.5×10^{-2}

[a]Assumes that all components have the same radiative rate constant, kr.

The results indicate an insensitivity to the wavelength range used in the calculations which suggests that the $F_i(\lambda)$ are not dependent on emission wavelength (Fig. 11).

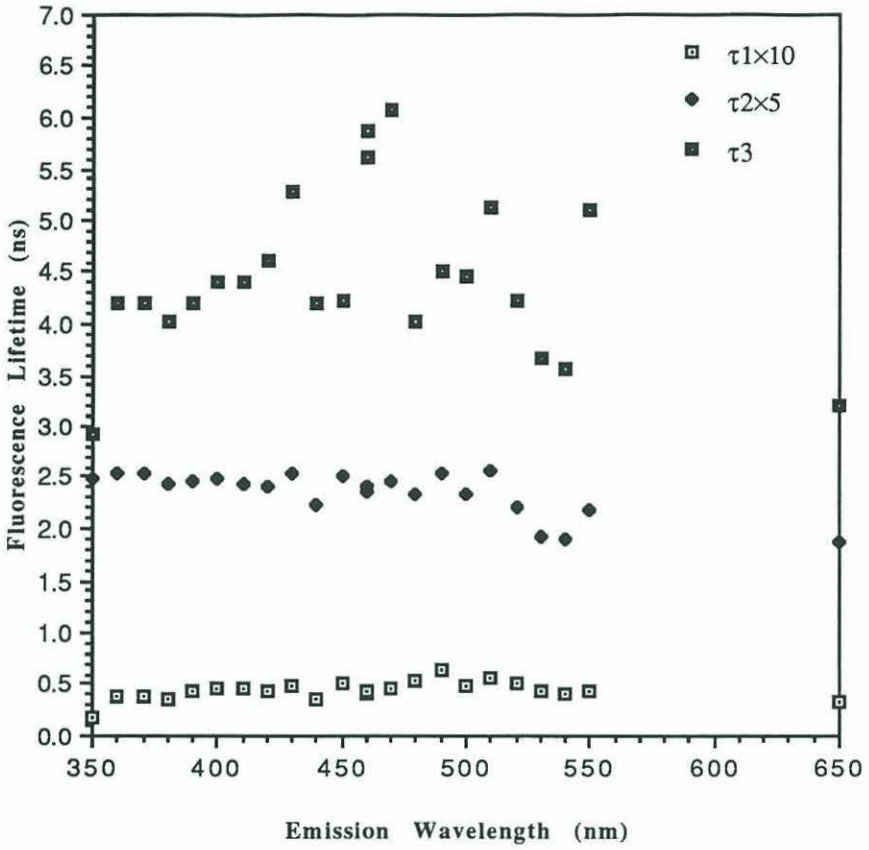

Figure 9. The three deconvoluted fluorescence lifetimes of SRHA in standard buffer vs emission wavelength. τ_2 values are multiplied by 5 and τ_3 values by 10 to make trend comparison easier. Excitation was at 290 nm.

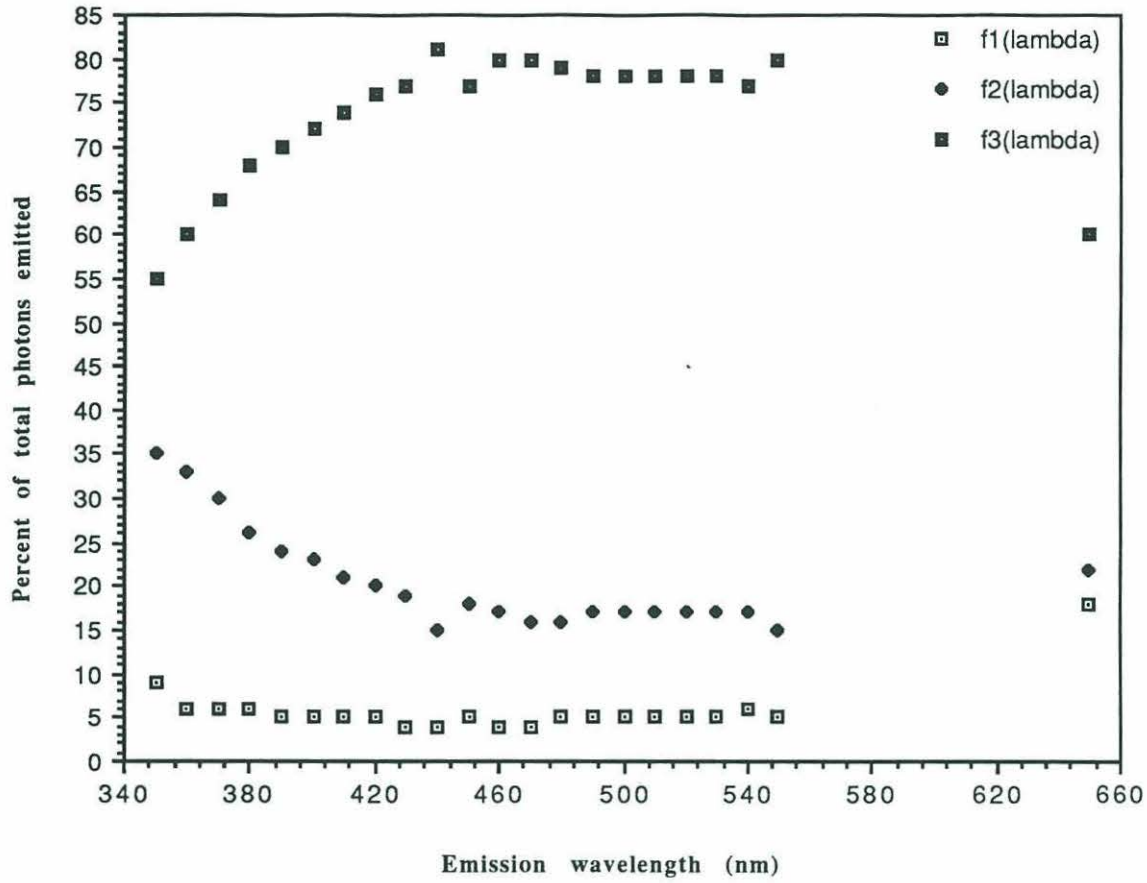

Figure 10. Wavelength dependence of the fractional fluorescence contribution of the three component species of SRHA for excitation at 290 nm.

Contribution to Steady-State Fluorescence

Of great interest are the fractional contributions of the three components. From the time-resolved data, the fractional contribution of each of the three individual lifetimes to the total steady-state fluorescence was calculated (22). The shortest lived component, τ_1, represents between 61 and 85% of the total decay. However, its contribution, f_1, to the steady-state fluorescence is only 4 to 21%. Thus steady-state measurements grossly misrepresent the abundance (and also the importance) of the short-lived, picosecond time range components. Multiplying the fractional contribution of each fluorescence lifetime by the fluorescence intensity at the corresponding wavelength leads to a graphic comparison of this issue (Fig. 11).

Comparisons between types of HA and solvents

The differences between excitation at 590 nm and 290 nm with emission at 650 nm on a 20 ns time scale are minimal for SRHA (Table II). No large differences were observed between SRHA and ORHA fluorescence lifetimes, and the change of solvent from buffer to seawater does not result in a discernible difference. These results agree with the results of Milne et al. (1985) who found very little variation between several types of CDOM in solutions of different pHs and salinities.

Comparison with other workers

Previously Milne et al. (1987) found that they could fit their data with a single exponential decay. We can compare our data with theirs by recombining the three individual exponentials into an average lifetime, $\langle\tau\rangle$, (2). This study's average lifetimes for ORHA (3.21-3.53 ns), SRHA in buffer (3.45 ns) and in seawater (3.37-3.41 ns) at 650 nm show only slight variations 3.4 ($\pm$ 0.2) in agreement with results by Milne et al. (1987). However their values, 2.2 ($\pm$ 0.2) at 460 nm, differ significantly from those of

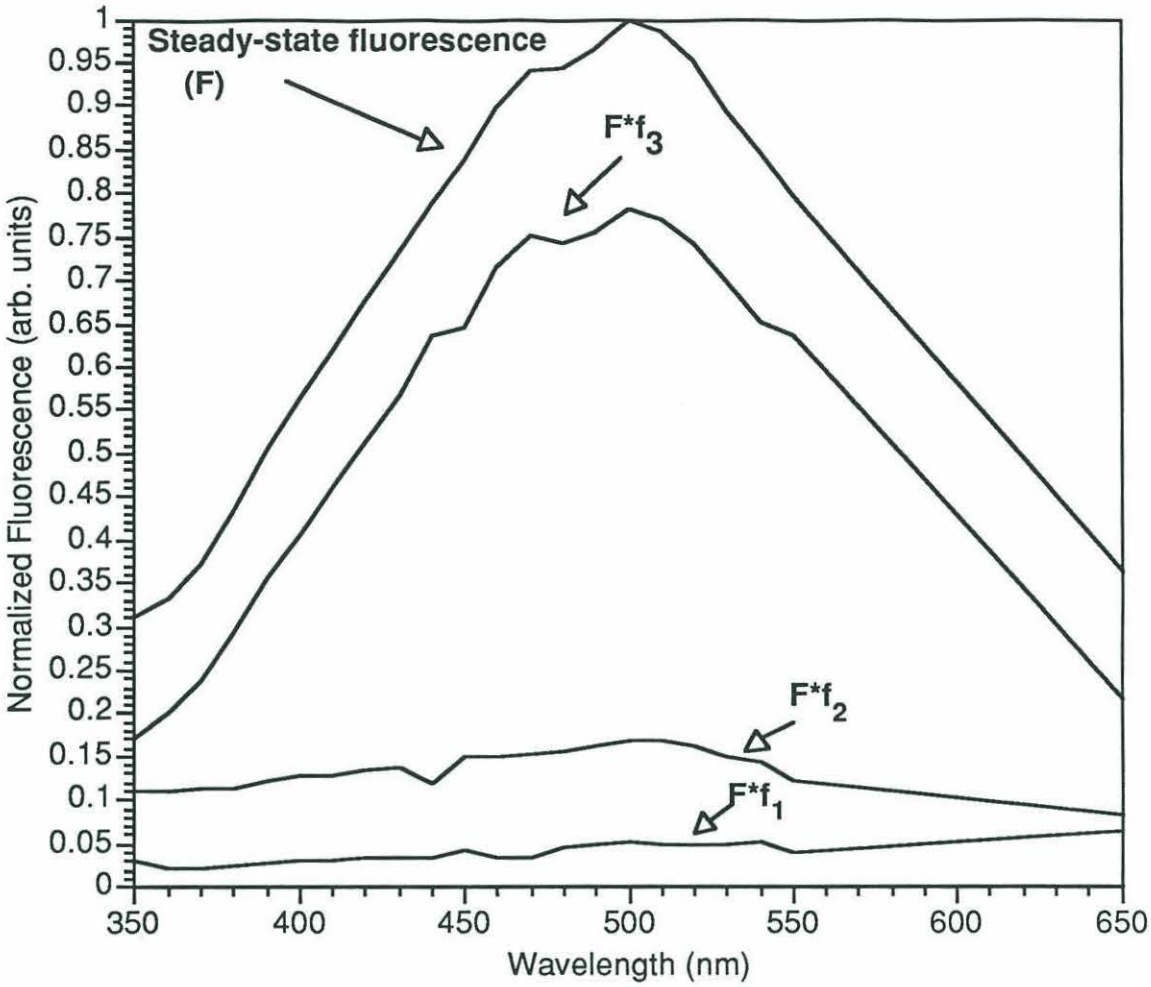

Figure 11. Fraction contribution of each of the three time-resolved lifetimes (f_i) to the steady-state fluorescence spectrum (excitation 290 nm) vs emission wavelength.

this study, 4.55 - 4.75 ns for SRHA in buffer at 460 nm. This may be due to the different time scales investigated.

Conclusions

The above data show that at least three individual lifetimes can be distinguished by iterative deconvolution. The majority of fluorescent chromophores in HA have very short (20-60 ps) lifetimes. From steady-state quantum yields and time-resolved fluorescence data across a suite of emission wavelengths the individual chromophore quantum yields can be calculated assuming identical radiative rate constants. Shorter fluorescent lifetimes for a given chromophore center within CDOM result in smaller quantum yields and may be caused by very rapid competing intramolecular dark pathways such as energy or electron transfer

Preliminary work investigating changes in time-resolved fluorescent lifetimes due to different sources of CDOM (Orinoco vs Suwanee Rivers), solution types (seawater vs standard buffer) has shown little variability due to these modifications. Excitation at 590 nm resulted in lifetimes, τ_i, and fractional contributions, c_i, for wavelengths above the excitation wavelength (640-660 nm) that were similar to those resulting from excitation at 290 nm.

Future Work

The results of this study should be included in future models of the effect of sensitization of compounds near or sorbed to CDOM as well as within individual CDOM chromophores in the environment. Our work should be expanded to include excitation at additional wavelengths, especially those in the solar ultraviolet and visible range. Also, other portions of CDOM such as fulvic acids which constitute an important component of marine organic matter. The application of deconvolution routines that can distinguish more than three independent lifetimes to this data will help determine if the absorption and

fluorescence spectra of CDOM is caused by a limited number of individual compounds with broad spectroscopic characteristics or a continuum of individual species with narrow ones. The utilization of a frequency modulated fluorescence spectrometer may assist in answering a number of these questions.

References

Amador, J. A., Alexander, M., and Zika, R. G., 1989. Sequential photochemical and microbial degradation of organic molecules bound to humic acid. Appl. Environ. Microbiol., 55: 243-2849.

Blough, N. V., Zafiriou, O. C., and Bonilla, J., 1993. Optical absorption spectra of waters from the Orinoco River outflow: Terrestrial input of colored organic matter to the Caribbean. J. Geophys. Res., 98: 2271-2278.

Bricaud, A., Morel, A., and Prieur, L, 1981. Absorption by dissolved organic matter of the sea (yellow substance) in the UV and visible domains. Limnol. Oceanogr., 26: 43-53.

Carter, C. W., and Suffet, I. H., 1982. Binding of DDT to dissolved humic materials. Environ. Sci. Technol., 16: 735-740.

Chiou, C. T., Malcolm, R. L., Brinton, T. I., and Kile, D. E., 1986. Water solubility enhancement of some organic pollutants and pesticides by dissolved humic and fulvic acids. Environ. Sci. Technol., 20: 502-508.

Fisher, A. M., Winterle, J. S., and Mill, T., Primary photochemical processes in photolysis mediated by humic substances. In Zika, R. G., and Cooper, W. J. (Eds.), Photochemistry of Environmental Aquatic Systems, 1987, ACS symposium series # 327, Washington, D.C., 141-156.

Gauthier, T. D., Shane, E. C., Guerin, W. F., Seitz, W. R., and Grant, C. L., 1986. Fluorescence quenching method for determining equilibrium constants for polycyclic aromatic hydrocarbons binding to dissolved humic materials. Environ. Sci. Technol., 20: 1162-1166.

Green, S. A., 1992. Applications of Fluorescence Spectroscopy to Environmental Chemistry. Ph.D. Thesis. MIT/WHOI, WHOI-92-24.

Green, S. A., and Blough, N. V., submitted. Optical absorption and fluorescence properties of chromophoric dissolved organic matter in natural waters.

Hatcher, P. G., Bortiatynski, J. M., Minard, R. D., Dec, J., and Bollag, J.-M., 1993. Use of high-resolution ^{13}C NMR to examine the enzymatic covalent binding of ^{13}C-labeled 2,4-dichlorophenol to humic substances. Environ. Sci. Technol., 27: 2098-2103.

McCarthy, J. F., and Jimenez, B. D., 1985. Interactions between polycyclic aromatic hydrocarbons and dissolved humic material: Binding and dissociation. Environ. Sci. Technol., 19: 1072-1076.

Milne, P. J., Odum, D. S., and Zika, R. G., 1987. Time-resolved fluorescence measurements on dissolved marine organic matter. In Zika, R. G., and Cooper, W. J. (Eds.), Photochemistry of Environmental Aquatic Systems, 1987, ACS symposium series # 327, Washington, D.C., 132-140

Power, J. F., Sharma, D. K., Langford, C. H., Bonneau, R. and Joussot-Dubien, J., 1987. Laser flash photolytic studies of a well-characterized soil humic substance. In Zika,

R. G., and Cooper, W. J., (Eds.) Photochemistry of Environmental Aquatic Systems, 1987, ACS symposium series # 327, Washington, D.C., p 157-173.

Zepp, R. G., Baughman, G. L., and Schlozhauer, P. F., 1981a. Comparison of photochemical behavior of various humic substances in water: I. Sunlight induced reactions of aquatic pollutants photosensitized by humic substances. Chemosphere, 10: 109-117.

Zepp, R. G., Baughman, G. L., and Schlozhauer, P. F., 1981b. Comparison of photochemical behavior of various humic substances in water: II. Photosensitized oxygenations. Chemosphere, 10: 119-126.

Zepp, R. G. and Schlotzhauer, P. F., 1981. Comparison of the photochemical behavior of various humic substances in water. III. Spectroscopic properties of humic substances. Chemosphere, 10: 479-486.

Zepp, R. G., Schlotzhauer, P. F., and Sink, R. M., 1985. Photosensitized transformations involving electronic energy transfer in natural waters: Role of humic substances. Environ. Sci. Technol., 19: 74-81.